City Research Online

City, University of London Institutional Repository

This is the accepted version of the paper.

This version of the publication may differ from the final published version.

Permanent repository link: https://openaccess.city.ac.uk/id/eprint/31000/

Link to published version:

Studies of multimode fibre linked white light interferometric sensor systems

by

QI WANG

A thesis submitted for the Degree of Doctor of Philosophy

CITY UNIVERSITY

Department of Electrical, Electronic and Information Engineering

Northampton Square, London EC1V 0HB

November 1997

Table of Contents

List of the figures

List of Tables

Acknowledgements

Declaration

The author hereby grants powers of discretion to the City University Librarian to allow this thesis to be copied in whole or in part without further reference to him. This permission covers only single copies made for study purposes, subject to normal conditions of acknowledgement.

Abstract

This thesis undertakes a detailed analysis of both the phase and intensity noise in a multimode fibre linked white light interferometric system. Several signal processing schemes have been introduced to ease the central fringe identification and to increase the accuracy of the central position measurement.

A detail investigation of modal noise induced by the multimode fibre link in the WLI system has been carried out. The relationship between modal noise and the parameters of the illuminating source and the linking optical fibre, including the coherence length of the source, the length of the linking fibre, the core diameter of the fibre and type of the fibre have been experimentally studied. A supporting theory has been developed and the results from the experiment are in good agreement with those from the theoretical analysis.

Two signal processing schemes have been developed to increase the relative intensity of the central fringe of the output in a dual wavelength system. One uses an electrical circuit to square the output of the two wavelength system directly, and the other uses two detectors to detect the different wavelengths components of the output of the system. Then, these two output are multiplied and squared using an analogue electrical circuit. With the use of these signal processing schemes, the central fringe becomes more dominant. The comparison of the two signal processing schemes has also been given.

A system consisting of two Michelson interferometers linked with a multimode fibre and illuminated with a dual wavelength source is investigated. The output signal to noise ratio of the system is measured by using a curve fitting method when different linking fibres are used. The result show that the output signal to noise ratio of the system increases as the core diameter of the linking fibre increases when the linking fibre is deliberately shaken. The effect of the modal noise on the central position measurement is also investigated.

A signal processing scheme based on curve fitting algorithm using a cosine function is introduced for this system. The theoretical resolution of the system with the use of the signal processing scheme is given when both intensity noise and phase noise is present. The displacement measurement repeatability of the system is experimentally measured over a displacement range of 80μm. The results show that the measured repeatability (standard deviations) of the system with the use of the signal processing scheme is better than 5nm, which is very close to the value of the theoretical resolution of, 1.9nm.

Chapter 1

Introduction

1.1 Optical fibre sensors

Optical fibre sensors have been intensively researched for many years because they have many potential advantages over electrical sensors. These advantages include their immunity to electromagnetic interference, their ability to realise long-distance sensing, their small size, their resistance to chemical corrosion and their potential for multiplexing [1, 2, 3]. They are also versatile, because an optical beam is characterised by a number of independent parameters including its intensity, wavelength spectrum, phase and polarisation, and each of these parameters may be sensitive to the applied measurand. Hence, a wide range of sensing mechanisms are available.

The technological developments of optical fibres have led to the emergence of the optical fibre sensor. The two main types of optical fibres used in these sensors are the monomode fibre and the multimode fibre. Monomode fibre is designed to guide a single transverse mode, i.e. the coherence of the transmitted light is maintained. In contrast, multimode fibre can transmit a large number of modes and the phase delays at the far end of the fibre varies for each mode.

Sensors may be classified in several ways, most simply as either intrinsic or extrinsic. In an *intrinsic* fibre sensor, the transduction mechanism is based on the modulation of the waveguide properties induced by the measurand and the fibre is both the sensor and the path of the light beam. In an *extrinsic* system, the fibre is not the sensing device, it only

allows the propagation of the light beam from the illuminating source to the sensing element and from the sensing element to the photo detector.

1.2 Optical fibre interferometric sensors

One of the various types of optical fibre sensors reported, optical fibre interferometric sensors, are receiving considerable attention because of their high sensitivity [4, 5, 6]. In an optical fibre interferometric system, the optical path difference (OPD) of the sensor is modulated by the measurand and this OPD change can be measured by using a signal processing scheme.
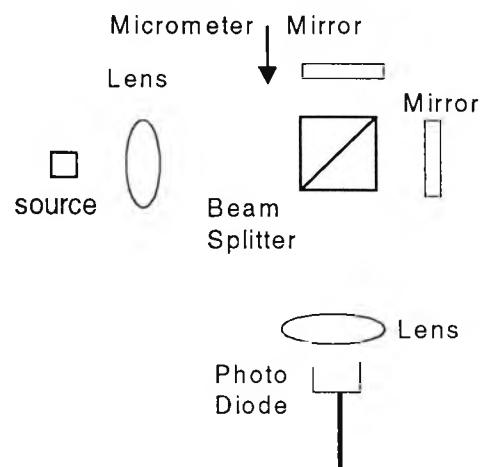
Fig.(1.1) Schematic showing a conventional Michelson interferometer.

Optical interferometry is a relatively old subject, and a large number of instruments based on interferometry were introduced many years ago. However, it is still a very active subject to research, especially since the invention of the optical fibre, as fibres can be used to fabricate interferometer and provide flexible connection for interferometer.

A conventional interferometer can be act as a displacement sensor. To illustrate this, consider a Michelson interferometer which is shown in Fig.(1.1). Light from a single wavelength source is divided by a beam splitter to produce both reference and sensing beams that propagate in each arm of the interferometer. The electric vectors E_r and E_s of these beams may be expressed as

$$E_r = A \exp[i(\omega t + 2\pi n x_r / \lambda)] \qquad (1.1)$$

and

$$E_s = B \exp[i(\omega t + 2\pi n x_s / \lambda)] \qquad (1.2)$$

where A and B are the amplitudes of the reference beam and the sensing beam respectively. x_r and x_s are the distances that the light travels in two arms of the interferometer; n is the refractive index of air, and λ and ω are the vacuum wavelength and the angular frequency of the light source respectively. After reflection by the mirrors, the two beams recombine at the output of the interferometer. The current, I_D, generated at the photo diode used to detect the output of the interferometer, under the condition that A is equal to B, is given by

$$I_D = \frac{I_0}{2}(1 + \cos(2\pi n(x_s - x_r) / \lambda)) \qquad (1.3)$$

where I_0 is the maximum output of the detector. From Eq.(1.3), the output of the photodiode is related to the mirror position x_s, and thus the position of the mirror can be measured by determining the phase change of the output of the photo diode providing the value x_r is held constant.

The Michelson interferometer shown in Fig.(1.1) can be realised using optical fibres, enabling a compact version to be made. Fig.(1.2) shows a schematic diagram of a fibre version Michelson interferometer. In this case, light from the illuminating source is coupled into the monomode fibre and then separated into two beams by the fibre coupler, which propagate in the sensing and reference arms. After reflection from the mirrors, the recombined beam is detected by the photo diode. The output of the photo diode can also be expressed by Eq.(1.3), where n is the refractive index of the fibre core, contrasting the refractive index of air in the conventional air path Michelson interferometer. When it acts as a sensing system, any length variation or refractive index variation in the sensing arm can be measured by calculating the phase change of the photodiode output, providing the effective optical path length of the reference arm is held constant.
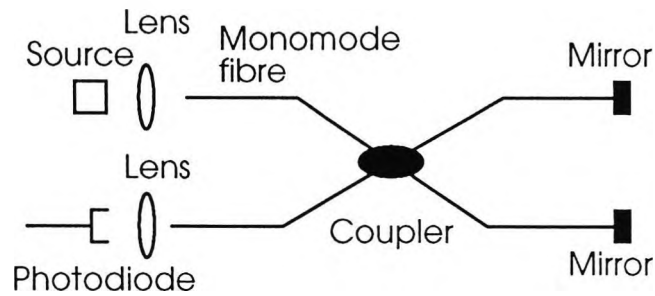
Fig.(1.2) Schematic diagram of a fibre version Michelson interferometer

Optical fibre interferometric sensors generally exhibit an extremely high sensitivity. The wavelength of the source used is often of the order of 1μm. Thus, if a system can measure a phase change of one percent of 2π radians, its resolution will then be 10 nm. However, conventional interferometric optical fibre sensors suffer from the problem that the relative phase difference is lost when the system is switched off and therefore the output become ambiguous beyond one "fringe" measurement. Optical fibre sensors based on "white light interferometry" have been developed to overcome this problem

4

[7, 8]. These white light or low coherence source interferometric sensors have the same potential sensitivity as conventional optical fibre interferometric sensors with the additional and very important benefit of providing an absolute measurement over a much wider range.

1.3 Optical fibre sensors based on white light interferometry

Optical fibre sensing systems based on white light interferometry have been intensively researched in recent years [7, 8, 9]. Compared with conventional optical fibre interferometric sensors, WLI systems have following substantial advantages: (1) A WLI system potentially has the same sensitivity as that of a conventional interferometric optical fibre sensor. (2) It can be used to determine quasi-static measurand, such as temperature, pressure, and strain with a corresponding displacement range much larger than a wavelength. (3) The system is immune to any fibre bending loss, fibre joint loss, source intensity drift, and source wavelength drift. The reason for these is that the output interferometric fringe pattern of a WLI system has a unique central fringe allowing an absolute displacement measurement to be realised and the central position of the output fringe pattern is independent from the slow change of the output intensity of the system and the drift of the average wavelength of the illuminating source.
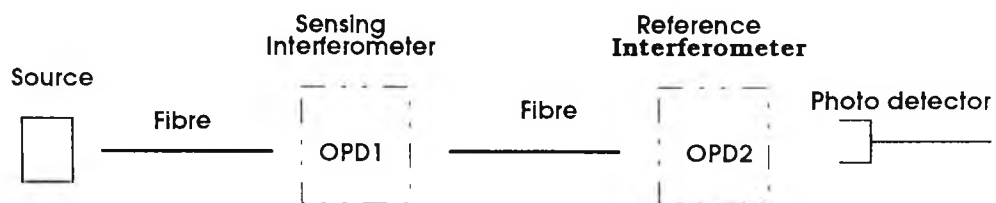
Fig.(1.3) Schematic diagram showing a white light interferometric system.

Fig.(1.3) is a schematic diagram of a typical WLI system. It consists of two interferometers. Light from the broad band (or "white light") source which has a short coherence length is launched into the sensing interferometer and then the reference interferometer. The output of the system is detected by a photo detector. When the optical path difference (OPD) of the reference interferometer is scanned, interference effects will only be observed under two primary conditions these being: (i) when the OPD of the reference interferometer is within the coherence length of the light source, and (ii) the difference between the OPD of the reference interferometer and the OPD of the sensing interferometer is within the coherence length of the light source. Optical fibre sensing systems based on white light interferometry usually operate under the second condition, where the maximum output intensity occurs when the OPD of the two interferometers are equal to each other. Therefore, any OPD change in the sensing interferometer can be absolutely measured by determining the central position change of the output interferometric fringe pattern.

In a fibre-based WLI system, optical fibre is used to provide a flexible connection within the instrument. Both monomode fibre and multimode fibre are capable of doing this. When monomode fibre is used, coupling difficulties arise due to narrow core diameter of the fibre. Hence, a comparatively expensive coupler and very high stable launch conditions of light into the system are necessary for the instrument. Multimode fibres can be used to overcome the coupling difficulties because they have a much larger core diameter than that of the monomode fibre otherwise used and the light is therefore much easier to couple into the fibre. In addition, by using a multimode fibre link, a WLI sensor system without moving parts can be realized [11]. However, the remaining problem for the system with a multimode fibre link is the presence of the modal noise that will reduce the output signal to noise ratio of the instrument.

Thus, suitable signal processing techniques are required to suppress noise and to give increased central position measurement accuracy. A noise rejection signal processing scheme based on the whole fringe pattern centroid algorithm has been proposed [10], which advantages are its short operational time and its resistance to noise. Other signal processing techniques have also been proposed [11]. These include the central full fringe centroid method and the central bright fringe centroid method. With the use of these techniques, the effect of noise can be suppressed considerably and give increased accuracy of the central position measurement.

To ease the central fringe identification problem, dual wavelength source techniques have been proposed [12, 13]. With two wavelength components in the source, a beat pattern is generated in the output of a WLI system and thus the relative intensity of the central fringe is considerably increased. With the use of this technique, the signal to noise ratio required to identify the central fringe may be reduced from typically about 50 dB for a single wavelength source system to about 25 dB [12]. The method used to select the suitable wavelengths of the source to optimise the system and obtain the highest relative intensity of the central fringe have also been reported [14,15].

To increase further the relative intensity of the central fringe, a three wavelength technique have been proposed [16, 17]. With three wavelength components in the source, the subsidiary fringes in the output of a WLI system have been seen to suppressed further. It has been reported [16, 17] that the signal to noise ratio required for the central fringe identification is about 13 dB when a suitable combination of wavelengths is selected.

The advantages of WLI systems have led to a large number of applications, although there are still problems existing which limit the measurement accuracy and the

7

measurement range of the WLI systems, as will be discussed in this thesis, together with ways to overcome them. WLI optical fibre sensors has been applied to pressure sensors [18, 19], to the measurement of strain and stress [20], to the sensing of temperature [21] and other special applications [22, 23]. It is also reported that an integrated optic Mach-Zehnder reference interferometer has been produced for a WLI system [24].

1.4 Aim of this work

The primary aims and objectives of this work are:

1. To investigate the relationship between modal noise and the parameters of the illuminating source and the linking multimode fibre in a white light interferometric (WLI) system. These parameters include the coherence length of the source, the length of the fibre, the core diameter of the fibre and type of the fibre.

2. To develop techniques applicable to the dual wavelength system which will increase the relative intensity of the central fringe.

3. To introduce and discuss a signal processing scheme based on a curve fitting algorithm, which will be used to reduce the effect of both intensity noise and phase noise, on the central position measurement.

1.5 Structure of the thesis

The structure of the thesis is as follows:

In Chapter 1, a brief review of the field of optical fibre sensors based on the white light interferometry is given.

In Chapter 2, the basic theory of white interferometry is introduced and the possible sources of noise in the system are discussed. Several illuminating sources and optical fibres used in a WLI system are also discussed.

In Chapter 3, an experimental investigation of the relationship between modal noise and the parameters of the illuminating source and the linking multimode fibre, which include the coherence length of the source, the length and the core diameter of the fibre and type of the fibre, is described. A supporting theory is included which helps to explain the experiment results.

Two techniques for dual wavelength system are discussed in Chapter 4, which can increase the relative intensity of the central fringe. One of the techniques is to square the summed output of two wavelength components and the other is to square the multiplied output of the two wavelength components. A theoretical simulation and a corresponding experimental investigation show that the signal to noise ratio required to identify the central fringe decreases as the power of the squaring operation increases. A comparison of the two techniques is also presented.

In Chapter 5, a WLI system consisting of two Michelson interferometers linked with a multimode fibre is described. Firstly, experiment results obtained on the output signal

to noise ratio of the system is given for different linking fibres and the effect of the modal noise on the central position measurement is investigated. Secondly, an investigation of the stability of the interferometers is presented. Thirdly, a signal processing scheme based on curve fitting algorithm is proposed, and the theoretical resolution of the system with the use of the signal processing scheme is given. Finally, the experimental results obtained on the displacement measurement repeatability of the system are presented.

In Chapter 6, conclusions are given and the potential for future research is discussed.

References

[1] T. G. Giallorenzi, J. A. Bucaro, A. Dandridge, G. H. Sigel, Jr., J. H. Cole, S. C. Rashleigh and R. G. Priest, "Optical Fibre Sensor Technology", IEEE Journal of Quantum Electronics, Vol. QE-18, No.4, pp626-665, 1982.

[2] D. A. Jackson and J. D. C. Jones, "Fibre Optic Sensors", Opt. Acta, Vol. 33, pp. 1469-1503, 1986.

[3] K. T. V. Grattan, "Recent Advances in Fibre Optic Sensors", Measurement, Vol.5, No.3, pp.122-134, July-September 1987.

[4] A. D. Kersey, "Recent Progress in Interferometric Fibre Sensor Technology", Proceedings of SPIE, Vol.1367, pp.1-12, 1990.

[5] A. Dandridge, "Fibre Optical Sensors Based on the Mach-Zender and Michelson Interferometers", in "Fibre Optic Sensors: An Introduction for Engineers and Scientists", Edited by E. Udd, pp.271-323, John Wiley & Sons, Inc., 1991

[6] D. A. Jackson, "Recent Progress in Monomode Fibre-Optic Sensors", Measurement Science and Technology, Vol.5, pp.621-638, June 1994.

[7] A. Koch and R. Ulrich, "Fibre-optic Displacement Sensor With 0.02μm Resolution by White Light Interferometry," in Proc. 7th Int. Conf. on Optical Fibre Sensors, Sydney, pp.201-207. 1990.

[8] H. C. Lefevre, "White Light Interferometry in Optical Fibre Sensor", Proceedings of the 7th international Optical Fibre Sensors Conference, pp.345-351, Sydney, Australia. 1990.

[9] K. T. V. Grattan and B. T. Meggitt. "Optical Fibre Sensor Technology" Chapter. 9, (Chapman & Hall, London, 1995).

[10] R. Dandliker, E. Zimmermann and G. Frosio, "Noise-Resistant Signal Processing for Electronically Scanned White-Light Interferometry", Proc. 8th Int. Conf. Optical Fibre Sensors, Monterey ,CA, Jan.1992, pp.53-56.

[11] S. Chen, A. W. Palmer, K. T. V. Grattan, and B. T. Meggitt "Digital Signal-processing Techniques for Electronically Scanned Optical-Fibre White-Light Interferometry" Applied Optics, Vol.31(28), pp6003-6010, 1992.

[12] S. Chen, K. T. V. Grattan, B. T. Meggitt, and A. W. Palmer, "Instantaneous Fringe-order Identificaton Using Dual Broadband Sources With Widely Spaced Wavelengths", Electron. Lett., Vol.29, pp. 334-335, (1993).

[13] Y. J. Rao, Y. N. Ning and D. A. Jackson, "Synthesized Source for White-light Sensing Systems", Opt. Lett., Vol.18(6), pp462-464, (1993).

[14] D. N. Wang, Y. N. Ning, K. T. V. Grattan, A. W. Palmer and K. Weir "Characteristics of Synthesized Light Sources for White Light Interferometric Systems", Optics Letters, Vol.18, No.22, pp.1884-1886, November 15, 1993.

[15] D. N. Wang, Y. N. Ning, K. T. V. Grattan, A. W. Palmer and K. Weir " The Optimized Wavelength Combinations of Two Broadband Sources for White Light Interferometry", Journal of Lightwave Technology. Vol.12, No.5, pp909-914, 1994.

[16] D. N. Wang, Y. N. Ning, K. T. V. Grattan, A. W. Palmer and K. Weir, "Three-wavelength Combination Source for White Light Interferometry", IEEE Photon. Technol. Lett., Vol.30(17), pp1440-1441, (1994).

[17] D. N. Wang, Y. N. Ning, K. T. V. Grattan, A. W. Palmer and K. Weir, "Optimized Multiwavelength Combination Sources for Interferometric Use", Applied Optics, Vol.33, No.31, pp.7326-7333, November 1994.

[18].G. Beheim, "Fibre-linked Interferometric Pressure Sensor," Rev. Sci. Instrum.,Vol. 58, pp. 1655-1657, 1987.

[19] W. J. Bock, W. Urbanczyk, J. Wojcik, and M. Beaulieu, "White Light Interferometric Fibre-Optic Pressure Sensor", IEEE Transaction on Intrumentation and Measurement, Vol. 44, No.3, pp694-697, June 1995.

12

[20] J. M. V. Oort and H. H. J. T. Kate, "A Fibre Optics Sensor for Strain and Stress Measurements in Superconducting Accelerator Magnets", IEEE Transaction on Magnets, Vol. 30, No. 4, pp2600-2603, July 1994.

[21] C. E. Lee and H. F. Taylor, "Fibre-Optic Fabry-Perot Temperature Sensor Using a Low-Coherence Light Source", IEEE Journal of Lightwave Technol., Vol.9, No.1, pp.129-134, January 1991.

[22] P. Sandoz and G. Tribillon, "Profilometry by Zero-order Interference Fringe Identification", Journal of Modern Optics, Vol. 40, No.9, pp1691-1700, 1993.

[23] K. Takada, K. Chida, J. Noda and S. Nakajima, "Trench Depth Measurement System for VLSI DRAM's Capacitor Cells Using Optical Fibre and Michelson Interferometer", Journal of Lightwave Technol. Vol.LT5, No.7, pp881-887, July 1987.

[24] M. V. Plissi, A. J. Rogers, D. J. Brassington, and M. G. F. Wilson, "Low-Coherence Interferometric Sensor System Utilizing an Integrated Optics Configuration", Applied Optics, Vol.34, No.22, pp4735-4739, August 1995.

Chapter 2

Principles of white light interferometry

Optical fibre sensing systems based on white light interferometry have been intensively studied over recent years [1-8]. This is usually called white light interferometric (WLI) system. In such a system, a broad band illuminating source, optical linking fibres, and interferometers are usually exploited (shown in Fig.(1.3)). Multimode fibres are very attractive for such systems because it has much larger core diameter than that of a single mode fibre so that the light beam from the illuminating source or from the sensing interferoemter is easier to be coupled into it. However, with a multimode linking fibre, modal noise is induced in WLI systems [9, 10, 11, 12], which reduces the output signal to noise ratio of the WLI systems.

In this Chapter, the theoretical output of a white light interferometric system consisting of two Michelson interferometers linked with an optical fibre has been derived. A discussion on intensity noise and phase noise associated with a WLI system is also included. In addition, optical sources and optical fibres for a typical WLI system are discussed.

2.1 Theory of white light interferometry

Suppose a white light interferometric system consisting of two Michelson interferometers linked with an optical fibre, which is shown in Fig.(2.1). The light beam from a broad band source is coupled into the first interferometer. Then, the light beam from the sensing interferometer is guided into the second interferometer, and the output of the system is detected by a photo detector.
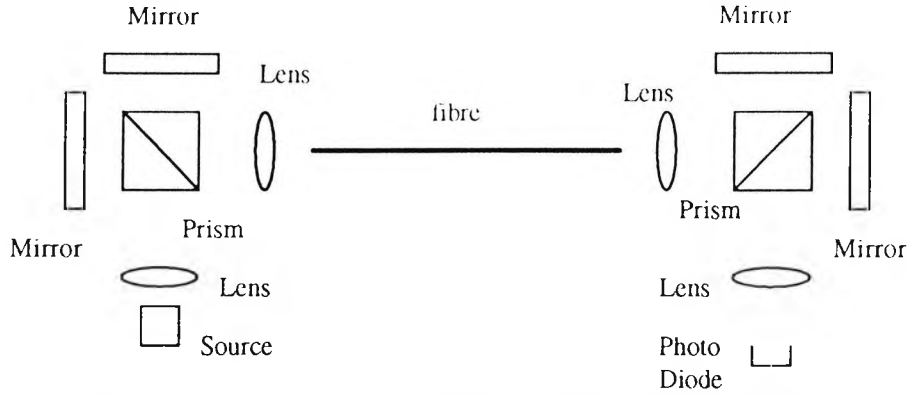
Fig.(2.2) Schematic diagram of a WLI system consisting of two Michelson interferometers with an optical fibre link

If the intensity transfer functions of the first interferometer and the the second interferometer, which can be regarded as sensing interferometer and reference interferometer, are $I_s(k)$ and $I_r(k)$ respectively. The resulting output intensity function of the system, I_D, will be of the form [1]

$$I_D = \int I_s(k) I_r(k) i(k) dk \qquad (2.1)$$

where k is the wave number and $i(k)$ is the power spectrum of the source, which may be expressed as [1]

$$i(k) = \frac{2I_0}{\sqrt{\pi}\sigma} \exp[-(\frac{k-k_0}{\sigma})^2] \qquad (2.2)$$

where k_0 is the central wave number and σ represents the half width of the spectrum of the Gaussion distribution. If both the sensing interferometer and the reference interferometer are of the Michelson type, the transfer functions of the interferometers, I_s and I_r are given by [2]

$$I_s = (1/2)(1 + \cos(k\,x_s))$$ (2.3)

and

$$I_r = (1/2)(1 + \cos(k\,x_r))$$ (2.4)

where x_s and x_r are the optical path differences (OPDs) of the sensing interferometer and the reference interferometer respectively. By substituting Eqs.(2.2), (2.3), (2.4) into Eq.(2.1), the output intensity function of the system, I_D, can be expressed as

$$I_D = \frac{I_0}{4} \int i(k)(1 + \cos(k\,x_s))(1 + \cos(k\,x_r))\,dk$$ (2.5)

When x_s, x_r are much larger than $1/\sigma$ and x_s approximately equals x_r, the output intensity function of the system can be simplified to [1]

$$I_D = \frac{I_0}{4}\{1 + \frac{1}{2}[\exp(-(\frac{2(x_s - x_r)}{L_c})^2)\cos(\frac{2\pi(x_s - x_r)}{\lambda})]\}$$ (2.6)

where $\lambda = \frac{1}{k_0}$ and $L_c = \frac{2}{\pi\sigma}$ are the central wavelength and the coherence length of the source respectively. Fig.(2.2) shows the output intensity fringe pattern of the system calculated from Eq.(2.6). In this case, I_0 is equal to unit, and the wavelength λ and coherence length L_C were chosen to be 0.78μm and 15μm respectively. It is noted that the position of the maximum output intensity, i.e. the central position of the output fringe pattern, occurs when the OPD difference of the interferometers is equal to zero. This is the key point for the system to realise effective optical fibre sensing. As a result, any variation of the OPD in the sensing interferometer can be measured absolutely by determining the central position of the output intensity fringe pattern.

16
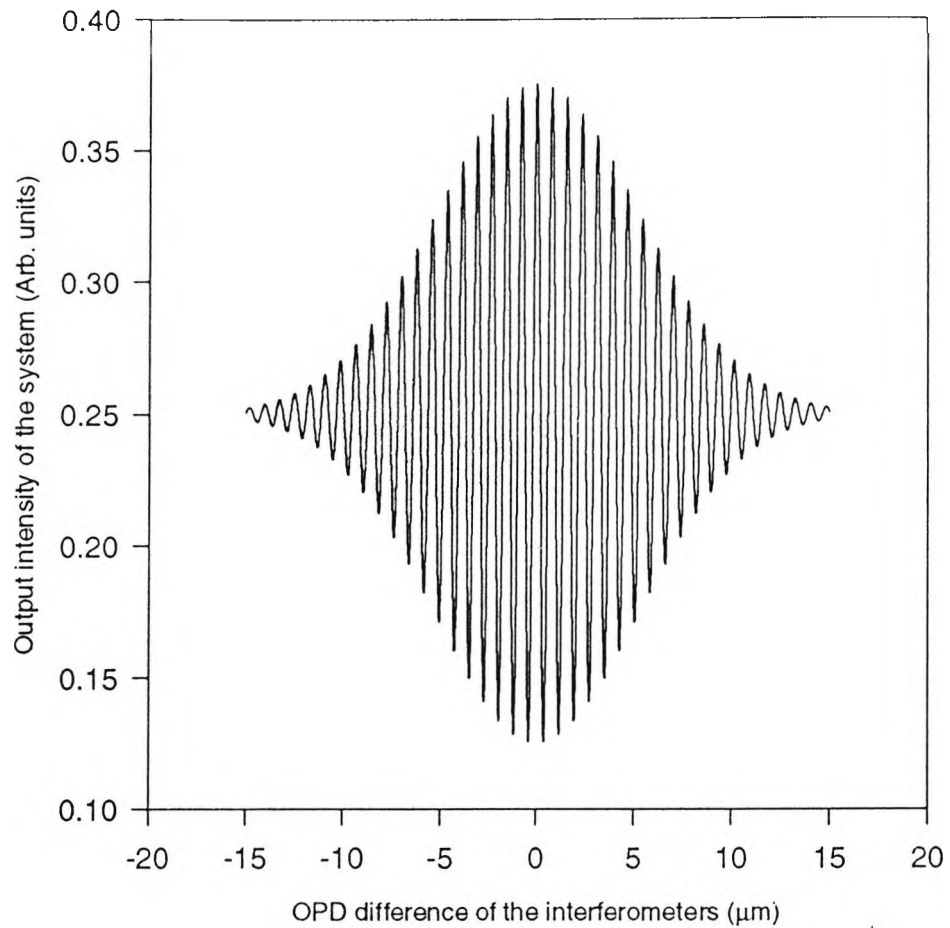
Fig.(2.2) Output fringe pattern obtained from Eq.(2.6)

2.2 Noise in a white light interferometric system

In a WLI system with monomode optical fibre link, there is no modal noise in the system and therefore a high output signal to noise ratio may be obtained. However, due to the difficulty of coupling the optical beam into the monomode fibre, high accuracy fibre couplers are required, resulting in a high cost to fabricate the system and difficulties in alignment.

If a multimode fibre is used to couple the sensing and reference interferometers, the above problems associated with monomode fibre linked systems are more easily overcome because multimode fibres have a much larger core diameter. In addition, with a multimode fibre link, a WLI sensing system without moving parts can be realized [7].

However, difficulties arise in any WLI system using multimode linking fibres as modal noise is introduced by the multimode fibre link when the multimode fibre is perturbed [9,10,11,12]. The level of induced modal noise in such a system may be higher than that of the noise induced by the intensity fluctuations of the illuminating source or the noise from the photodetector.

In the theoretical output of the WLI system shown in Eq.(2.6), noise has not been considered. In any WLI system, the output of a WLI system may be characterised by two major parameters, the output intensity and the OPD of the interferometer. These two parameters may fluctuate randomly in a practical system. The random fluctuation of the output intensity may be defined as *intensity noise* and the random fluctuation of the OPD of the interferometers may defined as *phase noise*. The possible sources of noise in the WLI system are discussed below:

1)   Thermal noise and shot noise of the photo detector [13].

Thermal noise (also called Johnson noise and Nyquist noise) originates within the photodetector load resistor R_L. Electrons within any resistor never remain stationary. They randomly move because of their thermal energy, even with no voltage applied. Thus, a randomly varying current exists, which induces thermal noise. The rms value of the thermal noise is given by

$$i_T = \sqrt{\frac{4kT\Delta f}{R_L}} \qquad\qquad (2.7)$$

where k is the Boltzmann constant, T is the absolute temperature, R_L is the photodetector load resistance, and Δf is the receiver bandwidth. Thermal noise is normally distributed, and contributes to the intensity noise in the WLI system.

Shot noise originates from the discrete nature of the electrons, and for example with a photodetector, the optical signal generates discrete charge carriers. Each carrier contributes a single pulse to the output current instead of a continuous current. This will induce the shot noise at the output of the detector. Its rms value is expressed as

$$i_s = \sqrt{2eI\Delta f} \qquad\qquad (2.8)$$

where e is the magnitude of the charge on an electron, I is the average detector current, and Δf is the bandwidth of the receiver. Just like thermal noise, shot noise is normally distributed noise, and contributes to the intensity noise in the WLI system.

2)   *Source noise* is the noise induced by semiconductor low coherence sources, such as light-emitting diodes and superluminescent diodes [14, 15]. When a semiconductor low coherence source is driven by an electrical current, photons will be emitted from it, which are generated independently and randomly. The optical output of the source is the sum of the effects of a large number of emitted photons [16]. As a result, the output intensity of the source fluctuates randomly. It is reported that the overall source noise, from the low coherence semiconductor source, exceeds the normal shot noise and thermal noise by 17dB when the output power of a source with a 50nm bandwidth is about 1mW. However, even with this type of source, it is possible

for an optical system to achieve a signal to noise ratio of about 10^5 (100dB) if only *source noise* is present.

It should be noted that the central position of the output fringe pattern is independent of the intensity and the wavelength drift of the illuminating source (see Eq.(2.6)). Thus, any low frequency intensity changes of the illuminating source or any average wavelength drift of the illuminating source will not induce an error to the central position measurement.

3)   *Modal noise* from the fibre link. When a multimode fibre is used to connect the components within the system, it will support the propagation of a large number of modes. Different modes travel different path lengths along the optical fibre. Hence, the intermodal coupling between the adjacent modes induces intensity noise when the multimode linking fibre is subjected to environmental perturbations, such as vibration or temperature variations. This the origin of the modal noise in the WLI system. The output signal to noise ratio of a multimode fibre linked system described in Chapter 3, if only modal noise is present, is given by

$$S/N_1 = \frac{\sqrt{M}(1 + C(\Delta L)\cos(2\pi\Delta L/\lambda))E(I_i)}{\sqrt{[1 + (C(\Delta L))\cos(2\pi\Delta L/\lambda)]^2 \xi + I_i^2 \chi_1}} \tag{2.9}$$

where

$$\chi_1 = \frac{1}{2}\{2C(\delta L_{i,i+1}) + C(\delta L_{i,i+1} + \Delta L)\cos(\frac{2\pi}{\lambda}\Delta L) + C(\delta L_{i+1,i} - \Delta L)\cos(\frac{2\pi}{\lambda}\Delta L)\}^2 \\ + \frac{1}{2}\{[C(\delta L_{i,i+1} + \Delta L) - C(\delta L_{i,i+1} - \Delta L)]^2 \sin^2(\frac{2\pi}{\lambda}\Delta L)\} \tag{2.9a}$$

and

$$C(\delta L_{i,i+1}) = \exp[-(2\delta L_{i,i+1} / L_c)^2]$$ (2.9b)

L_c is the coherence length of the source and $\delta L_{i,i+1}$ is the OPD between ith and (i+1)th mode at the far end of the fibre. M is the modal number transmitted in the fibre, $E(I_i)$ and $D(I_i)$ are the expectation value and the variance of the intensity of the light beam transmitted in the ith mode respectively.

Modal noise contribute intensity noise to the output of the WLI system. Its value is usually much larger than that of thermal noise, shot noise or source noise in a typical WLI system.

4)   *Noise from the capacitive position sensor.* The position of the mirror in the interferometer discussed in this thesis is measured with the use of a capacitive sensor (see section 5.3.2). Providing there is no vibration of the interferometers, the output noise from the position sensor and associated electrical circuit will cause a displacement measurement error. This kind of noise can be regarded as normally distributed, which contributes phase noise to the output of the system. Its value may typically be as small as 3 nm.

5)   *Vibration of the mirrors in the interferometers.* The presence of the vibration in the WLI system may cause fluctuations of the arm length difference (ALD) of the

21

interferometers, which induces phase noise in the output of the system. The frequency distribution of the noise is related to the natural frequency of the interferometers.

6)   *Position drift of the mirrors in the interferometers.* The ALD of the interferometer in the WLI system may change continuously due to the mechanical instability of the interferometers. This induces low frequency phase noise in the output of the WLI system.

7)   *Effects of atmospheric turbulence.* It is well known that air turbulence will cause the refractive index fluctuation of air, so that the OPD of an air path interferometer will fluctuate accordingly. This will contribute to intensity noise and phase noise in the output of a WLI system. The magnitude of the intensity noise will be proportional to the intensity of the light beam propagating in the interferometer and will depend on the arm length of the interferometers. The phase noise induced by the turbulence of air depends on the arm length of the interferometer.

Suppose n_I and n_p represent the intensity noise and the phase noise in the WLI system, respectively. Their mean values are zero and their rms values are σ_I and σ_p respectively. Eq.(2.6) can be rewritten as

$$I_D = \frac{I_0}{4}\{1 + \frac{1}{2}[\exp(-(\frac{x_s - x_r + n_p}{L_c})^2)\cos(\frac{2\pi(x_s - x_r + n_p)}{\lambda})]\} + n_I \qquad (2.10)$$

22

where n_I is induced by fluctuations of the illuminating source, by thermal noise and shot noise of the photodetector and by the modal noise of the fibre link. The modal noise is the main part of the intensity noise. The output intensity of the system, I_D, will fluctuate due to the presence of the intensity noise n_I. n_p is the phase noise which is induced by the vibration and the drift of the interferometers, by the noise from the capacitive position sensor, and by the air turbulence. The OPD of the system, $(x_s - x_r + n_p)$, fluctuates due to the presence of the phase noise n_p. It should be noted that the phase noise in the WLI system is not normally distributed. This is because the frequency distribution of the phase noise induced by the vibration is related to the natural frequency of the interferometers and the drift of the interferometers contributes low frequency phase noise to the output of the system.

2.3 Light sources for white light interferometry

In a WLI system, an illuminating light source, which has a very short coherence length, is needed for the operation of the system. These light sources should satisfy the requirements of the system in terms of power consumption, reliability, size, cost, spatial coherence, and coupling efficiency into optical fibres. A wide range of light sources have been investigated for this purpose [17]. A brief review of the illuminating sources, which are widely used in WLI systems, is given below:

1)   *Light emitting diodes* (LEDs). A light emitting diode (LED) is a semiconductor p-n junction operated under forward bias which transduces electrical energy into optical radiation. It is a widely used illuminating light source for WLI systems due to its low coherence length (without side fringe packages), low cost, high reliability, and

immunity to optical feedback. A typical LED has a spectral width of 60nm and a coherence length of about 10μm.

However, LEDs suffer drawbacks of low output power and poor coupling efficiency into optical fibres.

2)   *Multimode laser diodes*. The multimode laser diode is a competitive candidate for the use in WLI systems because it has a comparatively large output power and may be used to achieve high coupling efficiency into fibres [18, 19]. It is available with a wide range of emission wavelengths in the visible and near infrared range, typical 660nm, 780nm, 800nm, 850nm, 1.3μm and 1.5μm determined by the semiconductor material properties. A representative multimode laser diode, such as from the Sharp LT023 Series [20], has a spectral width of about 2nm and a corresponding coherence length of about 300μm.

Compared with the LED, the multimode laser diode has a larger output power and a higher coupling efficiency into the fibre. However, it has two main drawbacks: 1) It has a longer coherence length than that of a LED and 2) there are side fringe packages in the output fringe pattern when it is used as an illuminating source in a WLI system.

3)   *Superluminescent diode* (SLD). A superluminescent diode, which has been recently developed [21, 22], is a semiconductor p-n junction fabricated in a low fineness Fabry-Perot cavity. This kind of source offers several advantages over other kind of sources when it is used to illuminate WLI systems: 1) Its output power and coupling efficiency into a fibre are higher than that of a LED and 2) it has a shorter coherence length than that of a multimode laser diode and the output of a WLI system illuminated with such a source has lower level of the side fringe packages than that

24

illuminated with a multimode laser diode. A typical superluminescent diode has a spectral width of about 40nm and coherence length of about 15μm.

2.4 Optical fibre issues

There are two main types of optical fibre, *monomode fibre* and *multimode fibre*. The monomode fibre has a very small core diameter and transmits a single transverse mode only. In contrast, a multimode fibre has a much larger core diameter and supports the propagation of a large number of transverse modes. The total transmmited mode number M in a multimode fibre can be estimated by using the following equation [23]

$$N = \frac{q}{q+2} k_0^2 a^2 n^2 \Delta \qquad (2.11)$$

where a represents the radius of the fibre core, Δ is the grading parameter, n represents the axial refractive index, q represents the exponent of the power law profile. $q=2$ corresponds to a parabolic index profile and $q=\infty$ corresponds to a step index profile. k_0 is the wave number of the optical beam of the system.

Different modes travel at different velocities in a multimode fibre. As a result, they take different times to propagate through any particular length of a multimode fibre. Assume that the length of a step index fibre is L, its refractive index of the fibre core is n, and the ray makes a angle θ with the axis of the fibre. Then, the time delay t for a ray to propagate through length of the fibre L can be estimated as [23]

$$t = nL / c \cos(\theta) \qquad (2.12)$$

25

where c is the velocity of the light in vacuum. The above expression shows that the time delay vary against the angle θ as the modes propagated at different angles in a multimode fibre travel through different distance when they arrive at the far end of the fibre. The phase delay associated with the ray of each different mode is then a function of the angle θ when it reaches the far end of the fibre.

For a step index fibre, the time delay difference, δT_s between the extreme meridional ray and the axial ray may be expressed as [23]

$$\delta T_s = \frac{Ln\Delta}{c} \tag{2.13}$$

where Δ is the grading parameter for the fibre, c is the velocity of light in a vacuum, n is the refractive index of the fibre core and L is the length of the fibre.

For a graded index fibre, the time delay difference between the fundamental mode and highest-order mode, δT_g, is given by [23]

$$\delta T_g = \frac{Ln\Delta^2}{2c} \tag{2.14}$$

Typical values that may be relevant to a WLI system are: L taken as 1000m, n=1.5, and Δ=1%. As a result of Eq.(2.13) and Eq.(2.14), δT_s equal 50ns and δT_g 0.25ns, which represent about 15m and 75mm delay in length respectively. These calculated results imply that the average OPD between adjacent modes in a parbolic index fibre is much smaller than that in a step index fibre.

26

When a multimode fibre is subjected to perturbations, such as vibration or temperature differential variations, the so-called intermodal cross coupling will occur between these adjacent modes. The coupling between the guided modes transfers optical energy from the slower to the faster modes and vice versa. Hence, the phase of each mode at the far end of the fibre changes randomly due to the mode cross-coupling. This will induce the so-called modal noise [9, 10, 11], which will be discussed in detail in the next Chapter.

References

[1] D. N. Wang. "White Light Interferometric Sensor Systems" Thesis for Degree of Ph.D, Chapter.2, City University, London, 1995.

[2] K. T. V. Grattan and B. T. Meggitt. "Optical Fibre Sensor Technology" Chapter. 9, (Chapman & Hall, London, 1995).

[3] Th. Bosselmann and R. Ulrich, "High Accuracy Position-Sensing with Fibre-Coupled White light Interferometers", Proceedings of the 2nd International Optical Fibre Sensors Conference, pp.361-365, Stuttgart, Germany, 1984.

[4] G. Beheim, "Remote Displacement Measurement Using a Passive Interferometer With Fibre-optic Link", Appl. Optics, Vol.24, pp2335-2340, 1985.

[5] A. Koch and R. Ulrich, "Fibre-optic Displacement Sensor With 0.02μm Resolution by White Light Interferometry", in Proc. 7th Int. Conf. on Optical Fibre Sensors, Sydney, pp.201-207. 1990.

[6] R. Dandliker, E. Zimmermann and G. Frosio, "Noise-Resistant Signal Processing for Electronically Scanned White-Light Interferometry", Proc. 8th Int. Conf. Optical Fibre Sensors, Monterey ,CA, Jan.1992, pp.53-56.

[7] S. Chen, A. W. Palmer, K. T. V. Grattan, and B. T. Meggitt "Digital Signal-processing Techniques for Electronically Scanned Optical-Fibre White-Light Interferometry" Applied Optics, Vol.31(28), pp6003-6010, 1992.

[8] C. Belleville and G. Duplain, "White-Light Interferometric Multimode Fibre-Optic Strain Sensor", Optics Letters, Vol.18, no.1, pp78-81, 1993.

[9] S. Chen, A. W. Palmer, K. T. V. Grattan, and B. T. Meggitt, "Extrinsic Optical-Fibre Interferometric Sensor That Uses Multi-mode Optical Fibres: System and Sensing Head Design for Low-noise Operation," Opt. Lett. Vol.17, pp701-703 (1992).

[10]. Y. N. Ning, K. T. V. Grattan, A. W. Palmer, and K. Weir, "Measurement of Up and Down-Lead Fibre Sensitivity Caused by Lead in Multimode Fibre in an Interferometric System", Applied Optics, Vol.33, no.31, pp7529-35.

[11] Y. N. Ning, Y. Liu, B. M. A. Rahman, K. T. V. Grattan, and A. W. Palmer "Conditions for Suppressing Modal Noise Induced in a White Light Interferometer" Proceeding of Tenth Conf. on Optical Fibre Sensors, pp576-579, (Glasgow, 1994)

[12] Qi Wang, Y. N. Ning, K. T. V. Grattan, A. W. Palmer, "Effect of Multimode Fibre Core Diameter on Modal Noise Suppression in White-light Interferometry". Optical communication, Vol.118, pp473-478, 1995

[13] J. C. Palais "Fibre Optic Communications" 2nd Edition, Chapter 11, pp235, (Prentice-Hall International Inc.), 1988

[14] Aileen M. Yurek, Henry F. Taylor, Lew Goldberg, Joseph F. Weller, and Anthony Dandridge "Quantum Noise in Superluminescent Diode" IEEE Journal of Quantum Electronics, Vol. QE-22, no. 4, pp522-527, April 1986.

[15] Moshe Tur, Ehud Shafir, Kjell Bløtekjaer "Source Induced Noise in Optical Systems Driven by Low-Coherence Sources" Journal of lightwave technology, Vol. 8, no. 2, pp183-189, February 1990.

[16] J. W. Goodman, "Statistical Optics" New York: Wiley, 1985.

[17] E. Udd, "Light Sources", in "Fibre Optic Sensors: An Introduction for Engineers and Scientists", Edited by E. Udd, pp37-68, John Wiley & Sons. Inc., 1991.

[18] Y. N. Ning, K. T. V. Grattan, B. T. Meggit and A. W. Palmer, "Characteristics of Laser Diodes For Interferometric Use", Applied Optics, Vol.28, no.17, pp3657-61, September 1989.

[19] A. S. Gerges, T. P. Newson and D. A. Jackson, "Coherence Tuned Fibre Optic Sensing System, with Self-Initialization, Based on a Multmode Laser Diode", Applied Optics, vol.29, no.30, pp4473-80. October 1990.

[20] SHARP laser diodes. (1988). Laser Diodes User's Manual. Available from Access Pacific Ltd., Kymbrook School House, Kimbolton Road, Keysoe, Bedford MK44 2HH, U.K.

[21] C. B. Morrison, L. M. Zinkiewicz, J. Niesen and L. Figueroa, "High-Power Superluminescent Diode with Reduced Coherence Length", Electronics Letter, Vol.21, no.19, pp.840-841, September 1985.

[22] Y. Kashima, A. Matoba and H. Takano, "Performance and Reliability of InGaAsP Superluminescent Diode", IEEE Journal of Lightwave Technoloy, Vol.10, No.11, pp.1644-49, November 1992.

[23] A. K. Ghatak and K. Thyagarajan, "Optical Electronics" (Cambridge University Press), Chapter 13, 1989.

Chapter 3

Modal noise in a system consisting of a Michelson interferometer with a multimode lead fibre

3.1 Introduction

Optical fibre-based interferometric sensing systems have a considerable potential for high-precision measurement in many scientific and industrial applications [1]. Both intrinsic and extrinsic interferometric optical fibre sensors require the use of fibres to deliver the light beam from the light source to the sensing element, collect the modulated light beam from the sensing element, and then pass it to the detector that converts the optical signal into an electrical signal for further processing [2, 3, 4]. As has been discussed earlier, single-mode fibres are difficult to inject light into, and the cost of assembling such a single-mode fibre interferometric system increases because high-precision fibre couplers and components have to be employed.

There are distinct advantages in using multimode fibres, from the light-collection point of view, as lead fibres. In addition, a WLI sensing system without moving parts can be realised with the use of the multimode fibre [2]. However, when a multimode fibre is used to deliver light, an optical path difference (OPD) between each pair of adjacent modes is induced at the far end of the multimode fibre by the group delay time differences occurring among the modes in the fibre [5, 6]. Hence, if the fibre is subjected to environmental perturbations such as vibration and temperature variations, then the so-called intermodal cross-coupling effect [7] will be induced. As a result,

modal noise will be introduced and the signal to noise ratio of the optical intensity delivered by a fibre will be reduced [8, 9].

When a multimode fibre is used to provide link within a interferometric system, modal noise will also be present and the output signal to noise ratio of such a system will be reduced [10, 11, 12, 13]. It has been demonstrated that the modal noise in the output of such multimode fibre linked interferometric systems depends on the coherence length of the illuminating source [10, 11], the length of the multimode lead fibre [12], and the type of the lead fibre [2, 13].

In this Chapter, the work published in Refs. [10, 11, 12, 13] is discussed. A simple theory for the system consisting of a Michelson interferometer and a multimode lead fibre has been developed. Experimental investigations on the modal noise in the output of the system are carried out. These investigations include the dependence of the SNR of the system on the parameters of the illuminating source and the lead fibre. Following this introduction, the theoretical analysis of the output intensity and the rms value of the noise of the system is given. Then, the investigation of the dependence of the modal noise on the coherence length of the illuminating source is described. Furthermore, the investigation of the dependence of the modal noise on the length of the lead fibre is included. Next, the relationship between the modal noise and the characristics of the linking fibre is investigated. Next, the visibility reduction of the output of the system caused by the misalignment of the interferometer is studied theoretically and experimentally. Finally, a conclusion is given.

3.2 Theory and analysis

It is well known that the guided modes supported by a multimode fibre can be geometrically represented by a group of "allowable" rays that propagate along the fibre and their distance of travel depends on their angles of injection: the smaller the angle, the shorter the distance [14]. Clearly, the time taken for the arrival of the energy components at the far end of the fibre will very according to the propagation distances. If the OPD between the two modes is represented by a distance over which the associated energy components of these adjacent modes are separated at the far end of the fibre, then the magnitude of the OPD, $\delta L_{i,k}$, between the ith mode and the kth mode will increase during propagation and lie in the range

$$0 < \delta L_{i,k} < \delta L_{max} \tag{3.1}$$

where δL_{max} is the OPD between the fundamental and the highest-order modes.

To examine the output intensity from the fibre end a simple theoretical model can be introduced, assuming all modes are excited by the launched light beam at the input and then equally attenuated by the fibre. The output electrical field for the energy component of the ith fibre mode in an unperturbed fibre can then be written as [10]

$$E_i = E_{i,0}(x,y,z)\exp[j(\omega t + \phi_{i,0})] \tag{3.2}$$

where x, y, z represent the spatial position in a three demensional coodinate, $\phi_{i,0} = (2\pi / \lambda)\delta L_{i,0}$ is the optical phase difference between the ith mode and the zeroth mode at the far end of the fibre. λ is the wavelength of the light source, and

$E_{i0}(x,y,z)$, in which the explicit spatial dependence of the electric vector has been included, is the amplitude of the ith mode component.

As shown in Fig.(3.1), when the beam transported by each fibre mode reaches the interferometer, it will induce an OPD, $\delta L_{i,0}$, between the zeroth mode and the ith mode. These modes will then be divided by the interferometer, introducing an additional OPD, ΔL, between each mode. Thus the fields that arrive at the detector can be written as

$$E_{i1} = \frac{1}{4}E_{i0}(x,y,z)\exp[j(\omega t + \phi_{i,0})] \qquad (3.3)$$

$$E_{i2} = \frac{1}{4}E_{i0}((x+\Delta L),y,z)\exp\{j[\omega t + \phi_{i,0} + (2\pi/\lambda)\Delta L]\} \qquad (3.4)$$

Hence the output of the detector, the intensity, I, is given by

$$\begin{aligned} I &= [\sum_{i}^{M}(E_{i1} + E_{i2})][\sum_{k}^{M}(E_{k1}^{*} + E_{k2}^{*})] \\ &= I_{i=k} + I_{i \neq k} \end{aligned} \qquad (3.5)$$

where M is the number of modes, E_{k1}^{*}, E_{k2}^{*} represent the complex conjugates, of the electric vectors and

$$I_{i=k} = \sum_{i}^{M}I_{i}\{1 + C(\Delta L)\cos[(2\pi/\lambda)\Delta L]\} \qquad (3.6)$$

$$I_{i \neq k} = \sum_{i \neq k}^{M}I_{i}\{C(\delta L_{i,k})\cos[(2\pi/\lambda)\delta L_{i,k}] + C(\Delta L + \delta L_{i,k})\cos[(2\pi/\lambda)(\Delta L + \delta L_{i,k})]\} \qquad (3.7)$$

34

where

$$C(z) = \exp[-(2z / L_c)^2]$$ (3.7a)

and L_c is the coherence length of the source, I_i is the output intensity of the ith mode, which is proportional to the coupling efficiency and the mode attenuation, and $\phi_{i,k}$ and $\delta L_{i,k}$ are the optical phase differences and the optical path differences (OPDs) between the light beams delivered by the ith and kth modes at the far end of the fibre, respectively. ΔL is the OPD of the interferometer and λ is the average wavelength of the source.

From Eq.(3.5), Eq.(3.6), Eq.(3.7), the output, I, of the system shown in Fig.(3.1) can be expressed as

$$
\begin{aligned}
I &= I_{i=k} + I_{i\neq k} \\
&= \sum_i^M I_i\{1 + C(\Delta L)\cos[(2\pi/\lambda)\Delta L]\} \\
&\quad + \sum_{i\neq k}^M I_i\{C(\delta L_{i,k})\cos[(2\pi/\lambda)\delta L_{i,k}]\} \\
&\quad + \sum_{i\neq k}^M \{C(\delta L_{i,k} + \Delta L)[\cos(\frac{2\pi}{\lambda}\delta L_{i,k})\cos(\frac{2\pi}{\lambda}\Delta L) - \sin(\frac{2\pi}{\lambda}\delta L_{i,k})\sin(\frac{2\pi}{\lambda}\Delta L)]\}
\end{aligned}
$$ (3.8)

If there is no perturbation to the fibre, there is no mode cross-coupling induced and the OPD between modes in the fibre will not change. Hence, the multimode fibre can be approximated to a bundle of single mode fibres and there will be no modal noise in the system. If, however, the fibre is subjected to perturbations such as vibration or temperature variations, cross-coupling between the modes will be induced and the OPD, $\delta L_{i,k}$, will change randomly.

35

It is desired to investigate modal noise in such a system for the purpose of using multimode fibre in WLI systems. For the convenience of the discussion, define the SNR of the system as

$$S/N = \frac{E(I)}{\sqrt{D(I)}} \qquad (3.9)$$

where $E(I)$ and $D(I) = E[(I - E(I))^2]$ are the expectation value and the variance of the output, I, respectively. Since the values of the terms, $\cos(2\pi\delta L_{i,k}/\lambda)$ and $\cos(2\pi(\Delta L + \delta L_{i,k})/\lambda)$, are randomly distributed in the $[-1,1]$ range due to the fluctuation of the value of $\delta L_{i,k}$ providing the linking fibre is perturbed, the expectation value of the second term in the right-hand side of Eq.(3.8), $E(I_{i \neq k})$, is equal to zero. Therefore, the expectation value, $E(I)$, can be expressed as:

$$E(I) = \{1 + C(\Delta L)\cos[(2\pi/\lambda)\Delta L]\}\sum_{i}^{M} E(I_i) \qquad (3.10)$$

Assuming that the light energy transmitted in each mode is equal, the value of $E(I)$ may then be expressed as

$$E(I) = [1 + C(\Delta L)\cos((2\pi/\lambda)\Delta L)] \, M \, E(I_i) \qquad (3.11a)$$

where M is the number of modes transmitted in the fibre, and the average value of the Eq.(3.11a) will be the form

$$E(I) = M \, E(I_i) \qquad (3.11b)$$

36

The variance of the output is given by

$$D(I) = [1 + C(\Delta L)\cos((2\pi/\lambda)\Delta L)]^2 D\{\sum_i^M I_i\}$$

$$+ D\{\sum_{i,k}^M \{I_i C(\delta L_{i,k})\cos((\frac{2\pi}{\lambda})\delta L_{i,k})$$

$$+ I_i C(\delta L_{i,k} + \Delta L)[\cos(\frac{2\pi}{\lambda}\delta L_{i,k})\cos(\frac{2\pi}{\lambda}\Delta L) - \sin(\frac{2\pi}{\lambda}\delta L_{i,k})\sin(\frac{2\pi}{\lambda}\Delta L)]\}\}$$

(3.12)

Assuming that:

1) The optical power in nonadjacent mode I_i are statistically independent from each other and the variances of the optical power transmitted in each mode, $D(I_i)$, are equal to each other.

2) The mode cross coupling most commonly occurs between the adjacent modes [14] and only consider the contribution of the factors $\cos((\frac{2\pi}{\lambda})\delta L_{i,i+1})$ and $\cos((\frac{2\pi}{\lambda})\delta L_{i+1,i})$, which is the results of the interference between the adjacent modes, ignore the contribution of the other factors that are not generated between adjacent modes. The reason for this is that the OPD between the adjacent modes is shorter than the OPD between any other pair of modes and so they are the largest factors that contribute to the variance. The theoretical analysis is considerably simplified by this assumption.

3) The fluctuation generated by each pair of the adjacent modes are independent from each other and the variance contributed by them are equal to each other.

4)   The   values   of $E\{\sum_{i\neq k}^{M} I_i C(\delta L_{i,k}) \cos[\frac{2\pi}{\lambda}\delta L_{i,k}]\}$ and

$E\{\sum_{i\neq k}^{M} I_i C(\delta L_{i,k} + \Delta L)\cos[\frac{2\pi}{\lambda}(\delta L_{i,k} + \Delta L)]\}$ are equal to zero. The reason is that the

values of the factors $\cos[\frac{2\pi}{\lambda}\delta L_{i,k}]$ and $\cos[\frac{2\pi}{\lambda}(\delta L_{i,k} + \Delta L)]$ are randomly distributed

in the range [-1, 1] when the value $\delta L_{i,k}$ fluctuate under the condition that the fibre is perturbed.

5) Consider the case that the fluctuation of the value $\delta L_{i,i+1}$ is larger than the wavelength and smaller than the coherence length and so the fluctuation of the factors, I_i and $C(\delta L_{i,i+1})$, is much smaller than that of the factor $\cos[(2\pi/\lambda)\delta L_{i,i+1}]$.

The variance of the output can then be approximately expressed as

$$D(I) \approx M[1 + C(\Delta L)\cos(2\pi\Delta L/\lambda)]^2 \xi$$
$$+ (M-1)I_i^2 \{[2C(\delta L_{i,i+1}) + C(\delta L_{i,i+1} + \Delta L)\cos(\frac{2\pi}{\lambda}\Delta L)$$
$$+ C(\delta L_{i+1,i} + \Delta L)\cos(\frac{2\pi}{\lambda}\Delta L)]^2 D[\cos(\frac{2\pi}{\lambda}\delta L_{i,i+1})]$$
$$+ [C(\delta L_{i,i+1} + \Delta L) - C(\delta L_{i+1,i} + \Delta L)]^2 \sin^2(\frac{2\pi}{\lambda}\Delta L)D[\sin(\frac{2\pi}{\lambda}\delta L_{i,i+1})]\}$$

$$= M[1 + C(\Delta L)\cos(\frac{2\pi\Delta L}{\lambda})]^2 \xi$$

$$+ \frac{(M-1)}{2} I_i^2 \{[2C(\delta L_{i,i+1}) + C(\delta L_{i,i+1} + \Delta L)\cos(\frac{2\pi}{\lambda}\Delta L) + C(\delta L_{i,i+1} - \Delta L)\cos(\frac{2\pi}{\lambda}\Delta L)]^2$$

$$+ [C(\delta L_{i,i+1} + \Delta L) - C(\delta L_{i,i+1} - \Delta L)]^2 \sin^2(\frac{2\pi}{\lambda}\Delta L)\}$$

$$= M[1 + C(\Delta L)\cos(\frac{2\pi\Delta L}{\lambda})]^2 \xi + (M-1)I_i^2 \{\chi_1\}$$

(3.13a)

where

$$\delta L_{i+1,i} = -\delta L_{i,i+1}$$

(3.13b)

and

$$\xi = D(I_i) + \sum_i [E(I_i I_{i+1}) + E(I_{i-1}I_i)] - \sum_i [E(I_i)E(I_{i+1}) + E(I_{i-1})E(I_i)]$$

(3.13c)

and

$$\chi_1 = \frac{1}{2}\{2C(\delta L_{i,i+1}) + C(\delta L_{i,i+1} + \Delta L)\cos(\frac{2\pi}{\lambda}\Delta L) + C(\delta L_{i+1,i} - \Delta L)\cos(\frac{2\pi}{\lambda}\Delta L)\}^2$$

$$+ \frac{1}{2}\{[C(\delta L_{i,i+1} + \Delta L) - C(\delta L_{i,i+1} - \Delta L)]^2 \sin^2(\frac{2\pi}{\lambda}\Delta L)\}$$

(3.13d)

The rms value of the modal noise, N_1, in the system can then be expressed as

$$N_1 = \sqrt{D(I)} = \sqrt{M[1 + C(\Delta L)\cos(\frac{2\pi\Delta L}{\lambda})]^2 \xi + (M-1)I_i^2 \{\chi_1\}}$$

(3.13e)

From Eq.(3.13e), the modal noise in such a system depends on the OPD of the interferometer, the coherence length of the illuminating source, and the characteristics of the multimode fibre. By substituting Eq.(3.11a) and Eq.(3.13a) into Eq.(3.9), the SNR of the system can be expressed as

$$S \, / \, N_1 = \frac{M(1+\cos(2\pi\Delta L \, / \, \lambda))E(I_i)}{\sqrt{M[1+(C(\Delta L))\cos(2\pi\Delta L \, / \, \lambda)]^2 \xi + (M-1)I_i^2 \chi_1}} \qquad (3.14)$$

Usually, the number of modes, M, is much larger than one, Therefore, Eq.(3.14) can be simplified to

$$S \, / \, N_1 = \frac{\sqrt{M}(1+C(\Delta L)\cos(2\pi\Delta L \, / \, \lambda))E(I_i)}{\sqrt{[1+(C(\Delta L))\cos(2\pi\Delta L \, / \, \lambda)]^2 \xi + I_i^2 \chi_1}} \qquad (3.15)$$

From Eq.(3.15), the following theoretical result can be obtained:

A) *The signal to noise ratio of the output of the system increases when the coherence length of the source decreases.* When the fibre is perturbed, the OPD between the adjacent modes, $\delta L_{i,k}$, will change randomly due to the cross-coupling between the modes and the value of the term, $C(\delta L_{i,i+1})$, will decrease as the coherence length of the source decreases. Therefore, the value of the fact, χ_1, will decrease as the coherence length of the source decreases, resulting in an increase of the SNR in the output of the system. This theoretical conclusion will be verified by experiment, which will be discussed in sections 3.3 and 3.4.

B) *The signal to noise ratio of the output of the system increases when the fibre length increases.* The value of the OPDs between the adjacent modes at the far end of the

fibre, $\delta L_{i,i+1}$, increases as the length of the fibre increases so that the value of the term, $C(\delta L_{i,i+1})$, decreases as the value, $\delta L_{i,i+1}$, increases. Therefore, the value of the fact, χ_1, will decrease as the fibre length increases, resulting in the SNR increase in the output of the system. This theoretical conclusion will be verified by the experiment in the work reported in section 3.4.

C) *The signal to noise ratio of the output of the system is proportional to the square root of the number of modes transmitted in the fibre*. This can be easily seen from Eq.(3.15). Usually, a larger core diameter fibre have more modes allowed to transmit in the fibre, resulting in a higher SRN in the output of the system. An experimental investigation will be given in section 3.5 to verify this theoretical conclusion. However, if the core diameter of the fibre becomes too large, the output beam from the fibre will be difficult to collimate.

D) *Step index fibres are better as the linking fibre for a WLI system than graded index fibres*. This conclusion can be explained by the following two reasons:
1) Step index fibres have a much larger OPD between adjacent modes than that of graded index fibres (see section 2.4). This is similar to the situation discussed in (B). A higher output signal to noise ratio will be obtained when a step index fibre is used as a linking fibre in the case when the number of modes in step index fibre and the graded index fibre are about the same.

2) The number of modes in a step index fibre is twice that of a graded index fibre, when they have same core diameter and same refractive index difference [2], and from result (C) discussed above, the output signal to noise ratio of a WLI system with a step index linking fibre will be higher than that with a graded index linking fibre.

41

3.3 Comparison between modal noise in a system illuminated with a He-Ne laser and a system with a multimode laser diode

3.3.1 Experimental arrangement

Figure (3.1) shows the experimental arrangement used to study the effect of the modal noise induced by the lead fibre [10, 11]. Light from a high-coherence light source (a He-Ne laser) or a low-coherence light source (a multimode laser diode) was injected into a multimode fibre (50/125-OF0850, with a length of 2.2km) by means of a 10× objective lens. The light from the output end of the fibre was then collimated and launched into a Michelson interferometer. The interference optical output from the interferometer was converted into an electrical signal with an avalanche photodiode (APD) and analyzed with a spectrum analyzer. The OPD in the interferometer was modulated by the vibration of the mirror attached to a piezoelectric transducer (PZT). The frequency of the vibration was randomly chosen at 245Hz, and the amplitude of the vibration was adjusted so that only one interference fringe is generated by the vibration. Hence the rms value (in decibels) of the electrical output at 245Hz can be measured as the signal magnitude, and that at 80Hz can be obtained as the noise magnitude. Therefore, values of the SNR obtained under different experimental conditions can be studied and compared.

3.3.2 Experimental Results

In the first experimental investigation of modal noise in the system shown in Fig.(3.1), a He-Ne laser was used as a long-coherence-length light source. First, when there was no perturbation of the fibre, the values of the output signal and the noise from the APD were averaged 20 times; an average output S/N ratio of 51.0dB was obtained.

42

Fig.(3.2 (a)) shows one of the spectra taken in this case. Following that, a similar output signal was averaged over the same period when the fibre was shaken by hand. It was found possible to achieve consistent and repeatable results through the use of this technique. The average output SNR measured in this case was reduced to 30.1dB, resulting in a SNR reduction of 20.9dB caused by the perturbation of the fibre. Fig.(3.2 (b)) shows one of the spectra recorded in second case.
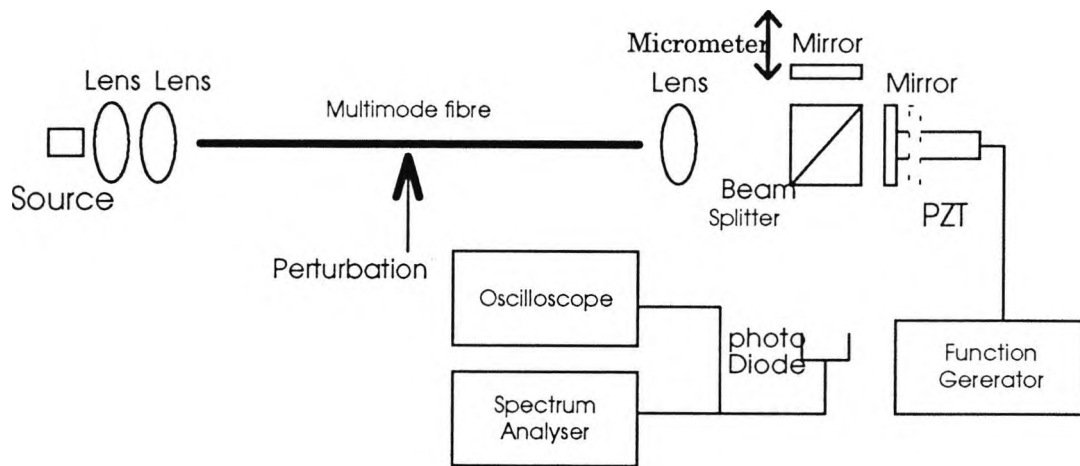
Fig.(3.1) Schematic interferometric system used for study of modal noise induced by the lead fibre.
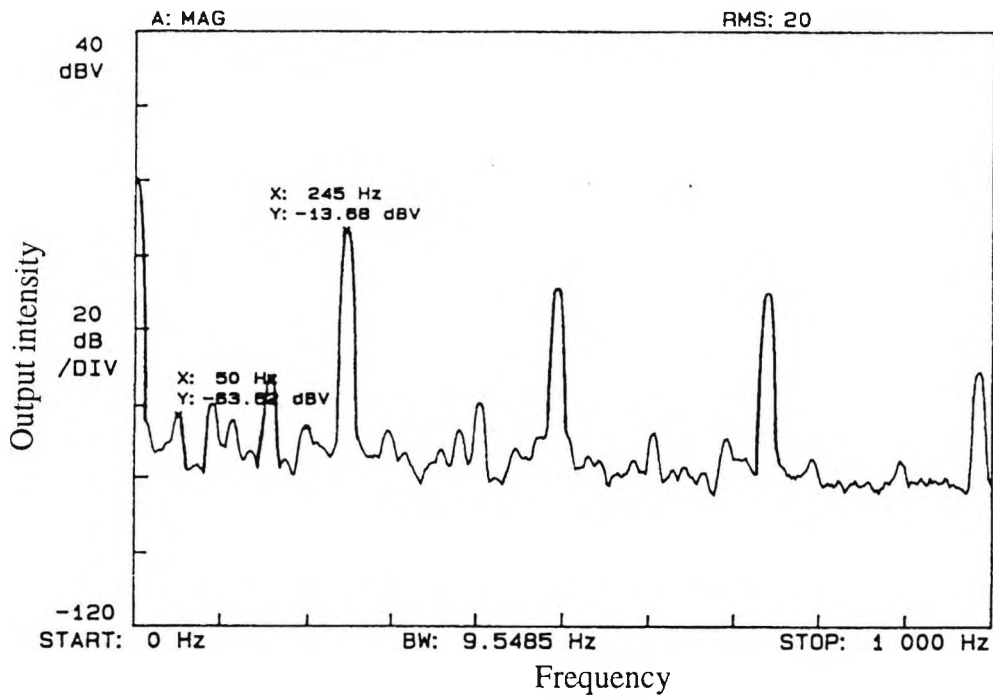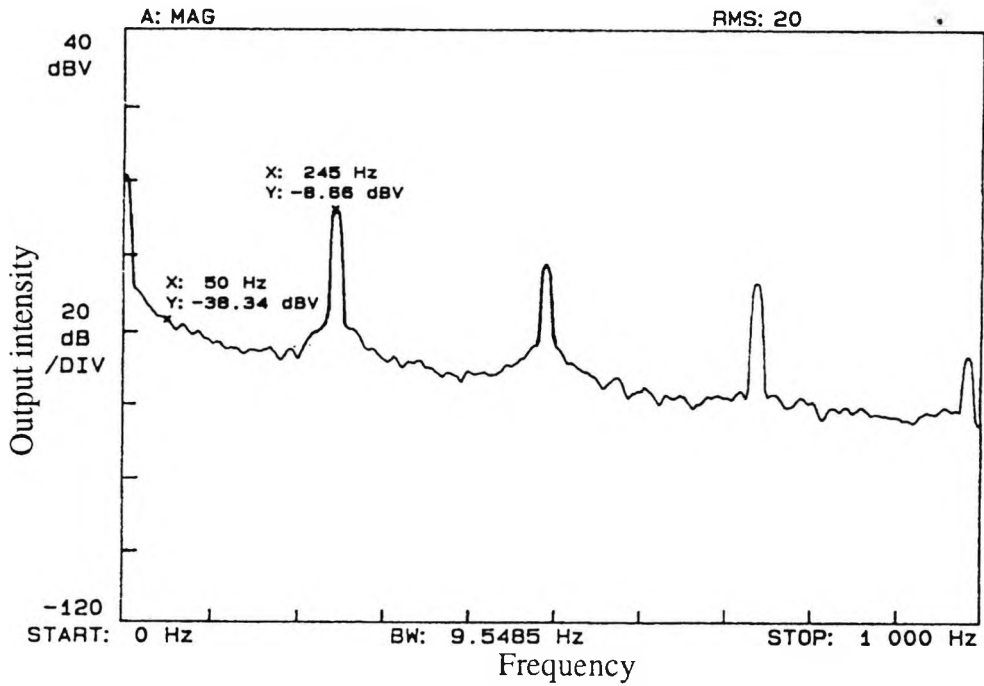
Fig.(3.2) Spectra of the output signal from the arrangement shown in Fig.(3.1) when a He-Ne laser is used as the source: (a) without perturbation on the fibre, (b) with perturbation on the fibre. BW, bandwidth.
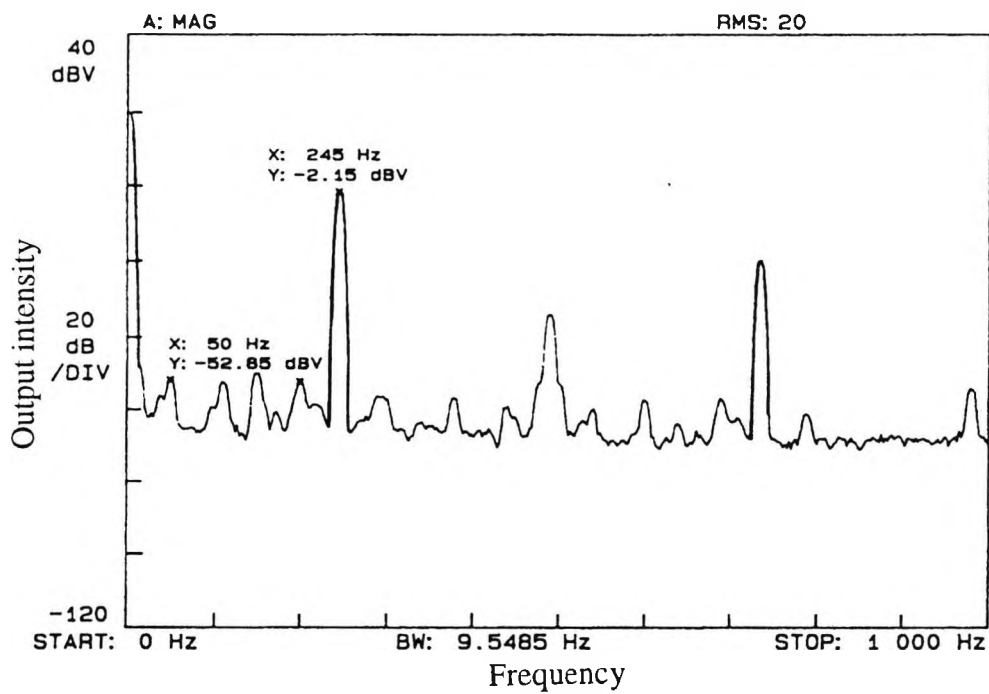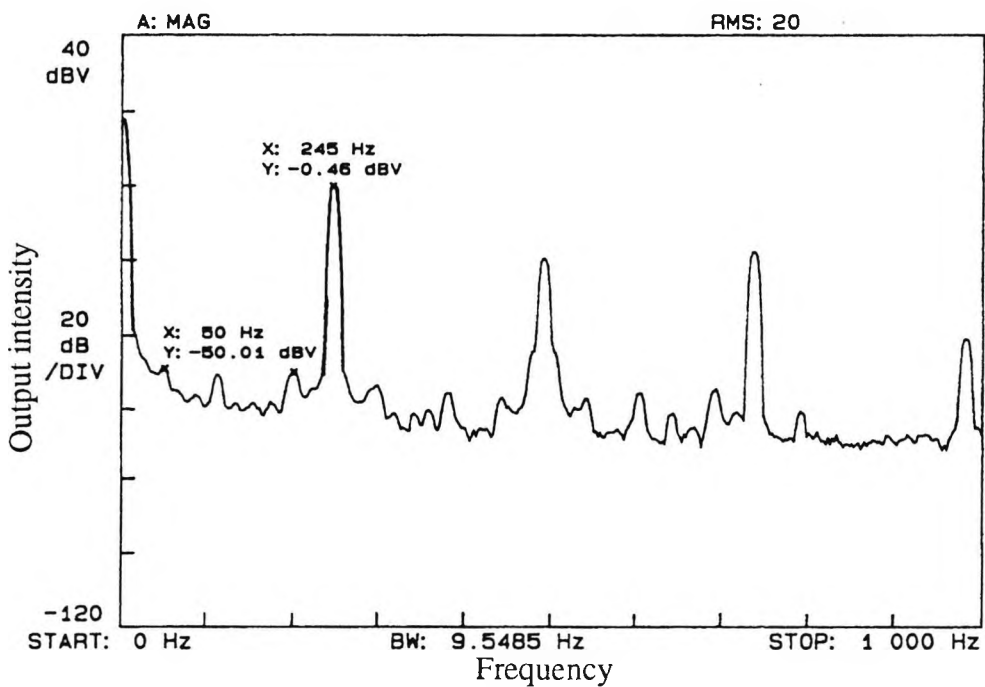
Fig.(3.3) Spectra of the output signal from the arrangement shown in Fig.(3.1) when a multimode laser diode is used as the source: (a)without shaking on the fibre, (b)with shaking on the fibre, BW: bandwidth.

In contrast, when a multimode laser diode was used to replace the He-Ne laser in the same arrangement, as shown in Fig.(3.1), average output SNRs of 52.0dB and 50.3dB were obtained for the cases without and with the perturbation of the fibre, respectively, resulting in only a 1.8dB SNR reduction when the fibre was perturbed. Typical recorded spectra for each situation are shown in Figs.(3.3 (a)) and (3.3 (b)). Comparing Figs.(3.2) and (3.3), it can be seen that the effect of the modal noise in the output of the system can be considerably suppressed as a result of a reduction of the coherence length of the light source employed. The measured results are summarised in Table (3.1), where the effect of the coherence length on modal noise is clearly shown.

Table (3.1). Summary of Experimental Results From the Experimental Arrangement Shown in Fig.(3.1)

	Average SNR Output (dB)		
Light Souce	Without Perturbation	With Perturbation	Average ΔS/N Ratio(dB)
He-Ne laser	51.0	30.1	20.9
Multimode laser diode	52.0	50.2	1.8

From the experimental results obtained, it can clearly be seen that, if an interferormeter is illuminated with a light source with a long coherence length by means of multimode fibres, the interferometric system becomes sensitive to environmental perturbations such as vibration and temperature variations, which may cause an intermodal cross-coupling effect. If, in contrast, the light source used is of low coherence then the modal noise induced by the fibre can be suppressed, provided that the OPD between the two

adjacent modes in the fibre is larger than the coherence length of the light source [14]. This is agreement with the theoretical conclusion obtained from Eq.(3.15).

3.4 Dependence of the modal noise on the length of the lead fibre

An experimental arrangement similar to that shown in Fig.(3.1) was used to investigate the dependence of the modal noise on the length of the fibre and the coherence length of the source [12]. The light from a single mode laser diode source (Sharp, LT022MCO) is injected into a Graded-index multimode fibre (50/125-OF0850) with lengths of 2, 20, 50 meters respectively, via a 10x objective lens. The fibres are wrapped on a separated portion of the cylinder roll (with a diameter of 170cm) in such a manner that only five turns are perturbed by shaking them (by hand) and thus in all cases the perturbation was approximately the same, regardless of the length of the fibre concerned.

The OPD between the two arms in the Michelson interferometer were set to a value, as close to zero as possible, and hence the effect of the modal noise on the peak intensity of the central interference fringe could be examined. In this case, the values of the OPD induced by the fibre mode delay were much larger than those of the OPD induced by the interferometer, and the noise levels detected at different values of coherence length were mainly caused by the modal noise. In order to measure and compare the reduction of the SNR due to the presence of modal noise, the spectral amplitude at 40 Hz was used as the reference noise level, and the corresponding SNR was determined to be about 60 dB for the unperturbed fibre. The noise amplitudes at the several other selected frequencies discussed (130, 270, 580, and 840 Hz) were also recorded, and an average SNR at a particular diode current could be obtained from the experimental data. When there was no perturbation of the fibre and the diode current was set to

47

40mA, the spectrum of the output signal was averaged 20 times and recorded, giving an average SNR without perturbation. Then the spectrum of the output signal was averaged over the same period whilst the fibre was shaken by hand and an average SNR with perturbation was obtained. It was found possible to achieve consistent and repeatable results using this technique.

The reduction of the SNR due to the perturbation, for each of the noise frequencies, was obtained by comparing the SNRs measured for both the unperturbed and perturbed cases, and then the values of the average SNR reductions for the laser diode currents from 40 mA to 60 mA, in steps of 5 mA, were measured. Similar measurements were taken for fibre lengths of 2, 20 and 50 meters respectively, and the results are shown in Fig.(3.4). The experimental results indicate that as the values of the laser diode current became larger (and hence the coherence length is increased), the modal coupling induced noise increases, resulting in a greater reduction in the value of the SNR of the output. Table (3.2) shows the coherence length of the laser diode against its driving current.

Table (3.2) Coherence length of the laser diode against its drive current

Current (mA)	40.0	45.0	50.0	52.0	54.0	56.0	58.0	60.0	62.0
Coherence Length (mm)	33	35	40	43	45	50	70	200	500

From the experimentally obtained results, which is shown in Fig.(3.4), the same trend in terms of the coherence length, which is determined by the drive current of the laser diode, and the modal-noise-induced SNR reductions can be observed. From Fig.(3.4),

48

it can be seen that for a given fibre length (less than a few thousand centimetres), the level of the modal-noise-induced SNR reduction increases as the coherence length increases, and these results match those discussed in last section.
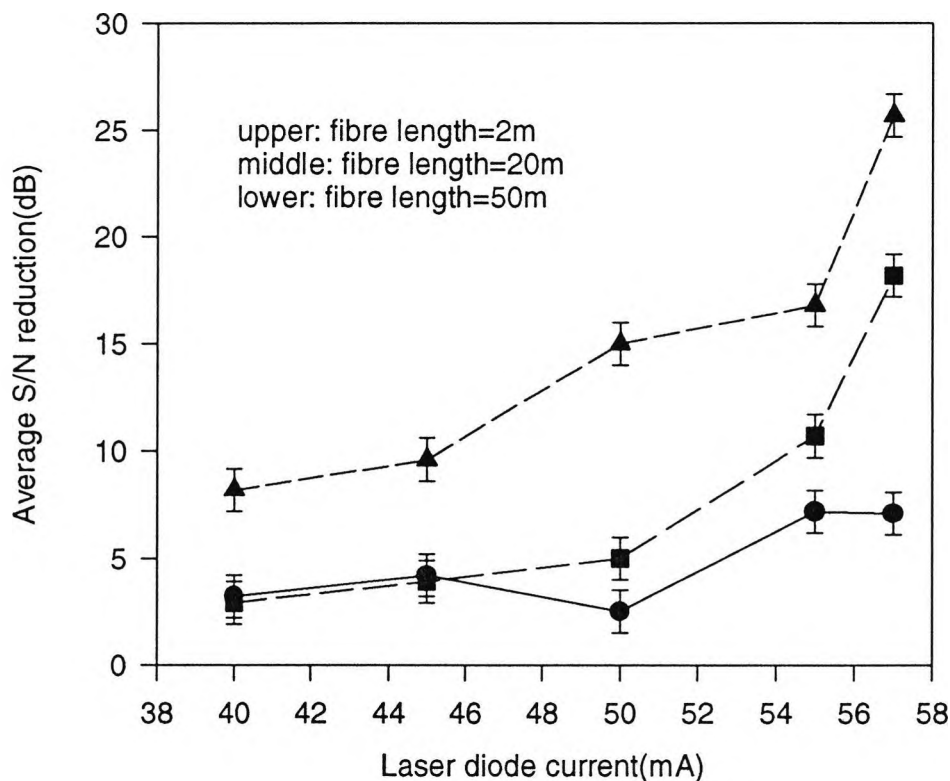

Fig.(3.4) Variation of the average S/N ratio reductions as a function of the diode currents for the different lengths of the fibre.

It can also be seen that, for a light source with a particular value of coherence length, the value of the average SNR reduction reduces as the length of fibre increases. For instance, for a diode with a coherence length of 60μm (corresponding to a drive current of 55 mA), the average SNR reduction is about 16 dB for a fibre of 2 meters in length, 11 dB for 20 meters and 7 dB for 50 meters. This is mainly due to the fact that as the fibre lengths increase, the OPDs between each pair of modes will increase. When these

49

OPDs become larger than the coherence length of the source, the corresponding modes will become incoherent with each other, the modal noise reaches its lowest level. This result also agrees with that expected from the theoretical analysis, as shown in Eq.(3.15).

In conclusion, this section has shown that there is a particular relationship between the modal noise induced and the length of the lead fibre employed. In order to suppress the modal noise in a white light interferometric sensor system, the length of the fibre selected has to be long enough so that the values of the OPDs (between a pair of modes within every modal group) are larger than the coherence length of the light source. Generally speaking, the shorter the coherence length chosen and the longer the fibre used, the lower the modal noise induced and thus the lower the reduction of the system SNR that is to be expected.

3.5 Dependence of modal noise in the system on the characteristics of the multimode lead fibre

An experimental arrangement similar to that shown in Fig.(3.1) is used to investigate the effect of modal noise induced by the lead fibre [13]. Light from a multimode laser diode (LT023MD) was injected into a multimode fibre, 5 meters in length, via an objective lens. The output light from the fibre was then collimated and launched into a Michelson interferometer which was adjusted to the "balanced position". The recombined output beam from the interferometer was focused by a lens and detected by a photodiode (with a receiving area of 41.3 mm^2), where its output was amplified and then analyzed with a spectrum analyzer. One of the mirrors in the interferometer was modulated at a frequency which was chosen to be 130 Hz, and the amplitude of the modulation was equal to half of the central wavelength of the illuminating source used,

50

so that only one interference fringe around the central fringe position was generated in the output signal of the interferometer. Part of the fibre (about 90 cm in length) was vibrated using an arrangement comprising an oval wheel driven by a motor at a frequency of about 3 Hz, inducing modal noise at the output. The root mean square (rms) value of the output, which was averaged 20 times, at the modulated frequency (130 Hz) is used as the "signal" and the output at 210 Hz is recorded as the average noise level. The above two frequencies were chosen to avoid 50Hz and its harmonics and the natural frequency of the interferometer.

In the experiment, the conditions of the experimental arrangement were kept unchanged while the different types of fibre were tested respectively, and therefore, the SNR of the system linked with the different fibres could be studied and compared. Four types of fibres (all of about 5 meters in length) with core diameters of 50μm (parabolic index), 100μm (step index), 200μm (step index), and 320μm (step index), were investigated.

Fig.(3.5) shows the results obtained experimentally. The mode number, M, was determined using the theoretical approach described by Snyder and Love [16], which can be expressed as

$$N = \frac{q}{q+2} k_0^2 a^2 n^2 \Delta \qquad (3.16)$$

where a represents the radius of the core, Δ is the grading parameter, n represents the axial refractive index, q represents the exponent of the power law profile. $q=2$ corresponds to a parabolic index profile and $q=\infty$ corresponds to a step index profile. k_0 is the wave number of the optical beam in the system. It should be pointed out that

the number of modes in the practical system may be smaller than that calculated from Eq.(3.16) because some modes may not fill in the practical system.
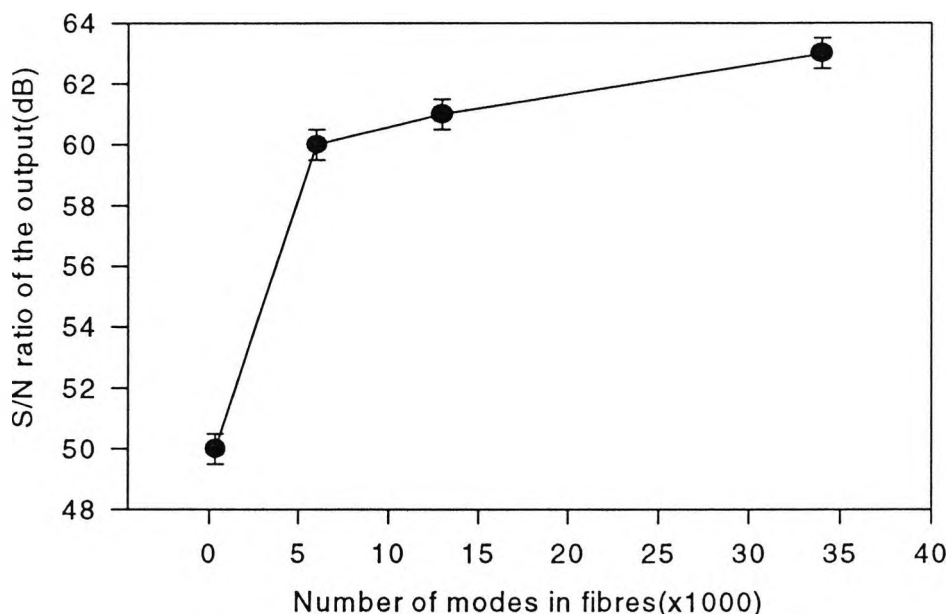

Fig.(3.5) Output S/N ratio of the system shown in Fig.(3.1) against the number of modes in the lead fibre when the fibre was shaken

The round dots in Fig.(3.5) represent the SNR obtained when these four types of fibres were used as the lead fibre. The error bar in Fig.(3.5) was estimated by repeating the measurement three times. From Fig.(3.5), it can be seen that the results from the experiment show a similar trend, as described by Eq.(3.15), i.e. as the core diameter of the fibre increases, allowing for a consequent increase in the mode number of the fibre, the S/N of the system is also seen to increase. It should be noted that the 50μm core diameter fibre used in the experiment is a parabolic index fibre, which has a much smaller OPD between its adjacent modes than that of the step index fibre [17] (see Section 2.4). This may be the reason that the signal to noise ratio of the system with 50 μm core diameter linking fibre is much lower than that of the system with other types

of linking fibre (see Eq.(3.15)). The experiment has been repeated several times. and the same trend was obtained each time.
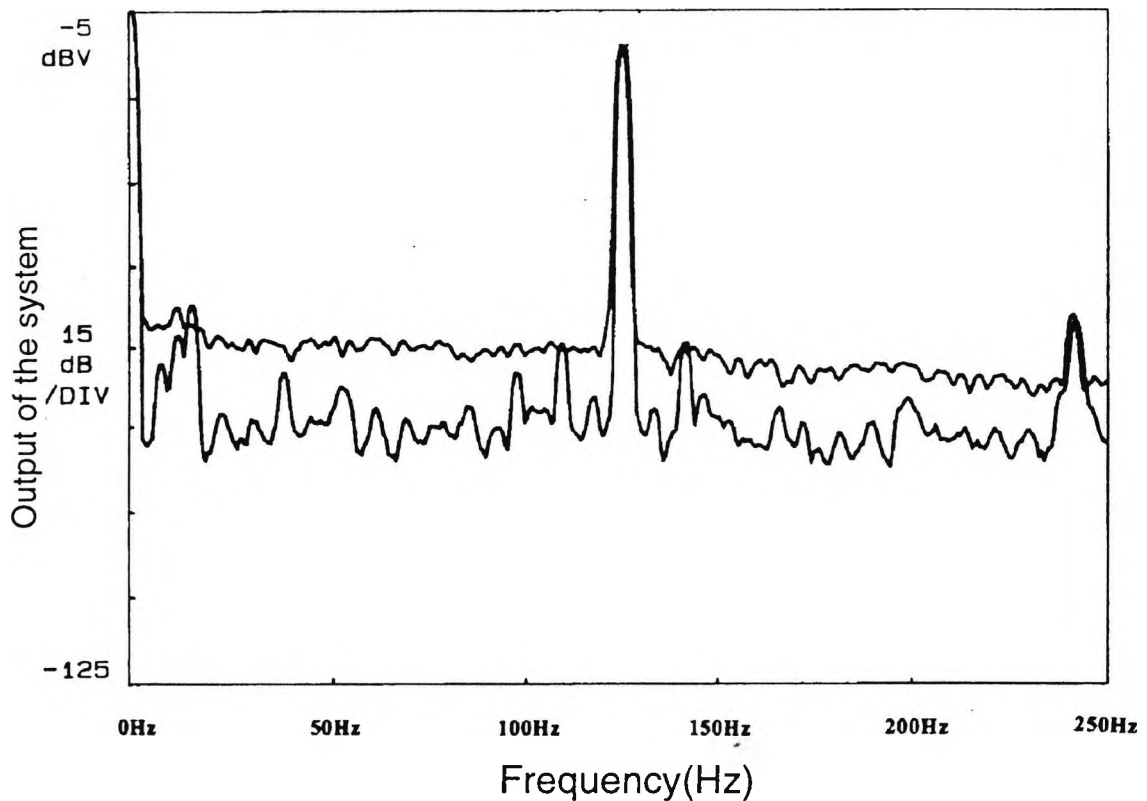

Fig.(3.6) Output spectrum of the system shown in Fig.(3.1). The upper curve was obtained with a 50μm core diameter fibre (parabolic index). The lower curve was obtained with a 320μm core diameter fibre (step index).

Fig.(3.6) shows a spectrum of the output obtained with a 50μm core diameter fibre (parabolic index, upper curve) and 320μm core diameter fibre (step index, lower curve) as the lead fibre, respectively. In the experiment, the output intensity from the fibre was held constant by using an optical filter when the lead fibre was replaced and the drive current of the laser diode maintained at a constant value in the experiment so that the coherence length of the source remained constant. From Fig.(3.6), it can be seen that the SNR of the system obtained with 320μm core diameter fibre (step index) is higher

than that with 50μm core diameter fibre (parabolic index). This can be explained by the fact that (1) the mode number in the 50μm linking fibre is smaller than that of the 300μm and (2) the OPD between adjacent modes in the parabolic index fibre is much shorter than that of the step index fibre [17] (see Eq.(3.15)). The graph shows some small peaks on the lower curve which are due to "pick-up" in the electrical signal processing system.

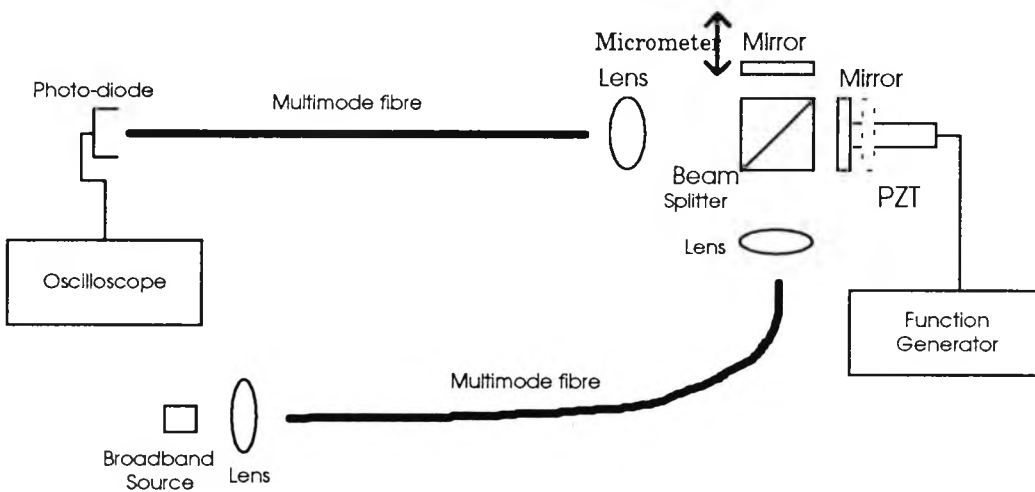## 3.6 Visibility reduction Caused by the misalignment of the interferometer

Fig.(3.7). Experimental arrangement to investigate the effect of the output fringe visibility reduction caused by the misalignment of the mirrors in the interferometer.

The theoretical output of a WLI system shown in Eq.(2.6) was obtained under the condition that the interferometers are perfectly aligned. In a practical system, misalignment may occur. For the system shown in Fig.(3.7), situation may occur where one of the mirrors is tilted with an angle θ, and the area of the spot size is A. The output of the interferometer then may be expressed as

54

$$I_s = \int (\frac{I_0}{2})(1 + \exp(-(\frac{2x}{L_c})^2)\cos(\frac{2\pi x}{\lambda}))(\frac{dA}{A}) \qquad (3.17)$$

where x is the OPD of the interferometer, λ is the central wavelength of the source, L_C is the coherence length of the source and I_0 is the total output intensity of the system. The integration covers the whole area of the light spot. To simplify the analysis, a square light spot with a side length e and a mirror rotation of angle θ around an symmetrical axis of the square, which is parallel to one of the sides of the square, may be assumed. Then Eq.(3.17) can be rewritten as

$$
\begin{aligned}
I_s &= (\frac{I_0}{2})[1 + \exp(-(\frac{2x_0}{L_c})^2) \int_{-e/2}^{e/2} \cos(\frac{2\pi (x_0 + y\theta)}{\lambda}) \frac{dy}{e}] \\
&= (\frac{I_0}{2})\{1 + \exp(-(\frac{2x_0}{L_c})^2) \frac{\lambda}{2\pi\theta e} [\sin(\frac{2\pi (x_0 + y\theta)}{\lambda})]_{-e/2}^{e/2}\}
\end{aligned}
\qquad (3.18)
$$

$$I_s = (\frac{I_0}{2})(1 + \exp(-(\frac{2x_0}{L_c})^2)(\frac{\sin(\frac{2\pi\theta e}{\lambda})}{\frac{2\pi\theta e}{\lambda}})\cos(\frac{2\pi x_0}{\lambda})) \qquad (3.19)$$

When the misalignment angle θ is equal to $\lambda/2e$, the term $|\frac{\sin(2\pi\theta e/\lambda)}{2\pi\theta e/\lambda}|$, which represent the visibility of the output from the system, is equal to zero. Therefore, the output fringe visibility of the system is equal to zero. If the dimension of the light spot is about 1mm and the central wavelength of the illuminating source is $0.78\mu m$, the angle at which the output fringe visibility is zero is equal to 3.9×10^{-4} rad.

An experiment has been carried out to investigate the effect on the visibility reduction caused by the misalignment of the interferometer. The light beam from a multimode

laser diode is coupled into a multimode fibre, after which, the output from the multimode fibre is collimated and launched into a Michelson interferometer. The output of the interferometer is coupled into another multimode fibre, and finally, the output of the system measured from the far end of the fibre is detected by a photodiode. The multimode fibres in the system are about 5m in length. One of the mirrors in the interferometer is specially installed so that the misalignment angle of the mirror can be measured. The resolution of the angle measurement is about 2×10^{-4} rad.

The experimental results obtained are shown in Fig.(3.8), Fig.(3.9) and Fig.(3.10). Fig.(3.8) shows that the output fringe visibility of the system decreases as the misalignment angle increases. The visibility reaches a minimum value when the misalignment angle is equal to about 5×10^{-4} rad for three different fibres, which is very close to the theoretical value discussed above. The diameter of the spot of the light beams in the interferometer, in which the measurements were made, are about 1mm.

Fig.(3.9) and Fig.(3.10) show the output fringe visibility and output DC intensity of the system when 50μm core diameter fibre (parabolic index) and 320μm core diameter fibre (step index) are used respectively. The figures show that the output DC intensity of the system changes very slowly as the misalignment angle increases. This means that the output fringe visibility of the system is very sensitive to the misalignment angle, whereas the output DC intensity of the system is insensitive to the misalignment angle.
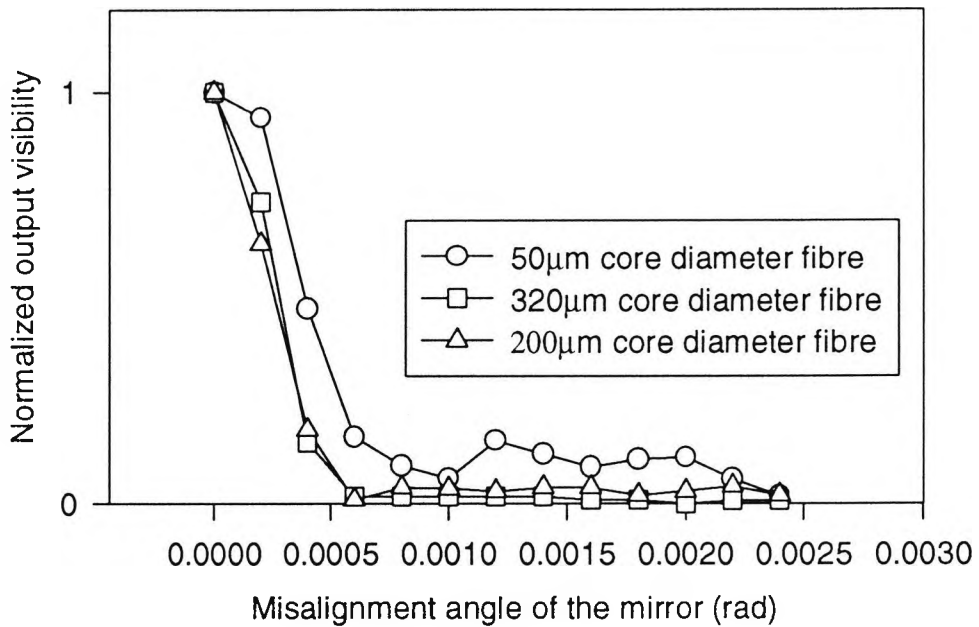
Fig.(3.8) Output visibility of the interferometer against the misalignment angle of the mirror
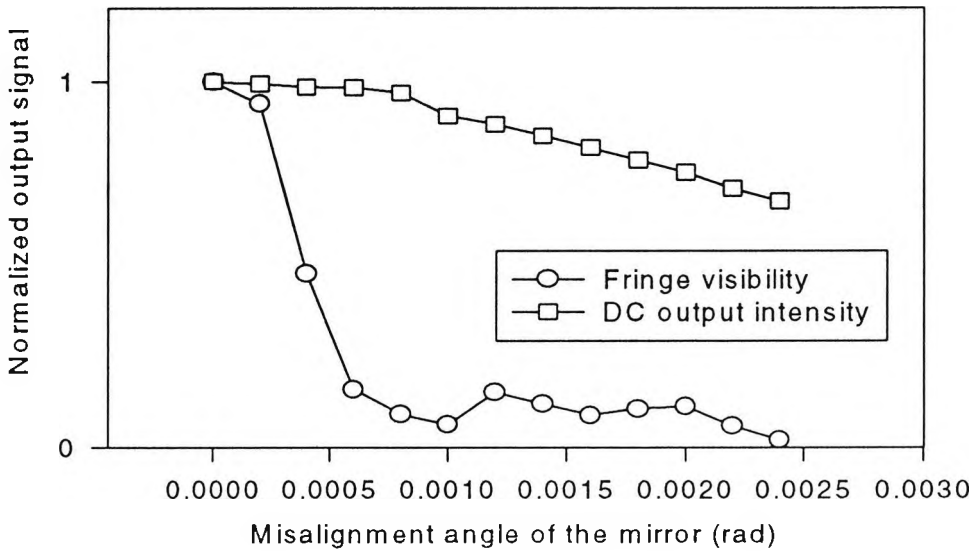

Fig.(3.9) Normalized output signal of the interferometer against the misalignment angle of the mirror when graded index linking fibre of 50mm core diameter is used
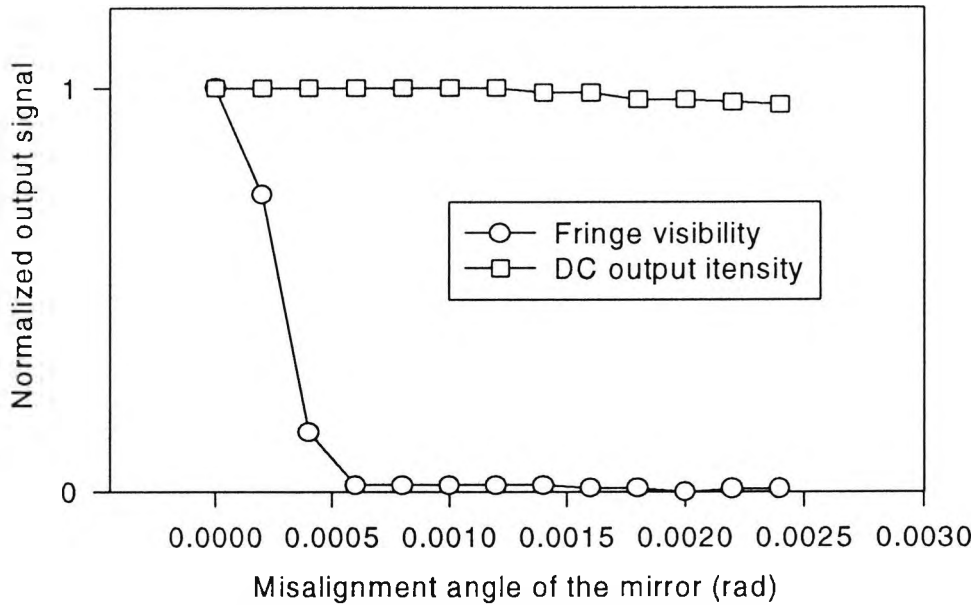
Fig.(4.10) Normalized output signal of the interferometer against the misalignment angle of the mirror when step index fibre of 320mm core diameter is used

3.7 Discussion

A theoretical analysis is given to estimate the SNR of the output of a multimode fibre linked WLI system, and the final equation for this analysis derived is given as Eq.(3.15). From Eq.(3.15), the following theoretical results can be obtained, under the condition that the lead fibre is perturbed:

1) The SNR of the output in such a system increases as the coherence length of the illuminating source decreases.

2) The SNR of the output in such a system increases as the length of the linking fibre increases.

3) The SNR of the output of the system is proportional to the square root of the mode number transmitted in the fibre. Hence, by using a larger core diameter linking fibre in such a system, a higher SNR can be obtained.

4) Step index fibres are better suited as a linking fibre, for a WLI system than parabolic index fibres, because step index fibres have a much larger OPD between adjacent modes.

In summary, in the experiments which have been carried out to investigate modal noise in a WLI system, the relation between modal noise and coherence length of the illuminating source has been studied (Section 3.3). It has been shown that the output signal to noise ratio of the system increases as the coherence length of the illuminating source decreases. This is in agreement with the first theoretical result from Eq.(3.15). In section 3.4, the modal noise effect on the length of the linking fibre is investigated. It is shown that the output signal to noise ratio of the system increases as the length of the linking fibre increases, which is in agreement with the second theoretical result from Eq.(3.15). In section 3.5, modal noise in a WLI system with different types of linking fibre has been investigated. It has been confirmed that 1) thick linking fibre induces less modal noise because it supports the propagation of more modes than thin fibre and 2) step index fibre induces less modal noise than parabolic index fibre because the OPD between the adjacent modes in step index fibre is much larger than that in parabolic index fibre. The experimental results obtained in section 3.5 are in agreement with the third and fourth theoretical results obtained from Eq.(3.15).

It should be clarified that the experimental investigation discussed in sections 3.3 and 3.4 are carried out by Dr. Y. N. Ning.

In summary, a series of results on a multimode linked white light interferometric system has been obtained and described, in agreement with the theoretical analysis. Next Chapter, techniques to enhance the relative visibility of the central fringe in a WLI system, with a synthetic source, will be discussed.

References

[1]. D. A. Jackson, "Monomode Fibre Optic Interferometers and Their Application in Sensing Systems," Opt. Fibre Sensors, Vol.132, pp1-33, 1987.

[2]. S. Chen, A. W. Palmer, K. T. V. Grattan, and B. T. Meggitt, "Extrinsic Optical-fibre Interferometric Sensor That Uses Multi-mode Optical Fibres: System and Sensing Head Design for Low-noise Operation," Opt. Lett., Vol.17, pp701-703, 1992.

[3]. D. Trouchert, F. X. Desforges, P. Graindorge, and H. C. Lefevre, "Remote Fibre Optic Measurement of Air Index with White Light Interferometry," presented at the Eighth Optical Fibre Sensors Conference, Montery, USA, January 1992.

[4]. W. V. Sorin, "Low-coherence Reflectometry For High Accuracy Sensing," presented at the Ninth Optical Fibre Sensors Conference, Florence, Italy, September 1993.

[5]. E. G. Rawason, J. W. Goodman, and R. E. Norton, "Experimental and Analytical Study of Modal Noise in Optical Fibres," IEE Conf., Publ. London, Vol.190, pp72-73, 1980.

[6]. J. V. Wright and B. P. Nelson, "Bandwidth Studies of Jointed Multimode Fibres," presented at the Seventh European Conference on Optical Communication, Copenhagen, Denmark, July 1981.

[7]. R. E. Epworth, "The Phenomena of Mode Noise in Analogue and Digital Optical Fibre Systems," presented at the Fourth European Conference on Optical Communication, Genoa, Italy, September 1978.

[8]. A. R. Mickelson and A. Weierholt, "Modal Noise-limited Signal-to-Noise Ratios in Multimode Optical Fibres," Appl. Opt., Vol.22, pp3084-3089,1983.

[9]. B. Daino, G. DE Marchis, S. Piazzolla, "Analysis and Measurement of Modal Noise in An Optical Fibre". Electronics Letters, Vol.15(23), pp755-756, 1979.

[10]. Y. N. Ning, K. T. V. Grattan, A. W. Palmer, and K. Weir, "Measurement of Up and Down-Lead Fibre Sensitivity Caused by Lead in Multimode Fibre in an Interferometric system", Applied Optics, Vol.33(31), pp7529-35.

[11]. Y. N. Ning, Y. Liu, K. T. V. Grattan, A. W. Palmer, and K. Weir, "The Relation Between the Coherence Length and Modal Noise in A Graded-index Multimode Fibre for White Light Interferometer System" Opt. Lett., Vol.19, pp372-374.

[12]. Y. N. Ning, Y. Liu, B. M. A. Rahman, K. T. V. Grattan, and A. W. Palmer "Conditions for Suppressing Modal Noise Induced in A White Light Interferometer" Proceeding of Tenth Conf. on Optical Fibre Sensors, pp576-579, (Glasgow, 1994)

[13]. Qi Wang, Y. N. Ning, K. T. V. Grattan, A. W. Palmer, "Effect of multimode Fibre Core Diameter on Modal Noise Suppression in White-light Interferometry". Optical Communications, Vol.118, pp473-478, 1995

[14]. H. Olesen, "Dependence of Modal Noise on Source Coherence and Fibre Length," in Progress in Optical Communication, P. J. B.Clarricoats, Ed. (Institution of Electrical Engineers, London,1980),Vol. 2, reprint series p4.

[15]. R. Olshansky, "Mode Coupling Effects in Graded-Index Optical Fibers" Appl. Optics, Vol.14, No.4, pp935-945, 1975.

[16] A. K. Ghatak and K. Thyagarajan, "Optical Electronics" (Cambridge University Press), Chapter 13, 1989.

[17] John M. Senior, "Optical Fibre Communications-Principles and Practice" (Prentice-Hall)

Chapter 4

Techniques to enhance the relative visibility of the central fringe in a WLI system with a synthetic source

4.1 Introduction

In Chapter 3, techniques to suppress the modal noise induced by the fibre lead was investigated. In order to obtain measurements from a WLI system with high accuracy, it is essential to identify the central fringe of the output fringe pattern and to determine the central position [1, 2]. However, in the system with a single wavelength illuminating source, the central fringe may not be identified simply through investigating its amplitude due to the presence of the modal noise. A dual wavelength technique has been proposed and developed to solve the problem [3, 4, 5]. With the dual wavelength technique, a fringe beating pattern is generated. Thus, the central fringe is enhanced. The SNR required to identify the central fringe of the output fringe pattern is reduced from about 50dB to about 25dB. In order to further enhance the relative intensity of the central fringe and suppress the side fringes, a three-wavelength-technique has also been proposed and described [6]. As a result, the SNR required to identify the central fringe is further reduced. Another approach [7] is to multiply the two different wavelength components in the output of the system and to obtain an increased relative amplitude of the central fringe. It has been shown that the SNR required to identify the central fringe of the multiplied output is lower than that of the conventional two wavelength system described by earlier workers [3, 4, 5].

In this Chapter, two simple, fast and low cost approaches based on multiplying and squaring are reported and compared. One uses an electrical circuit to square the output of a two

wavelength system directly [8]. The other uses two detectors to detect the different wavelength components from the system, which have been separated by a wavelength-selective mirror. Then, the outputs from the two detectors are multiplied and squared using an analogue electrical circuit [9]. The schematic diagrams of the two approaches are shown in Fig.(4.1) and Fig.(4.5). With the use of these techniques, the relative intensity of the central fringe of the output from a WLI system can be enhanced.
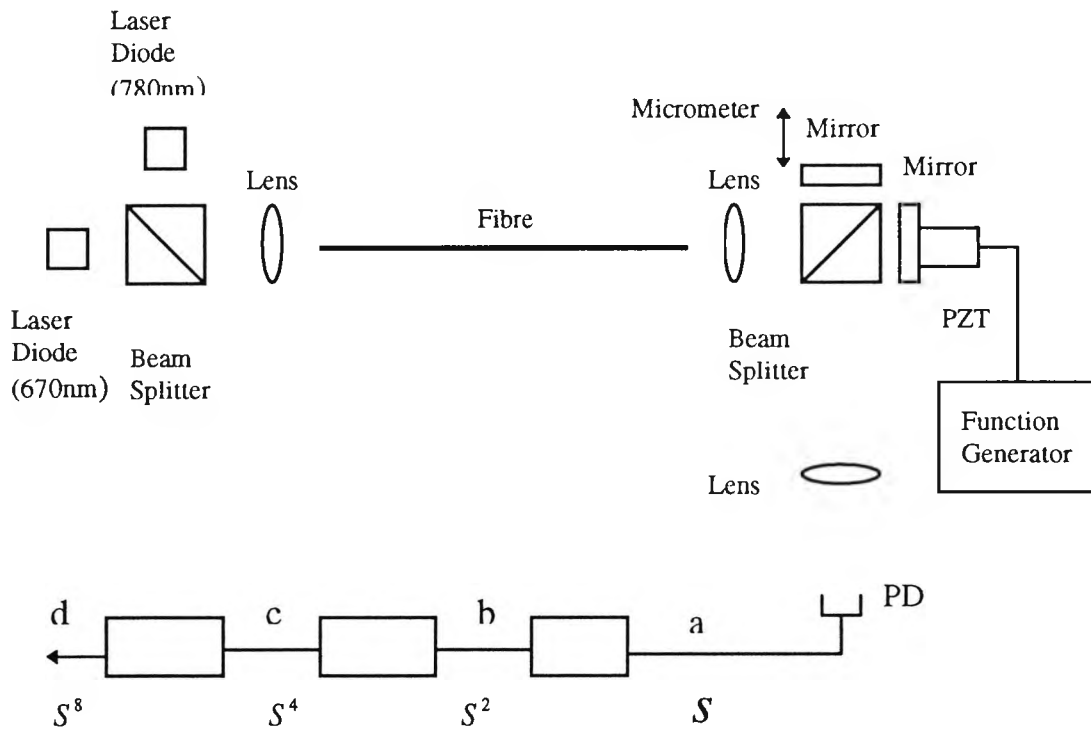

Fig.(4.1) Experimental arrangement of the scheme with one detector. (The experimental results were recorded at *a, b, c,* and *d*).

This Chapter is divided into four sections. Following this introduction, in Section 4.2, an investigation of the system with one detector is presented. In Section 4.3, an investigation of the system with two detectors is described. In Section 4.4, the dependence of the relative amplitude of the central fringe on the intensity ratio of the sources is investigated.

4.2 Enhancement scheme with one detector [8]

4.2.1 Theory

Consider a system shown in Fig.(4.1), the output intensities of the system, $I_1(\Delta L)$ and $I_2(\Delta L)$, when it is illuminated by two laser diodes with different wavelength can be expressed as [5]

$$I_1(\Delta L) = \frac{I_{01}}{2}[1 + \exp[-(2\Delta L / L_c)^2]\cos(2\pi\, \Delta L / \lambda_1)] \tag{4.1}$$

and

$$I_2(\Delta L) = \frac{I_{02}}{2}[1 + \exp[-(2\Delta L / L_c)^2]\cos(2\pi\, \Delta L / \lambda_2)] \tag{4.2}$$

where I_{01} and I_{02} are the maximum intensities detected by the photodiode when the laser diodes with central wavelengths of λ_1 and λ_2 are used respectively, ΔL is the OPD introduced by the interferometer and L_c is coherence length of the source. The beams from the two laser diodes are mutually incoherent. Hence, the output obtained from the system is a result of the intensity superposition of the two sets of the interference fringes. As a result, a fringe beat pattern is generated. The intensity of the system shown in Fig.(4.1), $I_a(\Delta L)$, can then be described by summing Eq.(4.1) and Eq.(4.2), which is given by

$$I_a(\Delta L) = I_1(\Delta L) + I_2(\Delta L) \tag{4.3}$$

In the case that $I_{01} = I_{02} = 1$, normalised output of a WLI interferometric system with a synthetic source can be written as
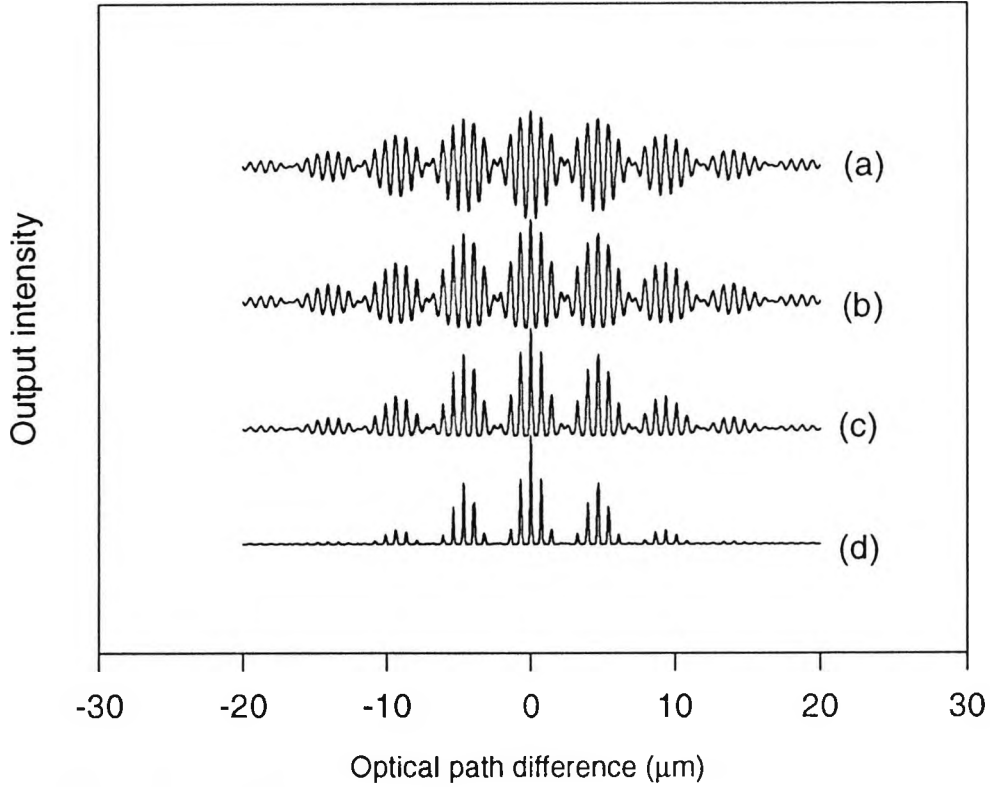
Fig.(4.2) Simulation results showing the output fringe patterns of the system with one detector when the number of the power is (a) n=1, (b) n=2, (c) n=4, (d) n=8.

$$I_a(\Delta L) = (1/4)\{2 + \exp[-(2\Delta L / L_c)^2][\cos(2\pi \Delta L / \lambda_1) + \cos(2\pi \Delta L / \lambda_2)]\}$$
$$= (1/2)\{1 + \exp[-(2\Delta L / L_c)^2][\cos(2\pi \Delta L / \lambda_a)\cos(2\pi \Delta L / \lambda_m)]\}$$

(4.4)

where $\lambda_a = 2\lambda_1\lambda_2 / (\lambda_1 + \lambda_2)$ is termed as the average wavelength and $\lambda_m = 2\lambda_1\lambda_2 / |\lambda_1 - \lambda_2|$ the modulation wavelength. When this output signal is fed into a simple three stage squaring circuit, the resulting output can be written as

$$I_a^n(\Delta L) = [I_a(\Delta L)]^n ,$$

(4.5)

where n=1, 2, 4, 8. $I_a^n(\Delta L)$ represents the output of the system before the first squaring operation, after the first, second and third squaring operation, respectively. With the use of

67

a simple computer program, the output intensity against the optical path difference for the cases of n=1, 2, 4, and 8 can be calculated. The results are shown in Fig.(4.2). In the calculation, the coherence length of the sources, L_c, is chosen to be 25μm and the wavelengths of the sources, λ_1, λ_2, are equal to 670nm and 780nm, which are typical values obtained from commercial supplies.

In order to determine the minimum value of the SNR required to identify the central fringe (SNR_{min}), the amplitude difference between the central fringe and second largest fringe within the zero-order fringe packet, ΔI_a^n, may be defined as the maximum noise level allowed for the identification of the central fringe, which can be written as

$$\begin{aligned}\Delta I_a^n &= I_a^n(0) - I_a^n(\lambda_a)\\ &= 1 - \{(1/2)[1 + \exp[-(2\lambda_a / L_c)^2]\cos(2\pi\lambda_a / \lambda_m)]\}^n\end{aligned} \qquad (4.6)$$

The value of the term $I_a^n(\lambda_a)$ is larger than zero and smaller than one. Therefore, the value of ΔI_a^n increases as the number n increases, resulting in a central fringe enhancement after the squaring process (see Fig.(4.2)). Clearly, if the level of the intensity noise in the system is equal to or greater than ΔI_a^n, the central fringe may not be identified simply through an inspection of its amplitude. In other words, if the normalised peak value of the central fringe is defined as a unit signal, the minimum SNR (SNR_{min}) required to identify the central fringe is given by

$$SNR_{min}(dB) = -20\log(\Delta I_a^n) \qquad (4.7)$$

It should be noted that the noise considered is the intensity noise. The reason is that the intensity noise changes the peak height of the fringes and therefore may cause the misidentification of the central fringe when the maximum visibility method [1] is used.

4.2.2 Experiment

In order to verify the theoretical results discussed in the last section, an experimental arrangement shown in Fig.(4.1) was used. The light beam from two multimode laser diodes, LT023MDO and LPM3 670, which central wavelengths were 780nm and 670nm respectively, was injected into a multimode fibre via a $10\times$ objective lens. The core diameter of the fibre is $200\mu m$ and the length of the fibre is about 4 meters. The collimated beam was modulated by a Michelson interferometer and detected with a photodiode. The output fringe patterns from the system were then recorded and the results are shown in Fig.(4.3), where (a), (b), (c) and (d) represent the results obtained before and after each stage of the squaring operation. The values of SNR_{min} for each case were measured and plotted in Fig.(4.4), in which the theoretical value of the SNR_{min} calculated from Eq.(4.7) against the number of the power n is also shown.

By comparing Fig.(4.2) and Fig.(4.3), it can be seen that the results obtained from the experiment are in agreement with those obtained theoretically. It is particularly important to see that the relative peak value of the central fringe becomes larger as the number of squaring operations increases. In Fig.(4.4), the squares represent the experimental data and the circles represent the results calculated from Eq.(4.7). It can be seen from the diagram that the value of the SNR_{min} is reduced as the number of the power increases. This is because the maximum value of noise defined here was the difference between the peak values of the two fringes. Hence, it can be directly increased by a squaring operation. As a result, the identification of the central fringe becomes easier after using the squaring operations.
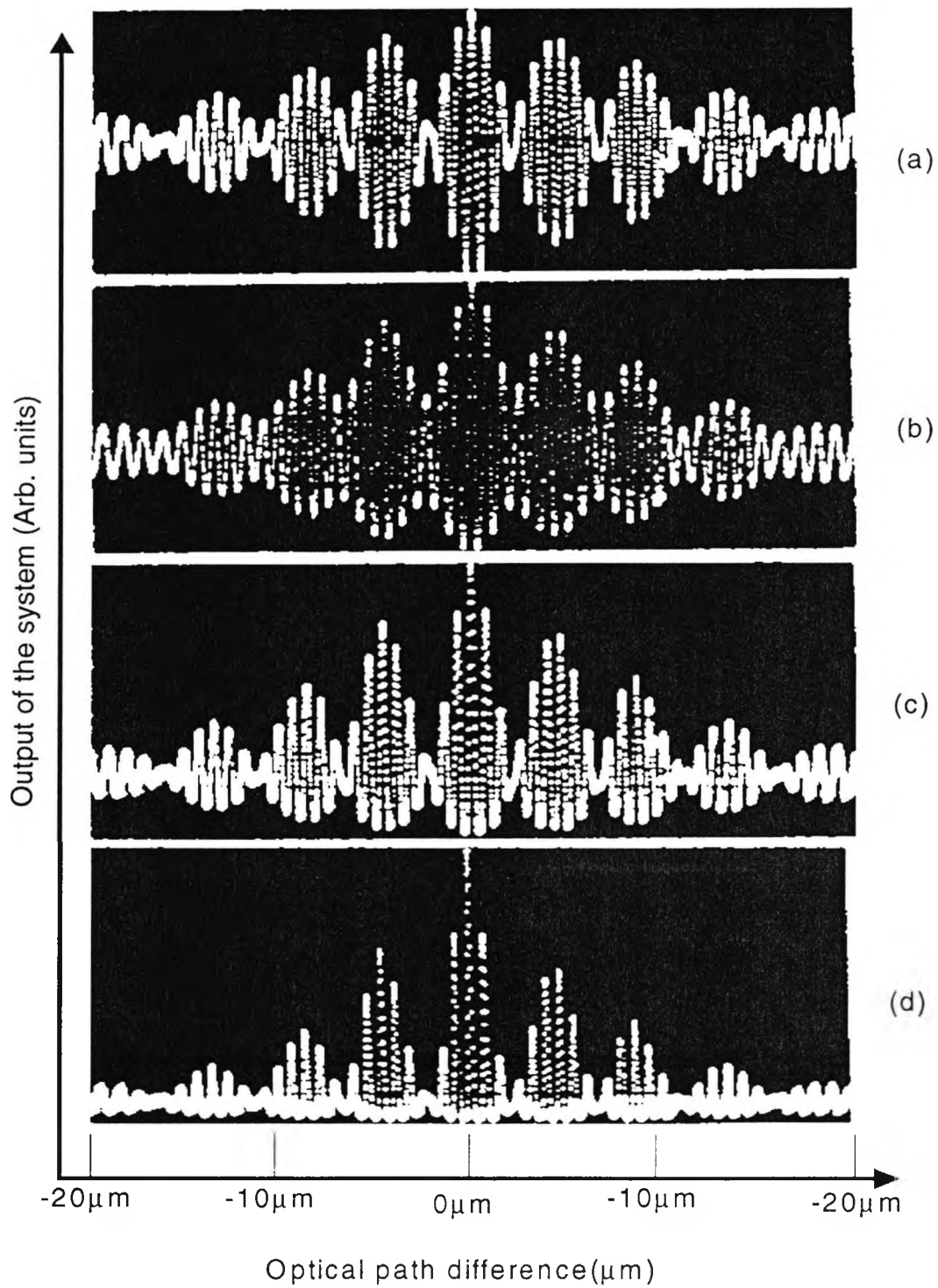
Fig.(4.3) Experimental results showing the output fringe pattern of the system shown in Fig.(4.1) when the number of the power is (a) n=1, (b) n=2, (c) n=4, and (d) n=8, respectively.
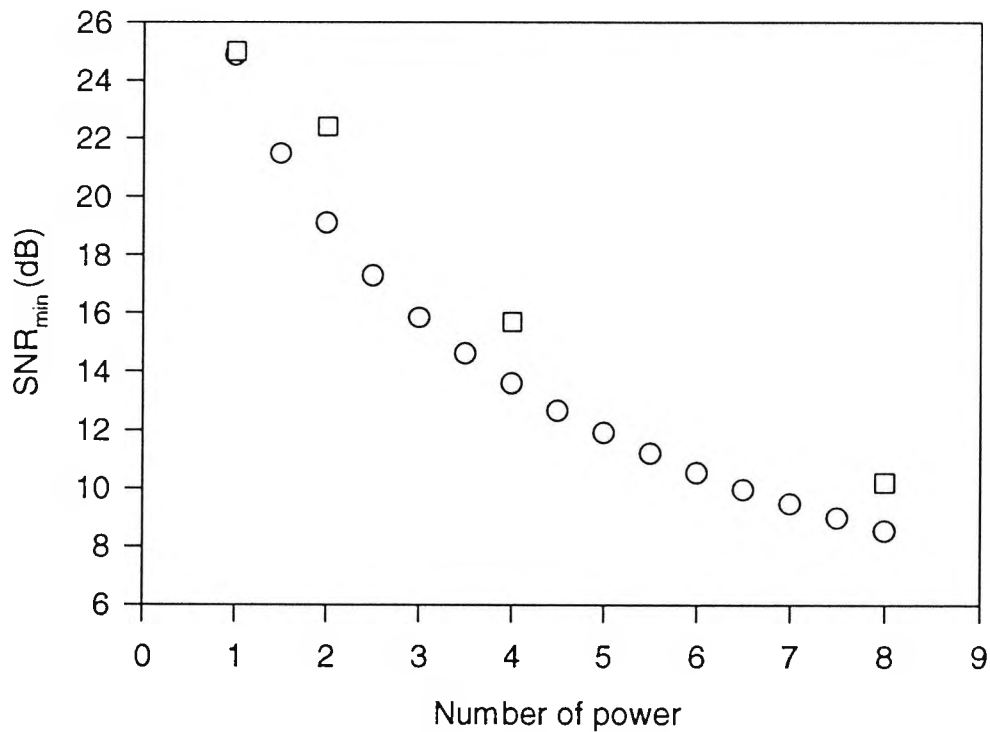
70

Fig.(4.4) Experimental results (squares) and theoretical results (circles) from the system shown in Fig.(4.1), showing that the values of the SNR$_{min}$ required to identify the central fringe are reduced as the number of the power increases.

It should be pointed out that the squaring operation may not increase the possibility of identifying the central fringe if noise with a value greater than the value of ΔI_a is present in the fringe pattern. The reason is that if the central fringe is lower than any other fringes due to the presence of noise, it will relatively be lowered after the squaring operations. However, if the noise level is lower than the value of amplitude difference between the central peak and the second largest peak, the squaring operation will enhance the central fringe, resulting in an easier central fringe identification in the consequent processing steps.

71

In summary, with the use of the multi-stage squaring signal processing approach, the central fringe in the output fringe pattern can be considerably enhanced. This can ease the central fringe identification.

4.3 Enhancement scheme with two detectors [9]

4.3.1 Theory

Consider the arrangement shown in Fig.(4.5). When the system is illuminated by the sources with wavelengths λ_1 and λ_2, the output intensities of the system, $I_1(\Delta L)$ and $I_2(\Delta L)$, can be expressed as

$$I_1(\Delta L) = \frac{I_{01}}{2}[1 + \exp[-(2\Delta L / L_c)^2] \cos(2\pi\Delta L / \lambda_1)] \tag{4.8}$$

and

$$I_2(\Delta L) = \frac{I_{02}}{2}[1 + \exp[-(2\Delta L / L_c)^2] \cos(2\pi\Delta L / \lambda_2)] \tag{4.9}$$

where λ_1, λ_2 are central wavelengths of the sources respectively, ΔL is the optical path difference (OPD) introduced by the interferometer, L_c is the source coherence length, and I_{01} and I_{02} are the maximum output intensity of the system with the sources. When the detected output signals are multiplied, the new output signal, $I_m(\Delta L)$, can then be written as

$$
\begin{aligned}
I_m(\Delta L) &= I_1(\Delta L)I_2(\Delta L) = I_a(\Delta L) + I_d(\Delta L) \\
&= \frac{I_0}{4}\{2 + \exp[-(\frac{2\Delta L}{L_c})^2]\cos(\frac{2\pi\,\Delta L}{\lambda_1}) + \exp[-(\frac{2\Delta L}{L_c})^2]\cos(\frac{2\pi\,\Delta L}{\lambda_2})\} \\
&\quad + \frac{I_0}{4}\{\exp[-2(\frac{2\Delta L}{L_c})^2]\cos(\frac{2\pi\,\Delta L}{\lambda_1})\cos(\frac{2\pi\,\Delta L}{\lambda_2}) - 1\}
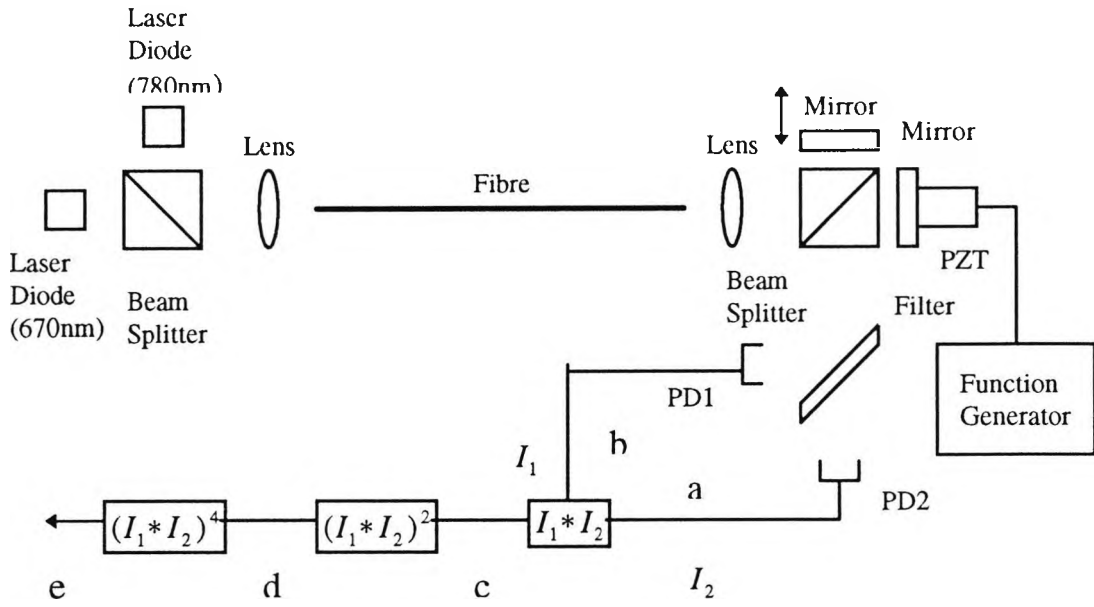\end{aligned}
\tag{4.10}
$$

72

Fig.(4.5) Experimental arrangement of the scheme with two detectors (the experimental results were recorded at a, b, c, d, and e respectively).

where

$$I_a(\Delta L) = \frac{I_0}{4}\{2 + \exp[-(\frac{2\Delta L}{L_c})^2]\cos(\frac{2\pi \, \Delta L}{\lambda_1}) + \exp[-(\frac{2\Delta L}{L_c})^2]\cos(\frac{2\pi \, \Delta L}{\lambda_2})\} \qquad (4.10a)$$

and

$$I_d(\Delta L) = \frac{I_0}{4}\{\exp[-2(\frac{2\Delta L}{L_c})^2]\cos(\frac{2\pi \, \Delta L}{\lambda_1})\cos(\frac{2\pi \, \Delta L}{\lambda_2}) - 1\} \qquad (4.10b)$$

$I_0 = I_{01}I_{02}$ represents the maximum output of the system after the multiplication process, $I_m(\Delta L)$ can be defined as multiplied output, $I_a(\Delta L)$ can be defined as summed output. The summed output I_a gives a fringe beat pattern with an average wavelength $\lambda_a = \frac{2\lambda_1\lambda_2}{\lambda_1 + \lambda_2}$,

and a modulation wavelength $\lambda_m = \dfrac{2\lambda_1\lambda_2}{|\lambda_1 - \lambda_2|}$. Its value can be calculated by Eq.(4.4). The

value of I_d, which is given by Eq.(4.10b), can be rewritten as

$$I_d(\Delta L) = \frac{I_0}{8}\{\exp[-2(\frac{2\Delta L}{L_c})^2][\cos(\frac{2\pi\Delta L}{\lambda_m / 2}) + \cos(\frac{2\pi\Delta L}{\lambda_a / 2})] - 2\} \qquad (4.11)$$

From Eq.(4.11), it can be seen that $I_d(\Delta L)$ is a result of the intensity superposition of two

terms, one with a wavelength $\lambda_m / 2$ and the other with a wavelength $\lambda_a / 2$. The fringe

peaks of $I_d(\Delta L)$ are located at $\Delta L = n(\lambda_a / 2)$, where $n = 0,1,2 \ldots$. In order to show the

relationship of the quantities, $I_m(\Delta L), I_a(\Delta L)$, and $I_d(\Delta L)$, the values calculated from Eqs.

(4.10), (4.10a) and (4.10b) were ploted in Fig.(4.6).

The amplitude difference between the central fringe and the first side fringes in the

multiplied output, ΔI_m is given by

$$\Delta I_m = \Delta I_a + \Delta I_d \qquad (4.12)$$

where ΔI_a can be calculated from Eq.(4.6) and ΔI_d is given by

$$\Delta I_d = \frac{I_0}{4}\{1 - \exp[-2(2\lambda_a / L_c)^2]\cos(2\pi\lambda_a / \lambda_1)\cos(2\pi\lambda_a / \lambda_2)\} \qquad (4.13)$$

Since the value of ΔI_d is larger than zero, the value of ΔI_m is larger than that of ΔI_a.

Therefore, the multiplied output has a larger amplitude difference between the central fringe

and the first side fringes than that of the summed output, resulting in a smaller SNR_{min} of the

multiplied output. This can easily be seen from Fig.(4.6), where the amplitude of the central

fringe in the multiplied output is equal to that in the summed output and the amplitude of

74

the first side fringes in the multiplied output is lower than that in the summed output. When the multiplied output is squared, the new output can be expressed as
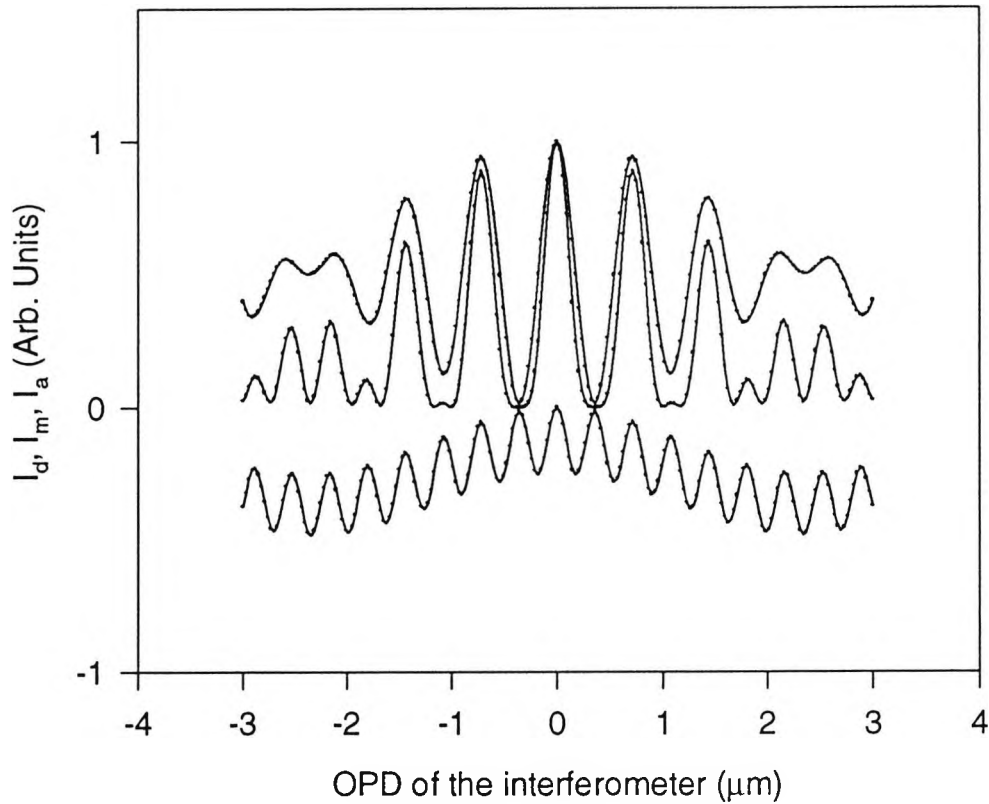

Fig.(4.6) The value of I_d (lower curve), multiplied output I_m (middle curve) and summed output I_a (upper curve) against the OPD of the interferometer.

$$I_m^n(\Delta L) = [I_1(\Delta L)I_2(\Delta L)]^n$$
$$= \{\frac{1}{4}I_0[1 + \exp[-(\frac{2\Delta L}{L_t})^2]\cos(\frac{2\pi\Delta L}{\lambda_1})][1 + \exp[-(\frac{2\Delta L}{L_t})^2]\cos(\frac{2\pi\Delta L}{\lambda_2})]\}^n \qquad (4.14)$$

where n equal to 1, 2, 4. $I_m^n(\Delta L)$ represent the output of the multiplier, the output of the first and the second squaring operation when n equal to 1, 2, and 4 respectively. With the use of a simple computer program, the output intensity against the OPD can be calculated

75

for the case before the multiplying, after the multiplying and after the further squaring processes respectively. In the calculation, the coherence length of the sources, L_c, were chosen to be 25μm and the wavelengths of the sources, λ_1, λ_2, are equal to 670nm and 780nm, respectively. The results of the calculation are shown in Fig.(4.7).
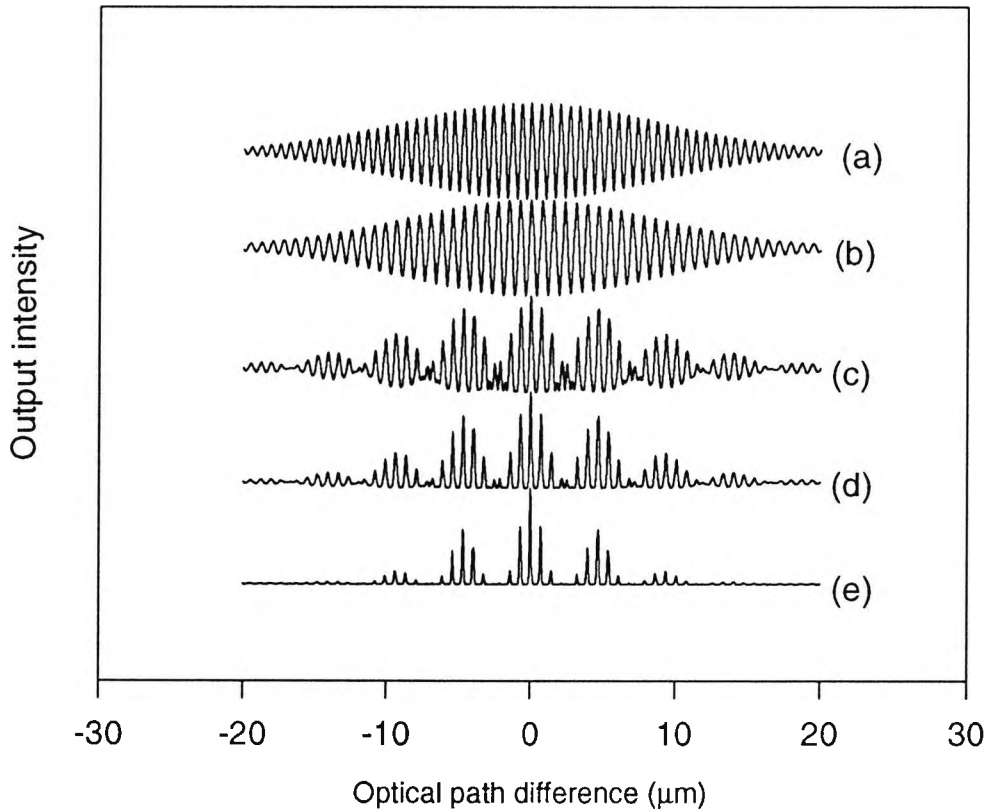
Fig.(4.7) Simulated results showing the output of the system with two detectors (given by Eq.(4.14)) when (a) a 670nm wavelength source is used (b) a 780nm wavelength source is used (c) n=1 (d) n=2 (e) n=4

Assume the maximum intensity of the multiplied output $I_0 = 1$. The amplitude difference between the central fringe and the first side fringe after the squaring operation, ΔI_m^n, can be written as

$$\Delta I_m^n = 1 - [I_1(\lambda_a)I_2(\lambda_a)]^n$$

$$= 1 - \{\frac{1}{4}[1 + \exp[-(\frac{2\lambda_a}{L_c})^2]\cos(\frac{2\pi\lambda_a}{\lambda_1})][1 + \exp[-(\frac{2\lambda_a}{L_c})^2]\cos(\frac{2\pi\lambda_a}{\lambda_2})]\}^n \quad (4.15)$$

The value of the factor $I_1(\lambda_a)I_2(\lambda_a)$ in Eq.(4.15) is larger than zero and smaller than one. Hence, the value of ΔI_m^n increases as the number n increases, resulting in further central fringe enhancement after each squaring process. This can easily be seen from Fig.(4.7).

Clearly, if the intensity noise in the system is equal to or greater than the amplitude difference, ΔI_m^n, between the central fringe and the second largest fringe, the central fringe cannot be identified directly through a simple inspection of its amplitude. In order to determine SNR_{min}, the value of ΔI_m^n is regarded as the maximum noise level allowed for the identification of the central fringe. This value can be obtained from Eq.(4.15). The value of SNR_{min} of the multiflied output in dB may be expressed as

$$SNR_{min}(dB) = -20\log(\Delta I_m^n) \quad (4.16)$$

4.3.2 Experiment

In order to verify the theoretical results of the multiplied output discussed above, the experimental arrangement shown in Fig.(4.5) was used where light from the two multimode laser diodes (LPM3 670 and LT023MDO), with central wavelengths of 670nm and 780nm respectively, was injected into a multimode fibre (with a core diameter of 200μm and a length of 4 meters) via a 10x objective lens. The collimated beam was modulated by vibrating one of the mirrors in the Michelson interferometer. The two different wavelength components were then separated by a wavelength-selective mirror (part No. 16 BH 16, supplied by Comer Instruments [10]) and detected with two photodiodes.

77

Since the output fringe patterns of the two wavelength components were measured simultaneously, they correspond to the same change of the OPD. The output signals before and after the multiplying operation and after each squaring operation were recorded. The results are shown in Fig.(4.8). It can be seen that the relative amplitude of the central fringe of the multiplied output has been increased considerably in comparison with the fringe patterns when the system illuminated by either of the sources. It has also been gradually enhanced as the number of the squaring operation increases, showing the same trend as that in Fig.(4.7). The values of the SNR_{min} for each case were measured and shown as squares in Fig.(4.9). The theoretical values of the SNR_{min} when the coherence length is 25μm were calculated from Eq.(4.16) and shown as circles in Fig.(4.9).

By comparing Fig.(4.7) and Fig.(4.8), it can be seen qualitatively that the results obtained from the experiment are in good agreement with those obtained theoretically. The figures show the same structure in both cases. It is also noted that the relative peak value of the central fringe increases as the number of squaring operations increases. As a result, the identification of the central fringe becomes easier in consequent process.

In Fig.(4.4) and Fig.(4.9), a similar trend can be seen in both the theoretical (circles) and experimental (squares) values of the SNR_{min}. The trend shows that the SNR_{min} is reduced as the number of squaring operations increase. This is because the maximum "noise" defined here was the difference between the peak values of the two fringes and it can be directly increased by the squaring operations. After the squaring operations, the identification of the central fringe becomes easier. It can also be seen from Fig.(4.4) and Fig.(4.9) that there was a difference (of about ~2dB on average) between the results obtained from the theoretical calculation (circles) and the experiment (squares). This may partially be explained by considering that the DC value in the normalized fringe pattern obtained from the experiment is relatively higher than that of the theoretical output fringe pattern.
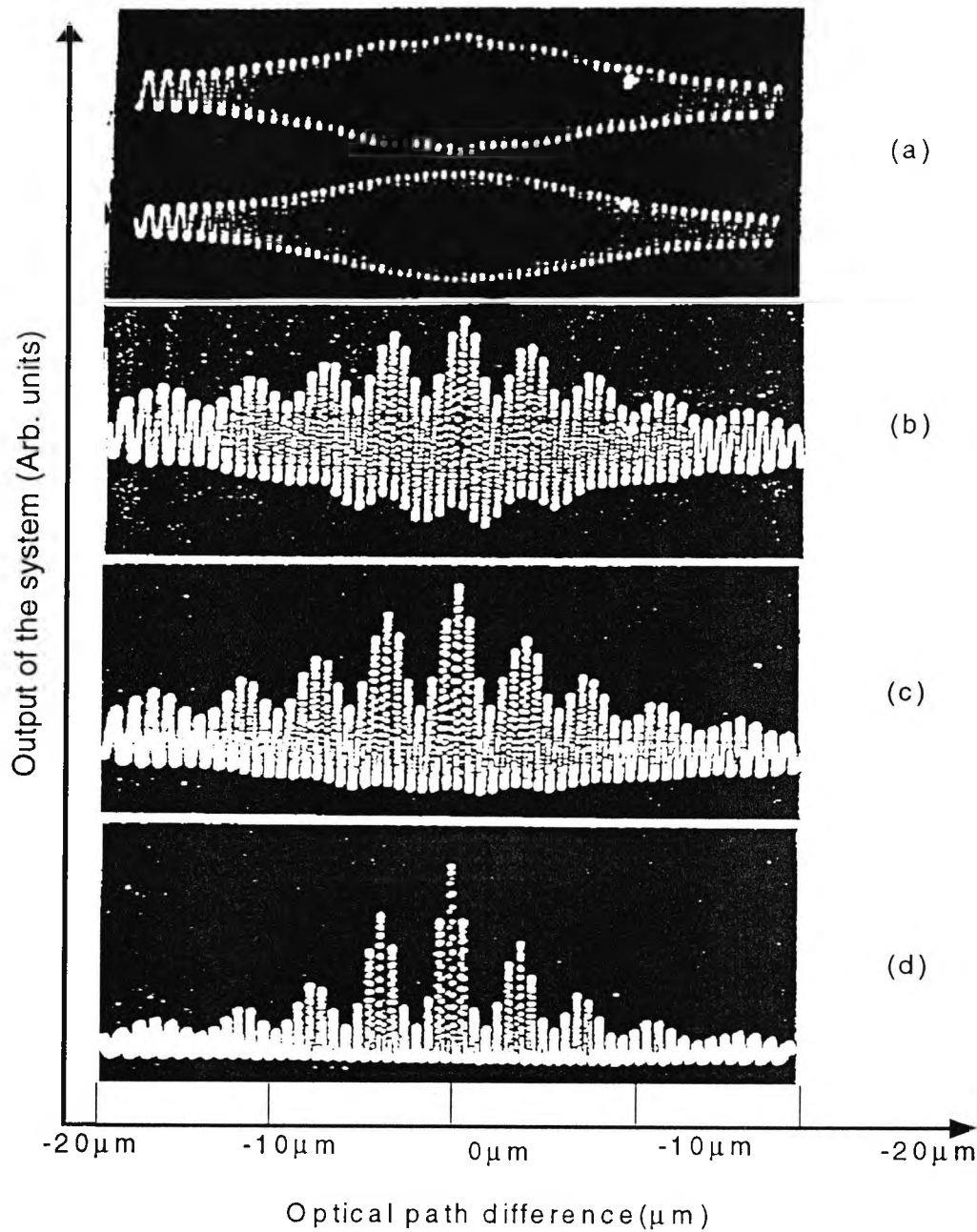
78

Fig.(4.8) Experimental output fringe patterns of the system shown in Fig.(4.5) in the cases (a) when the system was illuminated eather by 670nm wavelength source or 780nm wavelength source, (b) that the output obtained by multiplying the two wavelengths components, (c) that the output is obtained after the first squaring process, (d) that the output is obtained after the second squaring process.
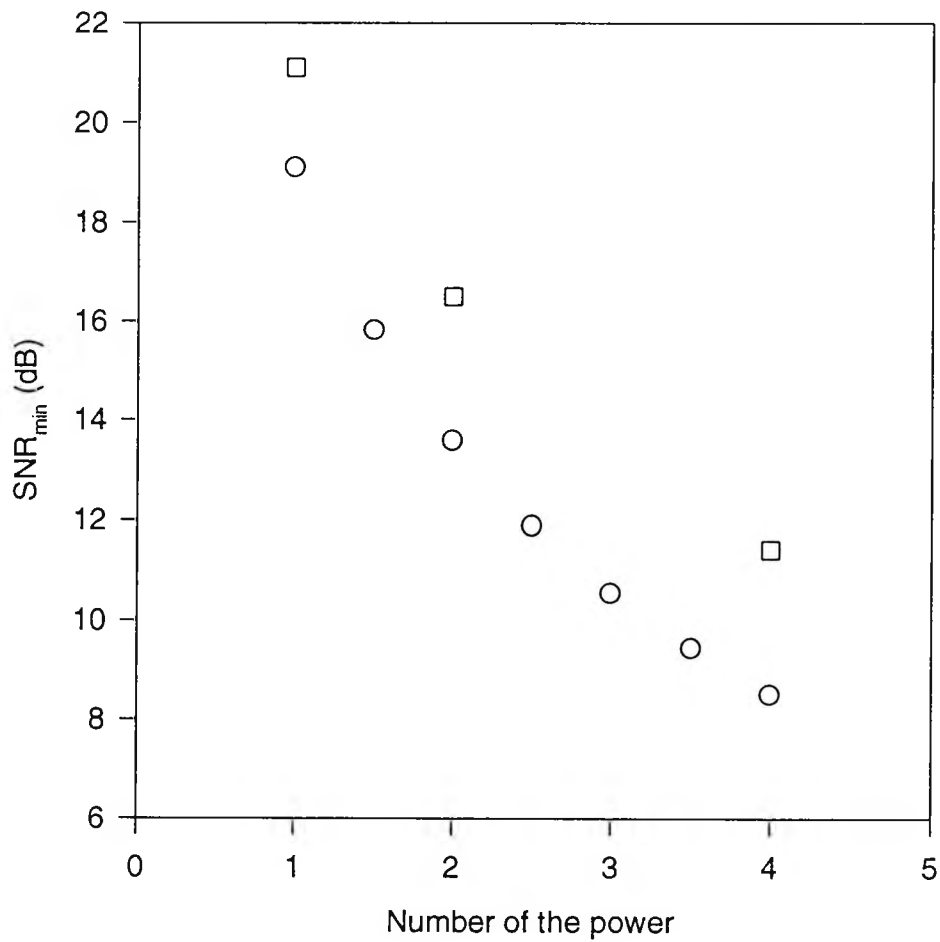
Fig.(4.9) Experimental results (shown as squares) and theoretical results (shown as circles) from the system described in Fig.(4.5), showing that the values of the SNR_{min} are reduced as the number of squaring processes increases

In summary, with the use of a low-cost optical filter to separate the sensing beam into two individual beams according to their wavelengths, the relative amplitude of the central fringe in the output fringe pattern can be considerably reduced, as illustrated, to a value of about 21dB. The relative amplitude of the central fringe can further be enhanced to a value of about 12dB by the squaring operations using a electrical circuit. Therefore, the central fringe identification after the signal processing becomes easier.

4.4 Dependence of the relative intensity of the central fringe on the intensity ratio of the two wavelength components

Two signal processing schemes have been discussed and analysed in the above sections. It should be noted that the discussion is limited within the case of $I_{01} = I_{02}$, which may not represents the case of a practical system and may not give the maximum relative intensity of the central fringe. From Eq.(4.3), the normalized output of the system with one detector (summed output), when the output intensities of the two sources are not equal, can be written as

$$I_a(\Delta L) = (\frac{1}{2(I_{01} + I_{02})})\{I_{01}[1 + \exp[-(\frac{2\Delta L}{L_c})^2] \cos(\frac{2\pi\Delta L}{\lambda_1})] + I_{02}[1 + \exp[-(\frac{2\Delta L}{L_c})^2] \cos(\frac{2\pi\Delta L}{\lambda_2})]\}$$

(4.17)

Define $R = \frac{I_{01}}{I_{02}}$, then Eq.(4.17) can be rewritten as

$$I_a(\Delta L) = (\frac{1}{2(1 + R)})\{R[1 + \exp[-(\frac{2\Delta L}{L_c})^2] \cos(\frac{2\pi\Delta L}{\lambda_1})] + [1 + \exp[-(\frac{2\Delta L}{L_c})^2] \cos(\frac{2\pi\Delta L}{\lambda_2})]\}$$

(4.18)

By multiplying Eq.(4.1) and Eq.(4.2), the normalized output of the system with two detectors (multiplied output) may be expressed as

$$I_m(\Delta L) = \frac{1}{4}[1 + \exp[-(\frac{2\Delta L}{L_c})^2] \cos(\frac{2\pi\Delta L}{\lambda_1})][1 + \exp[-(\frac{2\Delta L}{L_c})^2] \cos(\frac{2\pi\Delta L}{\lambda_2})]$$

(4.19)

81

It should be noted from Eq.(4.19) that the normalized output of the system with two detectors is independent of the intensity ratio of the two sources, $\dfrac{I_{01}}{I_{02}}$.

The SNR_{min} for the one-detector scheme can be expressed

$$SNR_{min}(dB) = -20\log(\Delta I_a) \qquad (4.20)$$

where ΔI_a is the amplitude difference between the central fringe and the first side fringes in the normalized output of the system with one detector. The SNR_{min} of the system with two detectors can be expressed as

$$SNR_{min}(dB) = -20\log(\Delta I_m) \qquad (4.21)$$

where ΔI_m is the amplitude difference between the central fringe and the first side fringes in the normalized output of the system with two detectors. In order to inspect the intensity ratio dependence of the SNR_{min}, the theoretical values of SNR_{min} of the summed output and multiplied output were calculated from Eq.(4.20) and Eq.(4.21) and the results are shown in the Fig.(4.10). The parameters, λ_1, λ_2 and L_c are chosen to be 0.67μm, 0.78μm, and 25μm, respectively. It can be seen from the diagram that the SNR_{min} for the system with two detectors (shown as lower straight line, which value is about 19dB) is lower than that for the system with one detector and is independent of the intensity ratio of the two sources. It can also be seen that the SNR_{min} for one-detector system (shown as upper

curve) is dependent on the intensity ratio of the sources and reaches its minimum value

(about 25dB) when the intensity ratio $\dfrac{I_{01}}{I_{02}}$ is about 0.85.
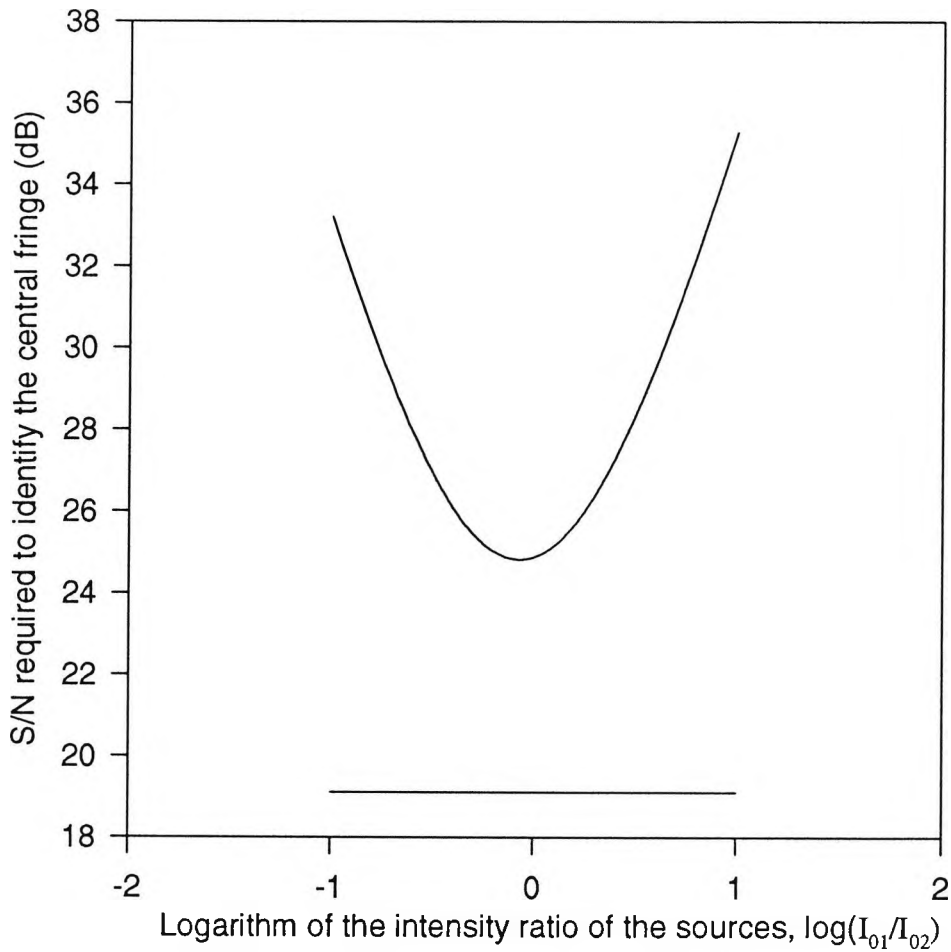
Fig.(4.10) SNR_{min} (without use of the squaring process) against the logarithm intensity ratio of the two sources, $\log(\dfrac{I_{01}}{I_{02}})$. The lower curve (the straight line) represents the result from the multiplied output (scheme with two detectors) and the upper curve represents the result from the summed output (scheme with one detector).

The results shown in Fig.(4.10) indicate that the relative amplitude of the summed output is lower than that of the multiplied output and necessitates similar intensities of the sources although it has a less complicated optical arrangement. On the other hand, the relative amplitude of the central fringe of the multiplied output is higher than that of the summed output and make unnecessary the similar intensities of the sources. This can be seen from Eq. (4.19) where the intensities of the sources are absent in the right side of the equation.

It should be noted that the intensity ratio to minimise the SNR_{min} of the system with one detector is equal to 0.85 instead of 1. In other words, the maximum relative intensity of the central fringe of the summed output occurs when the intensity from the source of the shorter wavelength, λ_1, is slightly lower than that from the source of the longer wavelength, λ_2.

4.5 Discussion

Two types of signal processing approaches have been developed, which can be used to increase relative amplitude of the central fringe of a WLI system with a dual wavelength illuminating source. The theoretical analysis and the experimental results have shown that the values of the SNR_{min} decreases as the number of the squaring operations increases.

The system with one detector has a relatively simple optical arrangement. Whereas, the system with two detectors has the advantage that its relative intensity of the central fringe is higher than that of the system with one detector and independent of the intensity ratio of the two wavelength components.

After identifying the central fringe of a WLI system, the actual central position of the central fringe need to be determined. In the next Chapter, a signal processing scheme base on curve

84

fitting algorithm will be proposed and analysed to measure the central position of the output from a WLI system.

References

[1] S. Chen, A. W. Palmer, K. T. V. Grattan and B. T. Meggitt, "Digital Signal Processing Techniques for Electronically Scanned Optical-fibre White Light Interferometry", Appl. Opt. Vol.31, pp 6003-6010, 1992.

[2] R. Dandliker, E. Zimmermann and G. Frosio, "Electronically Scanned White-light Interferometry: a Novel Noise-resistant Signal Processing". Opt. Lett. Vol.17(9), pp879-881, 1992.

[3] S. Chen, K. T. V. Grattan, B. T. Meggitt, and A. W. Palmer, "Instantaneous Fringe-order Identification Using Dual Broadband Sources with Widely Spaced Wavelength", Electron. Lett., Vol.29, pp. 334-335, 1993.

[4] Y. J. Rao, Y. N. Ning and D. A. Jackson, "Synthesized Source for White-light Sensing Systems", Opt. Lett., Vol.18(6), pp462-464, 1993.

[5] D. N. Wang, Y. N. Ning, K. T. V. Grattan, A. W. Palmer, and K. Weir " The Optimized Wavelength Combinations of Two Broadband Sources for White Light Interferometry", Journal of Lightwave Technology. Vol.12, No.5, pp909-914, 1994.

[6] D. N. Wang, Y. N. Ning, K. T. V. Grattan, A. W. Palmer and K. Weir, "Three-wavelength Combination Source for White Light Interferometry", IEEE Photon. Technol. Lett., Vol.30(17), pp1440-1441, 1994.

[7] Y. J. Rao, D. A. Jackson, "Improved Synthesized Source for White Light Interferometry", Electron. Lett., Vol.30(17), pp1440-1441, 1994.

[8] Q. Wang, Y. N. Ning, A. W. Palmer, K. T. V. Grattan "Central Fringe Identification in a White Light Interferometer Using a Multi-stage-squaring Signal Processing Scheme", Opt. commun. 117, pp241-244 1995.

[9] Y. N. Ning, Q. Wang, A. W. Palmer, K. T. V. Grattan, B. T. Meggitt, and K. Weir "Novel Signal Processing Scheme for Enhancing the Central Fringe in a White Light Interferometer" Proceeding of Sensors and their applications VII, pp149-154, 1995.

[10] Comar Imstruments, 70 Hartington Grove, Cambridge, UK, Manufacturer's Data, Section 7.7, 1993.

Chapter.5

A white light interferometric system linked with a multimode fibre

5.1 Introduction

Optical sensing systems based on white light interferometry have been increasingly investigated [1-6]. The performance of the system is dependent on how accurate the "central position" can be measured. Several signal processing schemes have been proposed to determine this central position, which include the whole fringe pattern centroid technique [6] and the central fringe centroid method [7]. However, with a single wavelength illuminating source, the central fringe of the output of the system can not be identified through simply investigating the amplitude of the fringes due to the presence of noise. In order to ease the central fringe identification, the system with a two wavelength source has been proposed and investigated[8][9]. With the two wavelength source technique, the signal to noise ratio required to identify the central fringe of the output of the system is considerably reduced from about 50dB to about 25 dB.

In addition to the single and dual wavelength techniques discussed earlier, a technique called dual-wavelength low-coherence interferometry (DWLCI) has been proposed and developed [10][11]. It allows the measurand to be determined by measuring the optical phase change between the reference interferometer and the sensing interferometer and the fringe number is obtained from the differential phase between the two sources with a small wavelength difference. However, this DWLCI technique requires an illuminating source with a very stable output wavelength, especially when a large measuring range is needed.

88

In this Chapter, a system comprising two Michelson interferometers linked with a multimode fibre was studied. The change of the arm length difference (ALD) of the sensing interferometer was determined by measuring the central position change of the output fringe pattern of the system utilizing a capacitive displacement sensor. Different types of multimode fibres were used to link the two interferometers and the corresponding characteristics of the system were investigated. A curve fitting signal processing scheme using a cosine function for reducing the noise effect and increasing the repeatability of the central position measurement has been studied both theoretically and experimentally.

5.2 Theory and analysis

In a system consisting of two Michelson interferometers linked with a multimode fibre (see Fig. (5.1)), the arm length difference (ALD) of the first interferometer is given by X_1 and
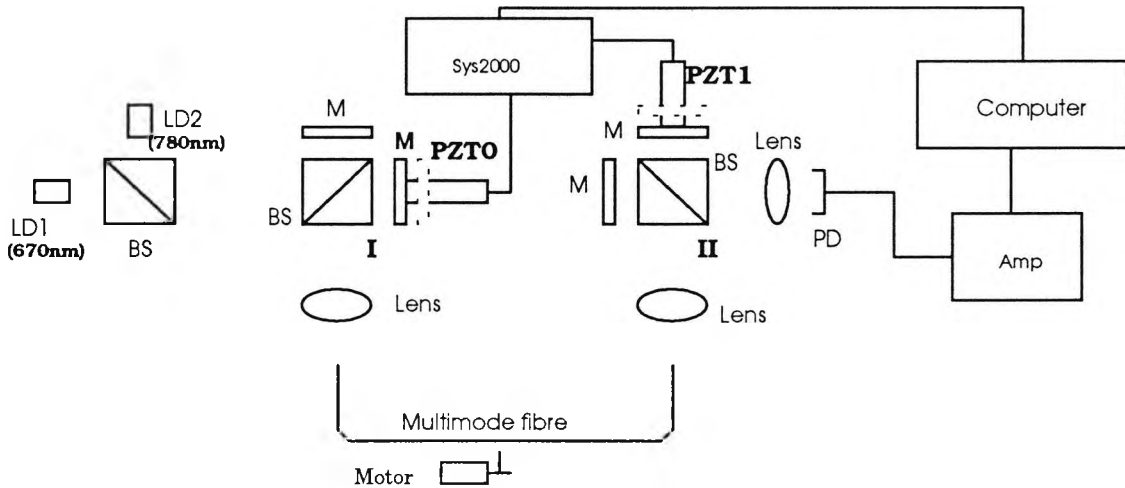
Fig. (5.1) The tandem interferometer system. **LD1**:670nm wavelength laser diode; **LD2**: 780nm wavelength laser diode; **BS**: beam splitter; **M**: mirror; **PZT0, PZT1**: piezoelectric actuators; **System2000**: controller for PZTs; **Amp**: amplifier; **I, II**: interferometers.

that of the second interferometer is given by X_2. The output power of the source is I_0, and the coherence length of the illuminating source is L_c. It may be assumed that the ALDs of the two interferometers are larger than the coherence lengths of the sources ($|X_1|$, $|X_2|>L_c$) and are approximately equal to each other ($X_1 \approx X_2$), and so the output of the system with a single wavelength illuminating source can be obtained from Eq. (2.6)

$$I(X) = \frac{I_0}{4}\{1 + \frac{1}{2}\exp(-(\frac{4X}{L_c})^2)\cos(\frac{4\pi X}{\lambda})\} \tag{5.1a}$$

where $X = X_1 - X_2$ is the difference of ALDs of the two interferometers, and λ is the wavelength of the source. Similarly to Eq. (4.4), the output of the system with a two wavelength source, in the case when the intensities of the two wavelengths components are equal to each other, is given by

$$I(X) = \frac{I_0}{4}\{1 + \frac{1}{2}\exp(-(\frac{4X}{L_c})^2)\cos(\frac{4\pi X}{\lambda_a})\cos(\frac{4\pi X}{\lambda_m})\} \tag{5.2a}$$

where $X = X_1 - X_2$ is the difference of the ALD of the two interferometers, $\lambda_a = \dfrac{2\lambda_1\lambda_2}{\lambda_1 + \lambda_2}$ is an average wavelength and $\lambda_m = \dfrac{2\lambda_1\lambda_2}{|\lambda_1 - \lambda_2|}$ is termed the modulation wavelength. From Eq. (5.1a) and Eq. (5.2a), it can be seen that the maximum amplitude of the AC component of the output from a tandem Michelson interferometer system is equal to half of that of the DC component. The central position of the visibility profile is located at $X_1 = X_2$, which means that any quasi-static variation in the value of X_1 can be determined by measuring X_2, when maximum output occurs. This is the key point of the use of the tandem interferometer system as an optical fibre sensing system.

Considering the noise in the practical system (see Section 2.2), Eq. (5.1a) and Eq. (5.2a) can be rewritten as

$$I(X) = \frac{I_0}{4}\{1+\frac{1}{2}\exp(-(\frac{4(X+n_p)}{L_c})^2)\cos(\frac{4\pi(X+n_p)}{\lambda})\} + n_I \qquad (5.1b)$$

$$I(X) = \frac{I_0}{4}\{1+\frac{1}{2}\exp(-(\frac{4(X+n_p)}{L_c})^2)\cos(\frac{4\pi(X+n_p)}{\lambda_a})\cos(\frac{4\pi(X+n_p)}{\lambda_m})\} + n_I$$

$$(5.2b)$$

where n_p and n_I are defined as the phase noise and the intensity noise, and their root mean square (rms) values are σ_p and σ_I respectively (see Section 2.2). In a practical system, the phase noise is usually induced by the vibration and the drift of the interferometers, by the noise of the capacitive displacement sensor and by the turbulence of air in the room. The intensity noise is usually induced by the fibre lead, by the source intensity fluctuations, and by the shot noise and the thermal noise from the detector. The noise induced by the fibre lead, which is called the "modal noise" [3], represents the main part of the intensity noise.

5.3 Experimental set-up

5.3.1.Introduction

Fig. (5.1) shows a schematic diagram of the experiment system used to investigate the system. The system consists of two Michelson interferometers linked by a multimode fibre. Multimode laser diodes (LDs) were used as the illuminating sources. The light beam passes through the first sensing interferometer, and is then launched into the multimode linking fibre. The output light beam from the multimode linking fibre is

collimated and injected into the second recovery interferometer. The output of the system is focused by a lens and detected with the photodiode (PD). Each Michelson interferometer has one mirror driven by a piezoelectric actuator (PZT0 & PZT1, type MTP105, manufactured by Queensgate Instruments Ltd)[12][13]. The analogue output of the detector was converted into a digital signal for computer processing. Part of the fibre (about 60cm in length) was deliberately shaken by an oval wheel driven by a motor. Thus, repeatable results for the noise generated could be obtained when such a fibre vibrating arrangement was utilized. Both LDs were driven with a current which is below the threshold, so that the corresponding coherence lengths of the outputs are relatively short (about 15μm).

In the experiment, the arm length differences (ALDs) of the two interferometers were set to be approximately equal to 2mm, and the resulting difference of the ALDs is smaller than the coherence length of the source. The PZT actuator in the reference interferometer (PZT1) was then scanned to obtain the output visibility fringe pattern of the system.

5.3.2 NanoPositioning system used (System2000)

System 2000 NanoPositioning [13] used in this system is a set of components that can be configured to control the PZT actuator. It is a closed-loop controlled system and the position of the PZT actuator is measured by a capacitance position sensor. Fig. (5.2) is a schematic diagram of the System2000 used to control a PZT actuator, which consists of a high voltage amplifier (DM100), a servo module (SM), and a PZT actuator with a capacitive displacement sensor (NS). The functions of the each components are shown in Fig. (5.2), and this components are described in detail below:
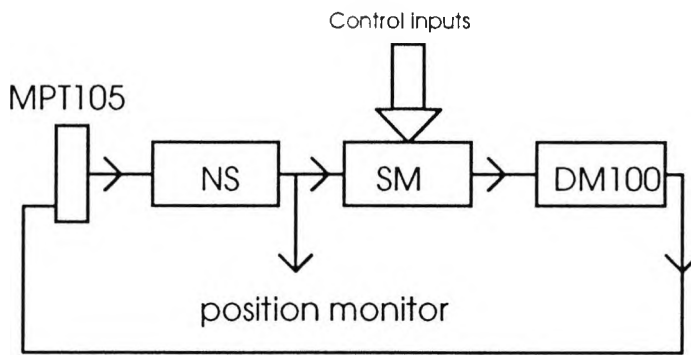
Fig. (5.2) Closed-loop controlled PZT actuator. NS-NanoSensor, SM-Servo Module.

Piezoelectric translator actuator MPT105

The PZT actuator (model MPT105) is a low voltage device with a multi-layer structure consisting of alternate in ceramic and metallic layers. Its range is 117.9μm. It was used to change the positions of the mirrors in the WLI system.

NanoSensor NS90

The NanoSensor (model NS90) is a capacitive displacement sensing device capable of resolving to better than 0.1nm. It has a range of more than 500μm and a frequency response of up to 5kHz. Its nonlinearity is 0.6% and output noise is 2.8nm (root mean square (rms)). Two sensor plates form a parallel plate capacitor. The relative position of these plates is measured by monitoring the change in capacitance as the gap between the plates alters. It was used to measure the displacement of the PZT actuator in the WLI system.

High voltage amplifier DM100

The DM100 is a high voltage amplifier which is used for driving the PZT actuator. It supplies a voltage in the range 0V to 170V to drive the PZT actuators over the full displacement range (about 100μm). The output of the amplifier can be controlled from an analogue signal (-15V→15V) through the front panel or via a 14 bit digital to analogue converter through the back plane connector. The gain of the amplifier is 16.

SM Servo Module

The SM Servo Module connects the output of the Nanosensor and the input of the DM100 high voltage amplifier to form a closed-loop for the servo controlling. Using the closed-loop control technique, the PZT translator can be positioned to within the accuracy to which the NanoSensor can measure, eliminating the non linearity, hysteresis and creep of the PZT translator.

The SM generates a command voltage from the external analogue input or digital inputs. (See Fig. (5.2)) This command is then compared with the NanoSensor output and the difference signal amplified and integrated. The resultant output can be used directly or an inverter can be switched in. The inverter is required to ensure negative feedback around the loop in systems. The gain of the amplification is selectable, via links on the circuit card, and the time constant of the integration is selectable by links and can be changed by a trimmer potentiometer accessible from the module front panel.

IEEE-488 Interface

The IEEE-488 is an optional model that allows the System2000 to be controlled by a computer via an IEEE-488 bus. It has Talk/Listener capability. The interface may be used to:

1) Set the output voltage of DM100 high voltage amplifier.
2) Read back position information from NS NanoSensor module (NS90).
3) Set a position of a closed loop system using the SM servo module.

Functions 2 and 3 are exploited in the system shown in Fig. (5.1) to set the positions of the mirrors and read back the positional information of the mirrors.

5.3.3 The program controlling the PZT actuator and collecting the output from the system

A program has been produced to position the PZT0, PZT1 and collect the intensity output from the WLI system. The flow chart of the program to obtain the output fringe pattern of the system is shown in Fig. (5.3). First, it sets the position of the PZT0, then scans the PZT1 to collect the data of the output fringe pattern. The scanning range and the scanning step size of the two PZT actuators can be changed by selecting the value of the parameters in the program.

5.3.4 Accuracy of the PZT actuators

From the user's guide of the System 2000, the resolution of the PZT actuator used in the system is about 2.8nm, which is estimated under the conditions of test of the
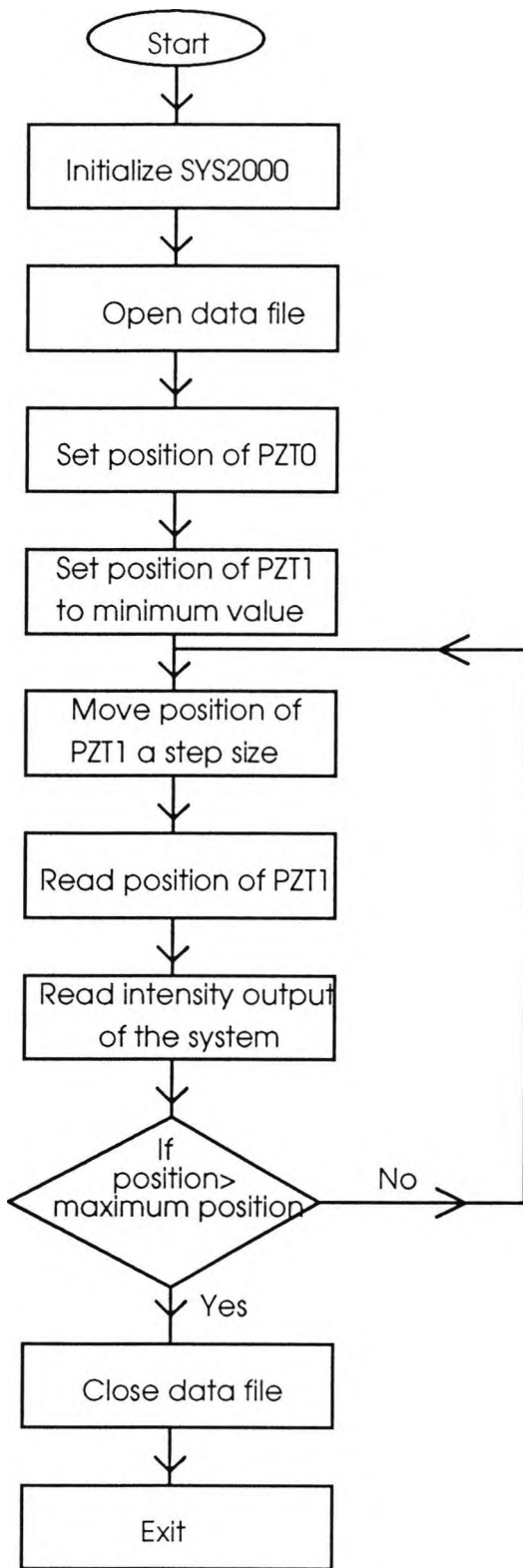
Fig. (5.3) Flow chart of the program for the data collection

manufacturer. When the PZT actuator was used in practice, the resolution of the PZT actuator was found to be poorer than that determined by the Nano Sensor due to the presence of vibration. In the experiment to investigate this, all the components of the system are put on a vibration-isolated table. However, there still is some vibration remaining, which will induce phase noise onto the output of the system.

The rms values of the error of the PZT1 are 4.7nm and 4.6nm for the coarse digital analogue converter (DAC) and the fine DAC respectively. The rms value of the error of the PZT0 is 6.8nm for both the coarse DAC and the fine DAC. The rms values of the errors, which were experimentally measured, are larger than that shown in the user's guide, namely 2.8nm. This is probably due to the remaining vibration of the vibration isolated table.

5.3.5 Low frequency stability of the interferometers

The low frequency stability of the interferometers in the experimental set up shown in Fig. (5.1) was investigated. Figs. (5.4a) and (5.4b) are the experimental results of the central position drifting of the output fringe pattern produced by the interferometers. They have shown that the central position of the interferometers drifts slowly. This "drifting" of the central position may be caused by the mechanical instability of the mirrors and may be removed by using a more sophisticated mechanical installation. From the Figs. (5.4a) and Figs. (5.4b), the displacement caused by the drift of the interferometers is about 1nm per minute and 3nm per minute for the interferometer with PZT0 and PZT1 respectively. The results of the central position measurement shown in Fig. (5.4a) and Fig. (5.4b) are obtained by using a central fringe curve fitting method, which will be discussed later in this Chapter. Each data point in the figures is an average result of six measurements and the length of the error bar is equal to the standard deviation of the measurements.

97
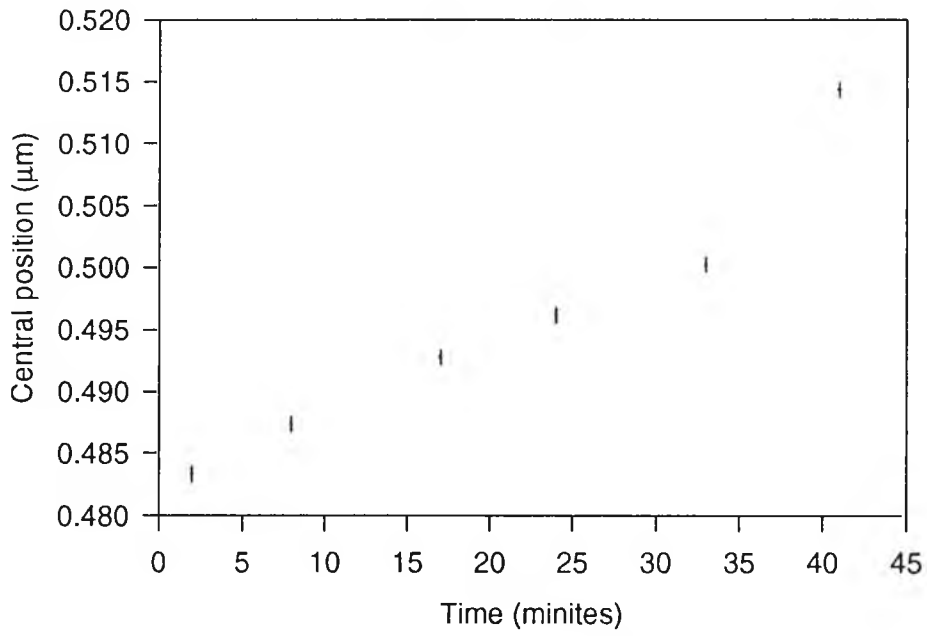
Fig.(5.4a) Drifting of the interferometer with PZT1
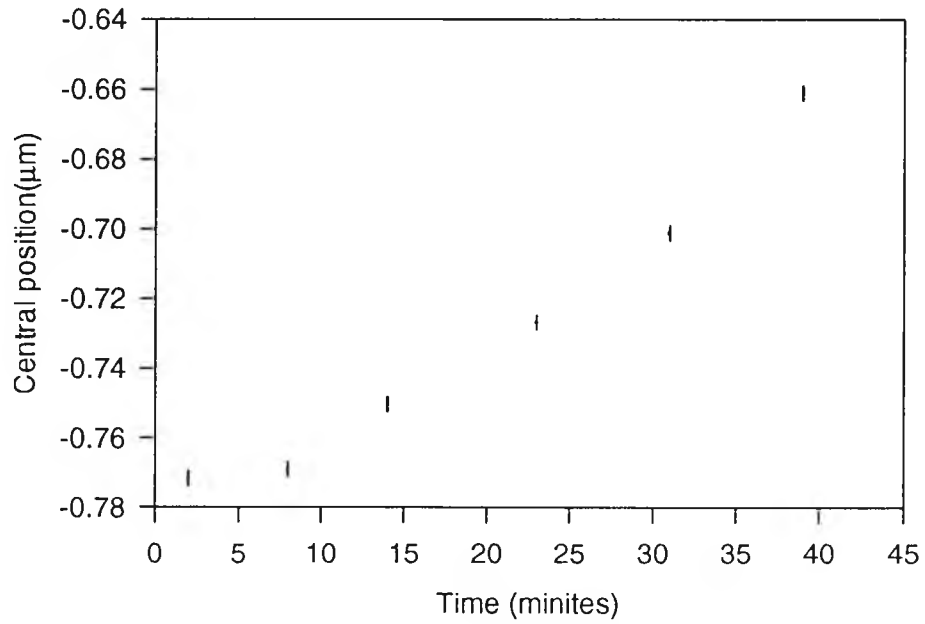
Fig.(5.4b) Drifting of the interferometer with PZT0

5.4 Modal noise in the system comprising two Michelson interferometers linked with a multimode fibre (system TMM)

5.4.1 Introduction

Modal noise in the system MM has been studied theoretically and experimentally in Chap.3. The results show that the output SNR in the system MM is proportional to the square root of the number of modes transmitted in the fibre and is dependent on the OPD between the adjacent modes of the fibre when the multimode fibre is shaken.

In this section, a system consisting of two Michelson interferometers linked with a multimode fibre (system TMM) has been investigated. A curve fitting technique has been introduced to assess the SNR of the output of the system. An actual position measurement using the system in the presence of modal noise has been carried out. It was found that the output SNR of the system and the repeatability of the displacement measurement vary with the types of linking fibre used. The experimental results were in agreement with those expected by the theoretical analysis.

5.4.2 Theory and analysis

According to the theoretical analysis in Chapter 3, it is reasonable to assume the following theoretical results for the system TMM:

1) The output SNR of the system TMM is proportional to the square root of the mode number transmitted in the fibre. when the fibre is perturbed

2) The output SNR of the system TMM increases as the OPD between the adjacent modes increases when the fibre is perturbed.

In order to assess the value of the noise in the output of the system, a curve fitting algorithm using a function describing the theoretical output of the interferometer has been introduced, which can be given by

$$y(x) = A \exp\{-[\frac{4(x - x_0)}{L_C}]^2\} \cos[\frac{4\pi(x - x_0)}{\lambda_a}] + B \qquad (5.4)$$

In this expression, A is the amplitude of the cantral fringe of the output pattern, B is the DC value of the output. L_C and λ_a are the coherence length and the average wavelength of the source, respectively. x is the position of the scanning mirror in the reference interferometer and x_0 is the central position of the central fringe. It should be noted that there is an extra factor of 2 compared with Eq.(2.6). This is because that x in Eq.(5.4) represents the position of the mirror in the interferometer while x_s and x_r in Eq.(2.6) are the OPD of the interferometer

When the function given by Eq.(5.4) is used to fit a fringe pattern obtained from experimental data, the sum of the squares for error (SSE) [6] can be minimised by adjusting the parameters, A, B, L_C, λ_a, and x_0 in the fitting process. The value of the SSE factor is given by

$$SSE = \sum_m (I_m - y(X_m))^2 \qquad (5.5)$$

where $[X_m, I_m]$ represent the experimentally obtained fringe pattern. X_m is the position of the PZT actuator and I_m is the output intensity of the system. The peak-to-peak value of

100

the central fringe $2A$ (see Eq.(5.4)) may be defined as the value of the signal, and the noise value, termed as N, can be defined as

$$N = \sqrt{\frac{1}{P} SSE}$$

(5.6)

where P is the number of data points in the digitised fringe pattern, and the value of SSE is defined by Eq. (5.5). The measured SNR, $(SNR)_m$ is then defined by

$$(SNR)_m = 20 Log(\frac{2A}{\sqrt{\frac{1}{P} SSE}})$$

(5.7)

In order to verify the determination of the SNR described by Eq.(5.7), a simulation has been carried out. A simulated output fringe pattern with the presence of the intensity noise can be expressed as

$$I_m = A \exp(-[\frac{4(md - x_0)}{L_C}]^2) \cos(\frac{4\pi (md - x_0)}{\lambda_a}) + B + n_I(m)$$

(5.8)

where $n_I(x)$ is the normally distributed intensity noise with an root mean square value σ_I. m is an integer and d is the sampling gap. It should be pointed out that the phase noise is ignored and only the intensity noise is considered. This is because we want to investigate the modal noise in the system, which is the main part of the intensity noise. The SNR associated with I_m (see Eq.(5.8)) can be defined as the given SNR $(SNR)_g$, we have

$$(SNR)_g = 20\log(2A / \sigma_I)$$

(5.9)

The SNR in the digitised fringe pattern given by Eq.(5.8) can also be determined by using the curve fitting algorithm discussed in this section. The SNR determined by the curve fitting algorithm is given by Eq. (5.7). Fig.(5.5) shows the curve fitting approach applied to the central fringe of the simulated fringe pattern. The jagged line is the simulated fringe pattern given by Eq.(5.8) when $(SNR)_g$ is equal to 30dB and the smooth solid line is the fitted curve of a cosine function, which SSE value is minimised.

Fig.(5.6a) shows a simulation result comparing the value $(SNR)_g$ (see Eq.(5.9)) and the value $(SNR)_m$ (see Eq.(5.7)). The data number P is chosen to be 800 in the simulation. It can be seen from Fig.(5.6a) that the value $(SNR)_m$ is approximately proportional to the vlaue $(SNR)_g$. Fig.(5.6b) shows the differences between the value $(SNR)_m$ and the vlaue $(SNR)_g$... This difference can be regarded as the error of the SNR measurement with the curve fitting approach. It can be seen from Fig.(5.6b) that the maximum SNR measurement error is about 0.5dB.

The simulation results shown in Fig.(5.6a) and Fig.(5.6b) indicate that the curve fitting approach can be used to assess the value of the intensity noise in the digitised fringe pattern. Compared with the method using a spectrum analyser, curve fitting technique offers several advantages: First, it is low cost. Second, it can derectly obtain the rms value of the noise over the whole frequency range.

The aim of the work described in next section is to experimentally investigate the modal noise of the system TMM when different types of multimode fibre link were perturbed. The details of the experimental arrangement are discussed below.
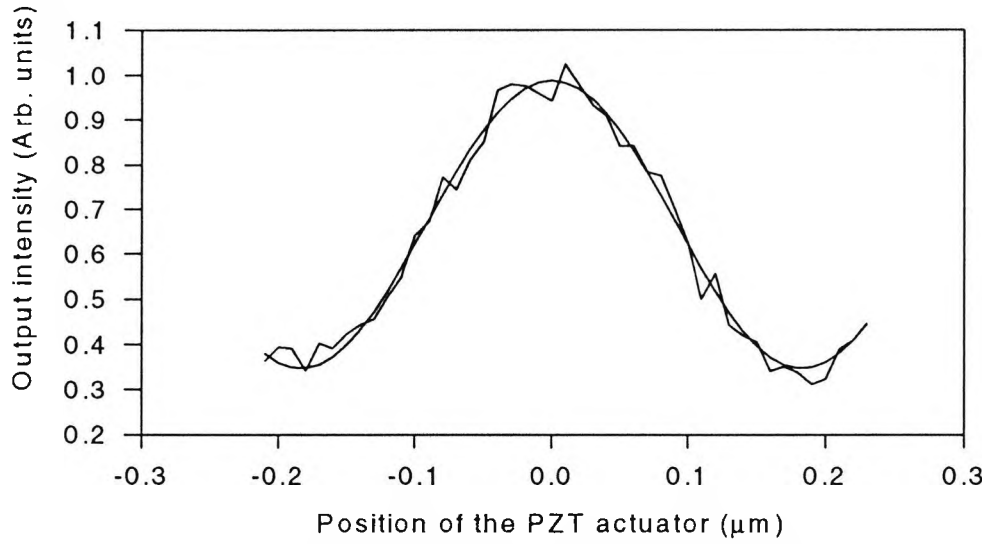
Fig.(5.5) Comparison between the curve fitting result and the central fringe of the simulated output fringe pattern when its SNR is 30dB.
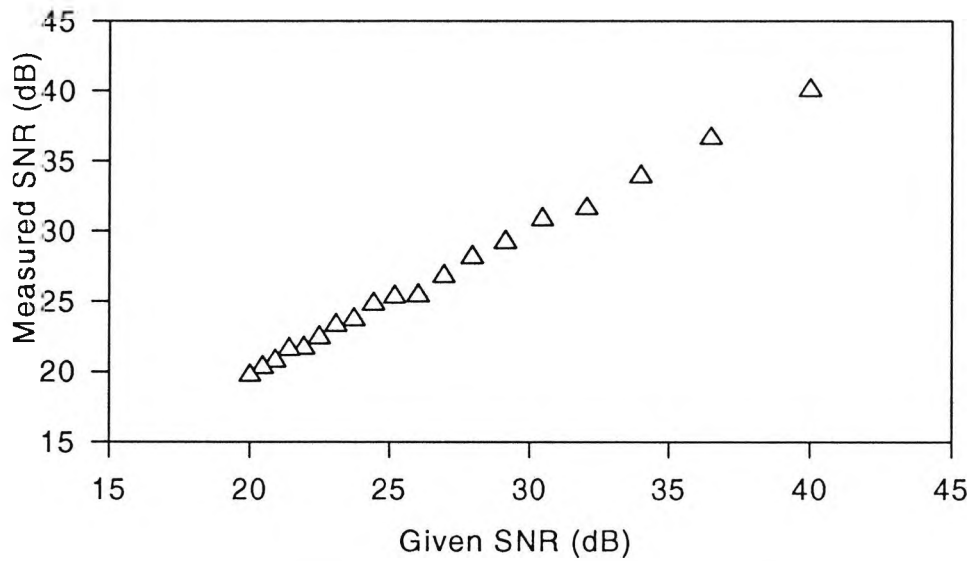
Fig.(5.6a) Simulated result comparing measured SNR and given SNR

103
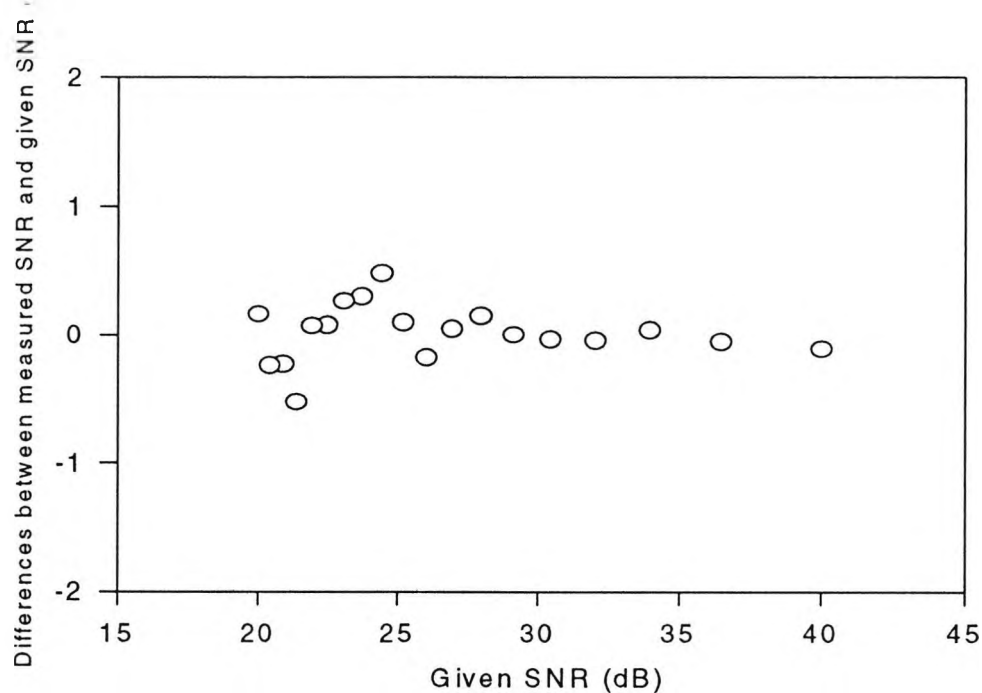
Fig.(5.6b) Simulated result showing the measured error of
the SNR using the curve fitting technique.

5.4.3 Experimental arrangement

Fig. (5.1) shows a schematic diagram of the experimental system used. The system consisted of two Michelson interferometers linked by a multimode fibre. Two multimode laser diodes (with wavelengths of 780nm and 670nm, respectively) were used as the illuminating sources. Several types of multimode fibres were used to connect the two interferometers. Part of the linking fibre (about 60cm in length) was deliberately shaken by an oval wheel driven with a motor. It was found that repeatable results for the noise generated could be obtained when such a fibre vibrating arrangement was utilized. The driving current of the LDs were below the threshold value. As a results, the corresponding coherence lengths of the LDs were relatively short (about 15μm).

104

In the experiment, the arm length differences (ALDs) of the two interferometers were set to be approximately equal to each other, so that the difference of the ALDs is smaller than the coherence length of the source. The PZT actuator in the reference interferometer (PZT1) was then scanned to obtain the output visibility fringe pattern of the system.

Fig.(5.7) shows an experimentally obtained fringe pattern from the system. Similar results for a one-interferometer system are described by Chen *et al* [8]. The fringe pattern was digitised and modal noise was present due to the shaking of the multimode fibre link. A curve fitting algorithm was applied on the fringe pattern and Eq.(5.7) was used to calculate the SNR of the output. In order to eliminate the phase noise, which was mainly induced by the vibration of the mirrors, the sampling gap of the raw data was simply set equal to the average sampling gap before using the curve fitting technique to measure the SNR. The results of SNR measurement is listed in Table(5.1) when a 50µm core diameter (parabolic index) and a 100µm core diameter (step index) linking fibre were used. $(S/N)_{50}$, $(S/N)'_{50}$, $(S/N)_{100}$ and $(S/N)'_{100}$ may be defined as the SNRs of the output when 50µm and 100µm core linking fibre were used. A prime denotes the value when the fibre was shaken. The SNR reductions in these two cases, $\Delta(S/N)_{50}$ and $\Delta(S/N)_{100}$, can be defined by

$$\Delta(S/N)_{50} = (S/N)_{50} - (S/N)'_{50} \qquad (5.10)$$

$$\Delta(S/N)_{100} = (S/N)_{100} - (S/N)'_{100} \qquad (5.11)$$
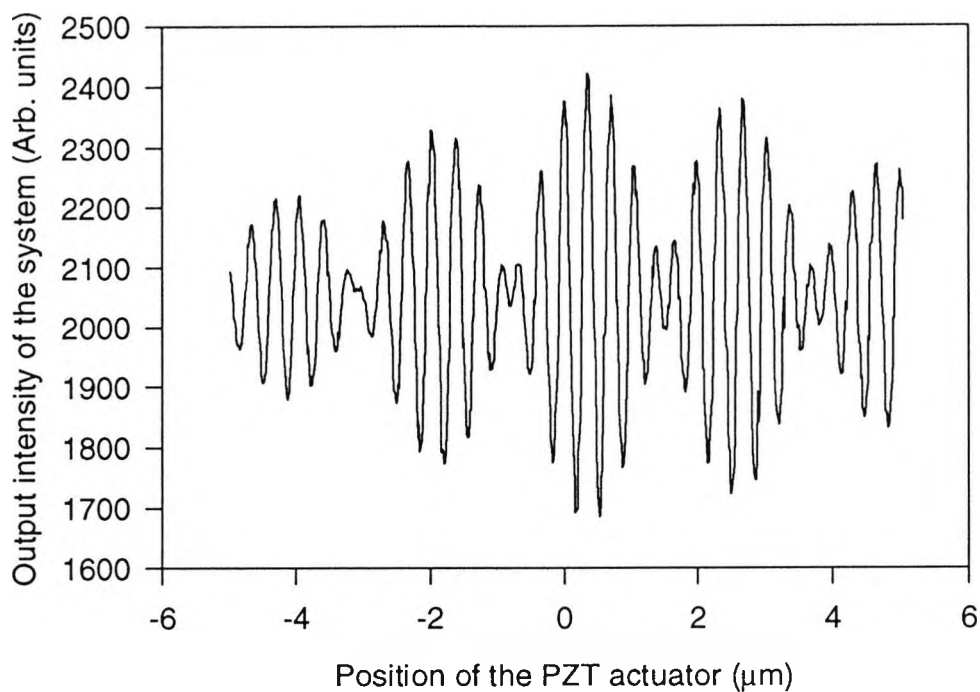
Fig.(5.7) Experimental output fringe pattern of the system

For each linking fibre, five measurements have been carried out, as shown in Table(5.1). From this table, it can be seen that the output SNR of the system with the 100µm core diameter fibre (step index) is higher than that with the 50µm core diameter fibre (parabolic index) by about 2dB. This experimental resut indicate that the step index multimode fibre is better as a linking fibre than parabolic index multimode fibre for the system TMM. This can be explained by the the following reason: (1) The mode number in the 100µm core diameter fibre is more than that of the 50µm core diameter fibre and (2) the OPD between adjacent modes in the parabolic index fibre is much smaller than that of the step index fibre. This result is in agreement with that expected by the theoretical analysis given in Section 5.4.2. In addition, this result is same as that obtained in Section 3.5, which means that step index multimode fibre and larger core diameter multimode fibre are better as

106

linking fibres for the system TMM and the system MM because they induce lower modal noise than parabolic index fibres.

Table (5.1). Measured SNR in the output of the system by using a curve fitting method.

	1	2	3	4	5
$(S/N)_{50}$	29.9dB	31.2dB	30.9dB	32.0dB	30.8dB
$(S/N)'_{50}$	27.2dB	28.2dB	28.4dB	28.6dB	27.1dB
$\Delta(S/N)_{50}$	2.7dB	3.0dB	2.5dB	3.4dB	3.7dB
$(S/N)_{100}$	32.1dB	32.5dB	32.7dB	33.1dB	33.0dB
$(S/N)'_{100}$	31.2dB	31.6dB	31.4dB	32.0dB	31.8dB
$\Delta(S/N)_{100}$	0.9dB	0.9dB	1.3dB	1.1dB	1.2dB

In the experiment, the interferometer I represents a sensing interferometer and the interferometer II represents a reference interferometer. In other words, PZT0 was used to set the displacement and PZT1 to measure the central position of the output fringe pattern. With this arrangement, an investigation of the modal noise effect on the central position measurement were carried out when different types of fibre links were used. The values of the arm length difference (ALD) of the sensing and reference interferometer were set to about 2mm. Then, the output fringe patterns were obtained by scanning the PZT actuator in the reference interferometer (PZT1). The central positions of the output fringe patterns were determined with the use of the maxmum visibility method. The repeatability E of the central position measurements represent the standard deviation of six consective measurements.

The measurement results are listed in Table 5.2, where the types of the fibres and the measurement repeatabilities (of standard deviations) with and without the fibre being shaken, E' and E, are shown. The central position was determined by using the maximum visibility method [7]. It can be seen from the table that the repeatability of the central position measurement was worse if the fibre was perturbed. This can be explained by the fact that modal noise was present when the linking fibre was shaken.

Table (5.2). Displacement measurement repeatability of the system with different linking fibres.

D & Type of the fibre	E	E'
single mode fibre	5.7nm	6.0nm
200μm (step index)	6.6nm	7.5nm
100μm(step index)	8.1nm	10.2nm
50μm(graded index)	9.0nm	19.0nm

It can also be seen from Table 5.2 the following trends:

1) The repeatability of the central position measurement became better as the core diameter of the linking fibre increases. This can be explained by the fact that the larger diameter fibre can support the propagation of more modes than thin fibre and the output SNR of the system increases as the number of the modes transmitted in the linking fibre increase.

2) The repeatability of the system with a step index linking fibre was better than that of the system with a parabolic index linking fibre. This can be explained by the fact that the OPD of the step index fibre between adjacent modes is much larger than that of the parabolic

108

index fibre (see Section 2.4) and modal noise in output of the system decreases as the OPD between the adjacent modes increases.

3) The measurement repeatability of the system with a single mode linking fibre was slightly better than that of the system with a 200μm core diameter linking fibre (step index). This may be explained by considering that the modal noise in the system TMM with a step index fibre was much lower than that of the amplitude of the central fringe. Therefore, its effect on the central position measurement was very low.

5.4.4 Summary

In this section, the SNR of the system TMM with different types of linking fibres has been measured experimentally. The results show that the output SNR of the system with a 100μm core diameter linking fibre (step index) was higher than that with a 50μm core diameter linking fibre (graded index). The displacement measurement repeatability of the system with different linking fibres was measured. The results showed that the repeatability (of standard deviations) of the system as the fibres were shaken were 6.0nm, 7.5nm, 10.2nm, 19.0nm when the system was linked with a single mode fibre, with a 200μm core diameter fibre (step index), with a 100μm core diameter fibre (step index) and with a 50μm core diameter fibre (parabolic index) respectively. The experimental results show that:

1) A step index fibre was better as a linking fibre for the system TMM than a graded index fibre as the OPD of a step index fibre between the adjacent modes is much larger than that of a graded index fibre.

2) The system TMM with a larger core diameter linking fibre induced less modal noise as it supports the propagation of more modes than a small core diameter linking fibre.

3) The displacement measurement repeatability using the system TMM with a single mode fibre was slightly higher than that with a 200μm core diameter linking fibre (step index).

Results 1) and 2) are in agreement with those expected by the theoretical analysis in Section 5.4.2.

5.5 A signal processing scheme using curve fitting algorithms

5.5.1 Introduction

From the system described in Fig.(5.1), a digitized output fringe pattern can be obtained by using a computer, as shown in Fig.(5.7). The central fringe of the output fringe pattern can be identified using the maximum visibility method [1] and the position where the maximum intensity ocurs can be regarded as a coarse central position. However, due to the presence of modal noise and the limitation of the sampling gap, the resolution of the coarse central position measurement is limited. In order to increase the resolution of the central position measurement, curve fitting techniques have been proposed and developed in this section. Following this introduction, a curve fitting algorithm using a fourth order polynomial is introduced. Then, a curve fitting algorithm using a cosine function is investigated, in which the theoretical resolution of the central position measurement is given.

5.5.2 Curve fitting signal processing approach using a polynomial

Polynomials are widely used function for curve fitting processing of experimental data. It is desirable to investigate such a technique for the purpose of determining the central position of a digitised interferometric fringe. With the use of a continous curve to fit the digitised fringe pattern, it is possible to reduce the effect of noise and improve the central position measurement of the output from a WLI system. The signal processing scheme introduced in this section consists of two main parts, which are

1) Identifying the central fringe by using the maximum visibility method [1].

111

2) Using a curve fitting technique to reduce the effect of noise presented in the fringe profile and thus to improve the central position measurement.

These are achieved by using the following steps

(a) *Determing the position of the maximum visibility of the output fringe pattern.* Suppose that $(X[i], I[i])$ are the raw data of the output fringe pattern of the system, where $X[i]$ represent the positions of the scanning mirror in the reference interferometer and $I[i]$ represent the corresponding output intensities of the system. The position of the maximum visibility of the fringe pattern is x_c', which may be defined as the coarse central position, providing the central fringe can be identified through simply investigating its amplitude. If a dual wavelength illuminating source was used in the system, the central peak can be identified by investigating the amplitude of the fringes because the relative intensity of the central fringe from a dual wavelength system is much higher than that of a single wavelength system [8, 9].

The coarse central position, x_c', was an approximate measured result. The noise in the system will induce a measurement error and the sampling gap of the digitied fringe pattern will limit the measurement accuracy. In order to increase the accuracy of the central position measurement, the following steps are required to obtain an improved result of the central position measurement. The new central positon can be termed as x_c, whose resolution can be much smaller than that of the sampling gap.

(b) *Subtracting the data set, $X[i]$, by x_c'.* The new values of the data set $X'[i]$ are then given by

$$X'[i] = X[i] - x'_c \tag{5.12}$$

After this signal processing step, the central position of the fringe pattern given by the new data set $(X'[i], I[i])$ is close to zero. Hence, it is easier to fit a polynomial curve to the central fringe of the new fringe pattern.

(c) *Fitting a fourth order polynomial to the central fringe.* The polynomial used for curve fitting, $y(z)$, is given by

$$y(z) = az^4 + bz^3 + cz^2 + dz + e \tag{5.13}$$

where a, b, c, d, and e are coefficients of the polynomial, by adjusting the values of the a, b, c, d, and e, the sum of squares for error (*SSE*) can be minimized [14]. The SSE factor is given by

$$SSE = \sum_i (I[i] - y(X'[i]))^2 \tag{5.14}$$

The curve which minimizes the *SSE* value is the fitted curve. After step (b), the central position of the data set becomes close to zero. However, due to the modal noise and the limitations of the sampling gap, the fringe central position, x'_c, was just an estimate of the central position of the raw data. Hence, the central position of the new data set $(X'[i], I[i])$ was not exactly equal to zero. The central position of the new data set Δx_c is a deviation of the coarse central position x'_c from the "real" central position. The following step is then used to estimate the value of Δx_c and determine the "real" central position.

(d) *Calculating the improved value of the central position of the raw data,* x_c, which is simply given by

$$x_c = x'_c + \Delta x_c \qquad\qquad (5.15)$$

where Δx_c is the position of the maximum visibility of the fitted curve, which is a deviation of the coarse central position from the "real" central position.

The resolution of the "real" central position can be smaller than the sampling gap, because the value of Δx_c is calculated from the equation governing the fitted curve which is a continuous function.

5.5.3 Curve fitting signal processing approach using a cosine function

The curve fitting approach can also be realised by using a cosine function because the central fringe of the output from a WLI system can be represented by a cosine function (see Eq.(2.6)). In this section, a curve fitting approach using a cosine function has been introduced and a theoretical investigation on the approach are included. The approach can be achieved by the following two steps:

(a)*Finding the central fringe of the output fringe pattern and determining the position of the maximum visibility,* x'_c, which may be defined as the coarse central position. This is a "first attempt" at determining the actual central position. With the use of a dual wavelength source in the system, the central fringe can be easily identified by using the maximum visibility method [7], which means that the error of the coarse central position can be much smaller than a wavelength. However, due to the presence of the noise and the limitation of the sampling gap, the resolution of the central position measurement is

114

restricted. In order to increase the resolution of the central position measurement, the curve fitting technique is used to obtain an improved central position in the next processing step.

(b)*Fitting a cosine function to the central fringe.* The cosine function, $y(x)$, is given by

$$y(x) = a\cos[4\pi(x - x_0)/\lambda_a] + b \tag{5.16}$$

where a is the amplitude of the central fringe, λ_a is equal to the wavelength of the source, b is the DC component of the output signal, and x_0 is the central position of the fringe pattern. The values of the parameters, a, b,λ_a, can be calculated from the experimental data set and the initial value of x_0 was set equal to the coarse central position x_c' at the beginning of the curve fitting signal processing. Then, by adjusting the value of x_0, the sum of squares for error (SSE) can be minimised. The SSE is given by [14]

$$SSE = \sum_m (I_m - y(X_m))^2 \tag{5.17}$$

where $[X_m, I_m]$ is the experimental data set, X_m is the position of the PZT actuator in the reference interferometer, I_m is the output light intensity of the system corresponding to the position X_m. If the values of a', b', λ_a', and x_0' are the values of parameters with which the value of the factor SSE was minimised, the best fitted curve can then be written as

$$y'(x) = a'\cos[4\pi(x - x_0')/\lambda_a'] + b' \tag{5.18}$$

where the value of the parameter x_0' of the fitted curve is the new central position of the output fringe pattern.

115

To investigate the method of the curve fitting signal processing scheme, suppose the central fringe of the output of the system with added random noise is expressed as

$$X_m = md + n_p(m) \tag{5.19a}$$

$$I_m = a\cos[4\pi\,(md - X_0 + n_p(m))/\lambda_a] + b + n_I(m) \tag{5.19b}$$

In this expression, m is an integer, d is the sampling gap of the PZT actuator, $n_p(m)$ and $n_I(m)$ are the phase noise and the intensity noise at the mth sampling point, which are assumed to be normally distributed noise with root-mean-square values of σ_p and σ_I, respectively. When a curve described in Eq.(5.16) is used to fit the simulated experimental data given by Eq.(5.19a) and Eq.(5.19b), the SSE value is given by

$$SSE = \sum_{m=1}^{N}(I_m - y(md))^2$$
$$= \sum_{m=1}^{N}\{a\cos(4\pi(m*d - X_0 + n_p(m))/\lambda_a) - a\cos(4\pi(m*d - x_0)/\lambda_a) + n_I(m)\}^2$$

$$\tag{5.20}$$

Assuming $\Delta x = x_0 - X_0$, in the case of $\sigma_p \ll \lambda_a$ and $\Delta x \ll \lambda_a$, Eq.(5.20) can be rewritten as

$$SSE = \sum_{m=1}^{N}\{-\frac{4\pi a}{\lambda_a}\sin(4\pi(m*d - X_0)/\lambda_a)(\Delta x + n_p(m)) + n_I(m)\}^2 \tag{5.21}$$

where $\Delta x = x_0 - X_0$ is the error of the central position measurement and N is the number of data points covered by the curve fitting. To obtain the value of Δx that minimises the SSE value, the following equation has to be satisfied

$$\frac{\partial (SSE)}{\partial (\Delta x)} = 2\sum_{m=1}^{N} \{(\frac{4\pi a}{\lambda_a}) \sin(4\pi (md - X_0)/\lambda_a)(\Delta x + n_p(m)) - n_I(m)\} \frac{4\pi a}{\lambda_a} \sin(4\pi (md - X_0)/\lambda_a)$$
$$= 0$$

(5.22)

From Eq.(5.22), the error of the central position of the ith measurement, Δx_i, is given by

$$\Delta x_i = \frac{\lambda_a}{4\pi a} \frac{\sum_{m=1}^{N} n_I(m) \sin(4\pi(md - X_0)/\lambda_a)}{\sum_{m=1}^{N} \sin^2(4\pi(md - X_0)/\lambda_a)} - \frac{\sum_{m=1}^{N} n_p(m) \sin^2(4\pi(md - X_0)/\lambda_a)}{\sum_{n=1}^{N} \sin^2(4\pi(md - X_0)/\lambda_a)}$$

(5.23)

where a is the amplitude of the central fringe, λ_a is the average wavelength of the source, X_0 is the central position of the central fringe, m is an integer, d is the sampling gap of the PZT actuator in the reference interferometer, and $n_p(m)$ and $n_I(m)$ are the phase noise and the intensity noise with their root mean square values, σ_p and σ_I respectively. From Eq.(5.23), the error of the central position measurement is dependent on the wavelength of the illuminating source, λ_a, i.e. the measurement error increases when a longer wavelength illuminating source is used. To simplify the analysis, it may be assumed $X_0 = 0$. Then the Eq.(5.23) can be simplified to

$$\Delta x_i = \frac{\lambda_a}{4\pi a} \frac{\sum_{m=1}^{N} n_I(m) \sin(4\pi(md)/\lambda_a)}{\sum_{m=1}^{N} \sin^2(4\pi(md)/\lambda_a)} - \frac{\sum_{m=1}^{N} n_p(m) \sin^2(4\pi(md)/\lambda_a)}{\sum_{m=1}^{N} \sin^2(4\pi(md)/\lambda_a)}$$

(5.24)

The theoretical resolution of the system, Δ, can then be expressed as

117

$$\Delta = \sqrt{\{\frac{1}{M}\sum_{i}^{M}(\Delta x_i)^2\}} \qquad (5.25)$$

where M is the number of repeated measurements. A calculation has been carried out according to Eq.(5.25). In the calculation, M was chosen to be 1000, λ_a was equal to $0.72\mu m$, the rms value of the phase noise σ_p was equal to 8nm. The SNR is defined as the peak-to-peak value of the central fringe divided by the rms value of the intensity noise $2a / \sigma_I$. The calculation result is shown in Fig.(5.6), where the triangles, squares and round dots represent the resolutions of the central position measurement when the SNR of the fringe pattern was 40dB, 30dB and 20dB respectively. It can be seen that the resolution improves as the number of the data points covered by the curve fitting, N, increases. This can be explained by considering that the noise effect was averaged by the curve fitting algorithm. Therefore, the more points that were covered by the curve fitting, the lower the noise effect on the central position measurement will be. In the case of N=36, it can also be seen that the resolution of the measurement was about 1.7nm, 1.9nm, and 3.0nm when the SNR of the fringe was equal to 40dB, 30dB, and 20dB respectively. The result indicate that the resolution of the central position measurement of a digitised fringe pattern with the curve fitting algorithm can be as better as 1/400 of a wavelength.

This resolution was similar to that obtianed by a system with a lock-in amplifier [10, 11].
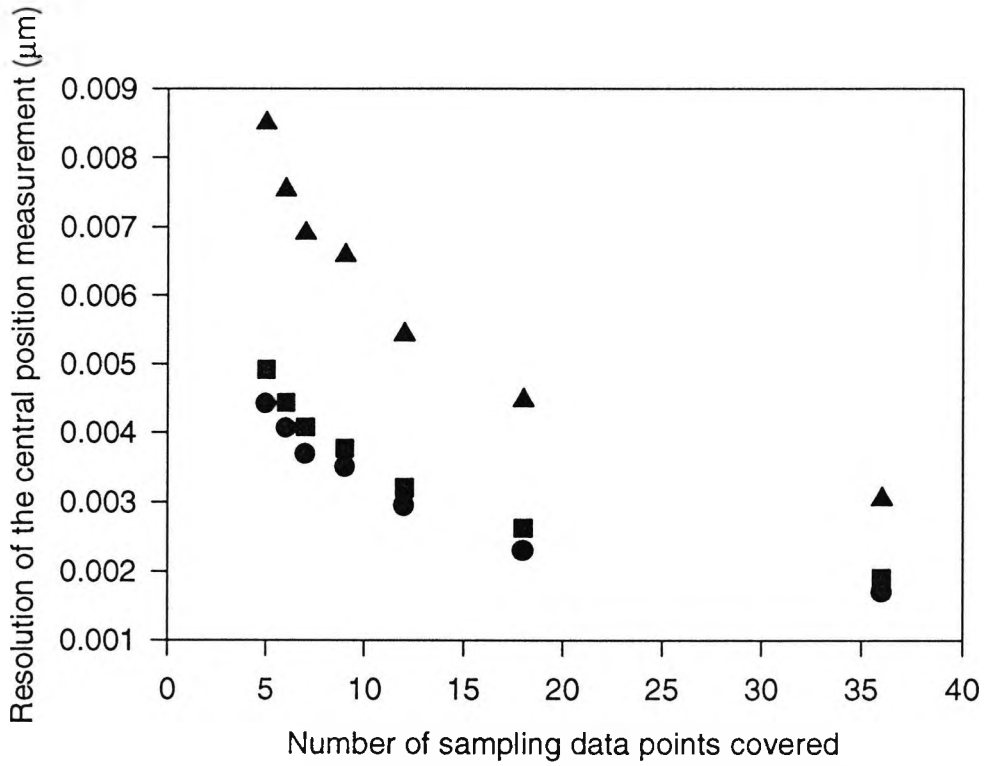
Fig.(5.8) Theoretical resolution of the central position measurement calculated from Eq.(5.21). The triangles, squares and round dots represent the resolutions when the S/N are 20dB, 30dB and 40dB respectively.

From Eq.(5.24), the theoretical resolution of the system can also be written as

$$\Delta = \sqrt{D(\Delta x)} = \sqrt{(\frac{\lambda_a}{4\pi a})^2 \frac{\sigma_I^2 \sum_{m=1}^{N} \sin^2(4\pi(md)/\lambda_a)}{[\sum_{m=1}^{N} \sin^2(4\pi(md)/\lambda_a)]^2} + \frac{\sigma_p^2 \sum_{m=1}^{N} \sin^4(4\pi(md)/\lambda_a)}{[\sum_{m=1}^{N} \sin^2(4\pi(md)/\lambda_a)]^2}}$$

(5.26)

In the case when $d << \lambda_a$, Eq.(5.26) can then be rewritten as

119

$$\Delta = \sqrt{(\frac{\lambda_a}{4\pi a^2}) \frac{\sigma_I^2 d}{[\int \sin^2(y)(dy)]} + \frac{4\pi d\sigma_p^2 \int \sin^4(y)(dy)}{\lambda_a [\int \sin^2(y)(dy)]^2}} \qquad (5.27)$$

If the curve fitting covers just one fringe, Eq.(5.23) can be rewritten as

$$\Delta = \sqrt{(\frac{\lambda_a}{4\pi a^2}) \frac{\sigma_I^2 d}{[\int_0^{2\pi} \sin^2(y)(dy)]} + \frac{4\pi d\sigma_p^2 \int_0^{2\pi} \sin^4(y)(dy)}{\lambda_a [\int_0^{2\pi} \sin^2(y)(dy)]^2}} \qquad (5.28)$$

and

$$\Delta = \sqrt{(\frac{\lambda_a}{4\pi a^2}) \frac{\sigma_I^2 d}{\pi} + \frac{4\pi d\sigma_p^2 \frac{3}{4}\pi}{\lambda_a \pi^2}}$$

$$= \sqrt{\frac{\lambda_a^2 \sigma_I^2}{8\pi^2 a^2 N} + \frac{3\sigma_p^2}{2N}} \qquad (5.29)$$

where $N = \frac{\lambda_a}{2d}$. Eq.(5.29) shows a theoretical resolution of the system when the curve

fitting covers just one fringe. It can be seen from the equation that the resolution of the

system increases either as the number of sampling data points N increases or as the rms

values of the noise, σ_I and σ_p, decrease.

To show the validity of the curve fitting signal processing method in practice, an

experiment was carried out to obtain the output fringe patterns of the WLI system under

the condition that the fibre is perturbed. Then, the curve fitting algorithm is applied to the

experimental data to reduce the noise effect and increase the repeatability of the central

position measurement. The details of the experiment are discussed below.

5.5.4 Experiment and results

Fig.(5.1) shows a schematic diagram of the system used for the investigation. In the experiment, the arm length differences (ALDs) of the two interferometers were set nearly equal to each other so that the difference between the ALD of the two interferometers was smaller than the coherence length of the source. The PZT actuator in the reference interferometer (PZT1) was then scanned to obtain the output fringe pattern of the system. Interferometer I operated as a sensing interferometer and interferometer II was used as a reference interferometer. In other words, PZT0 was used to set the displacement and PZT1 was used to measure the central position of the output fringe pattern.

Fig.(5.9) shows a result of the curve fitting approach on the central fringe. The jagged curve was drawn according the experiment data and the smooth curve was the fitted cosine function that was determined by Eq.(5.18). If the peak-peak value of the smooth curve is defined as the value of the signal and the value of the SSE divided by the number of the data points covered by curve fitting is defined as the value of the noise, the SNR calculated from Fig.(5.9) is about 31dB.

The reason that the curve fitting can improve the measurement results may be as follows. Firstly, the fitted curve is obtained with use of the least-mean-squares method, allowing the removal of the high frequency noise by averaging, and secondly, the fitted curve is a
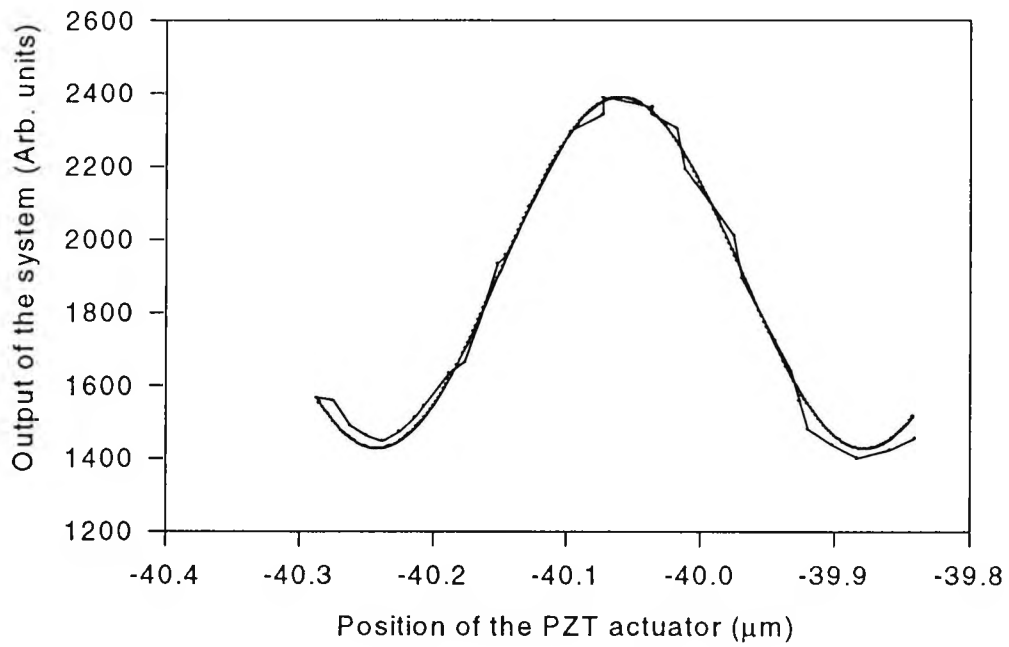
Fig.(5.9) Comparison between the Curve fitting result and
the raw data of the central fringe of output fringe pattern.
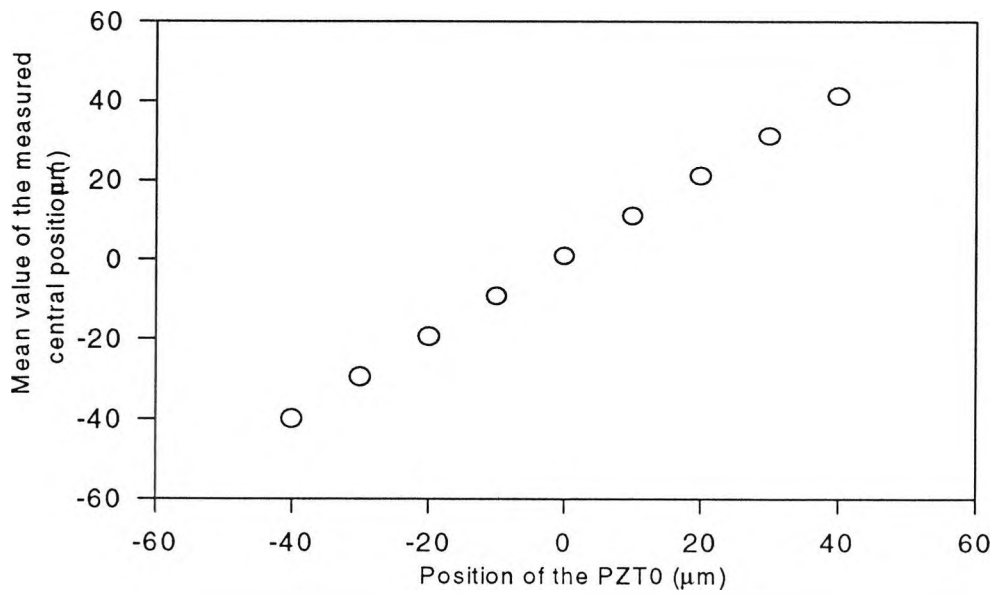
Fig.(5.10) Displacement meaurement results with use of the multimode
fibre linked interferometric system discussed.

continuous function instead of a series of separated experimental data points. This allows the resolution of the system to be smaller than that determined by the sampling gap of the PZT actuator.

The displacement of the mirror in interferometer I, which is set by PZT0, was measured by using the tandem interferometer system. Each measurement was repeated six times within a short period of about two minutes allowing negligible interferometer drift to be assumed. The sampling gap of PZT1 was about 12nm. The results obtained are shown in Fig.(5.10) where the x axis represents the displacement set by PZT0, and the y axis the mean value of the measured displacement using the curve fitting signal processing scheme discussed. The number of sampling data points that are covered by the curve fitting is 36. It can be seen from this diagram that the system gives a quite satisfactory measurement result with a 100μm core diameter linking fibre, even when the fibre was constantly shaken. The repeatability (of standard deviations) of each measurement is shown in Table 5.3, where D represents the mean value of the measured displacement, E represents the repeatability of the measurements without use of the curve fitting signal processing scheme (using just the maximum visibility method [7]), and E' represents the repeatability of the measurement using the curve fitting signal processing scheme. Measurements are obtained with the shaking of the linking fibre and thus modal noise is induced in the output of the system. From Table 5.3, it can be seen that the worst repeatability of the measurements obtained with the use of the maximum visibility method is about 30nm, and after using the signal processing scheme, the repeatability improved to values that are better than 15nm, where the total displacement range of measurement is 80μm. Comparing the experimental repeatability, taken as standard deviations, with the theoretical resolution shown in Fig.(5.8) when the number of the sampling data points covered by curve fitting is 36 and the SNR is about 30dB, it can be seen that most of the experimentally measured repeatability results are very close to the value of the theoretical resolution, 1.9nm. It is

123

noted that some figures of the experimentally measured repeatability listed in table 5.3 with use of curve fitting signal processing scheme are larger than that of the theoretical resolution. This may be due to the drift of the interferometer, which may possibly be removed by using a more sophisticated mechanical installation of the mirrors in the interferometers.

Table 5.3 Mean value of the measured displacements (D) and the repeatability of the displacement measurements, E and E' without and with the use of the cosine curve fitting scheme

D(μm)	-40.056	-29.720	-19.450	-9.239	0.910
E(nm)	9.0nm	9.0nm	7.7nm	7.4nm	4.4nm
E'(nm)	2.7nm	2.8nm	5.0nm	4.0nm	2.3nm

D(μm)	11.008	21.089	31.147	41.163
E(nm)	11nm	5.0nm	9.7nm	4.7nm
E'(nm)	2.7nm	3.3nm	1.2nm	1.8nm

It is found that a similar repeatability of the displacement measurement result has been obtained when a fourth order polynomial is used to carry out the curve fitting and the repeatability of the displacement measurement is dependent on the order of the polynomial used. From the experiment, the best repeatability of the displacement measurement is obtained when a fourth order polynomial is used.

5.5.5 Summary

In section 5.5, both a theoretical and an experimental investigation have been carried out for a multimode fibre linked WLI system. The theoretical resolution of the displacement measurement using a cosine curve fitting scheme is given by Eq.(5.29) and illustrated in Fig.(5.8). It is shown that the resolution of the system increases as the number of sampling data points increases and also as the rms values of the intensity noise and the phase noise decrease. The results from the experiment have shown that the SNR of the output from the system is about 31dB when a 100μm core diameter step index linking fibre is deliberately and reproduciably shaken and the noise effect on the central position measurement has been shown to be reduced by the curve fitting signal processing scheme discussed. After using the cosine curve fitting signal processing scheme, the short term displacement measurement repeatability (of standard deviations) of the system is better than 5nm over a measurement range of 80μm. Most of the experimentally measured repeatabilities are very close to the value of the theoretical possible resolution of 1.9nm.

It is also found that a similar repeatability of the displacement measurement has been obtained with the use of a fourth order polynomial to carry out the curve fitting.

Reference

[1] K. T. V. Grattan and B. T. Meggitt. "Optical Fibre Sensor Technology" Chapter. 9, (Chapman & Hall, London, 1995).

[2] A. Koch and R. Ulrich, "Fibre-optic Displacement Sensor with 0.02µm Resolution by White Light Interferometry," in Proc. 7th Int. Conf. on Optical Fibre Sensors, Sydney, pp.201-207. 1990.

[3] S. Chen, A. W. Palmer, K. T. V. Grattan and B. T. Meggitt, "Extrinsic Optical-fibre Interferometric Sensor That Uses Multimode Optical Fibres: System and Sensing Head Design for Low Noise Operation," Opt. Lett., Vol. 17, no. 10, pp. 701-703, 1992.

[4].T. Bossemann, "Multimode Fibre Coupled White Light Interferometric Position Sensor," Optical Fibre Sensors, NATO, ASI Series E: Applied Science, no. 132, pp 429-432, 1987.

[5].G. Beheim, "Fibre-linked Interferometric Pressure Sensor," Rev. Sci. Instrum.,Vol. 58, pp. 1655-1657, 1987.

[6] R. Dandliker, E. Zimmermann and G. Frosio, "Noise-Resistant Signal Processing for Electronically Scanned White-Light Interferometry", Proc. 8th Int. Conf. Optical Fibre Sensors, Monterey ,CA, pp.53-56, Jan. 1992.

[7] S. Chen, A. W. Palmer, K. T. V. Grattan, and B. T. Meggitt "Digital Signal-processing Techniques for Electronically Scanned Optical-Fibre White-Light Interferometry" Applied Optics, Vol.31(28), 6003-6010, 1992.

[8] S. Chen, K. T. V. Grattan, B. T. Meggitt, and A. W. Palmer, "Instantaneous Fringe-order Identification Using Dual Broadband Sources with Widely Spaced Wavelength", Electron. Lett., Vol.29, pp. 334-335, 1993.

[9] Y. J. Rao, Y. N. Ning and D. A. Jackson, "Synthesized Source for White-light Sensing Systems", Optical Letters, Vol.18, No.6, pp.462-464, 1993.

[10] A. D. Kersey and A. Dandrige, "Dual-wavelength Approach to Interferometric Sensing," in Proc. SPIE, Fibre Optic. Sensors II, Vol. 798, pp.176-181, 1987.

[11] Y. J. Rao, D. A. Jackson, "Universal Fibre-optic Point Sensor System for Quasi-static Absolute Measurements of Multiparameters Exploiting Low Coherence Interrogation," J. Lightwave Technol., Vol. 14, pp592-600, 1996.

[12] J. Eugene "Temporal Coherence Measurement System" Project for the degree of B. Eng., City Univ., London, 1994.

[13] System2000 manual and DRVR-PC2A manual (Queensgate Instruments Ltd).

[14] W. Mendenhall, R. L. Scheafer, and D. D. Wackerly. "Mathematical Statistics with Applications" Second Edition, Ch.11, p426, (Boston, Duxbury, 1978).

Chapter 6

Conclusion

6.1 Summary of this work

White light interferometric sensors have several advantages over the conventional interferometric optical fibre sensors which have been discussed. To provide a flexible connection within a WLI system, optical fibres are required. Multimode fibres are very attractive to provide the connections because it has a much larger core diameter so that the light beam is much easier to couple into the fibres. In Chapter 3, the relation between the signal to noise ratio of a WLI system and the parameters of illuminating source and linking fibres were investigated. This parameters include the coherence length of the source, the length of the linking fibre, and the type of the linking fibre. It has been shown both experimentally and theoretically that:

1) The signal to noise ratio of a WLI system increases as the coherence length of the illuminating source decreases.

2) The signal to noise ratio of a WLI system increases as the length of the linking fibre increases.

3) The signal to noise ratio of a WLI system is proportional to the square root of the mode number propagating in the multimode linking fibre.

4) Step index fibre is better suited for a WLI system than a graded index fibre because step index fibre has a much larger OPD between adjacent modes than graded index fibre. With

the knowledge gained in this work about modal noise, it will be easier to design a WLI system with a high signal to noise ratio. It should be noted that the first and the second result described above were obtained by Dr. Y. N. Ning and Dr. S. Chen has contributed to the third and fourth results.

To realize the absolute measurement, it is essential to determine the central position of the output fringe pattern with a high accuracy. With a single wavelength broad band source, such as a light emitting diode, a multimode laser diode or a superluminescent diode, the output fringe pattern of a WLI system is similar to that shown in Fig.(2.2) and the identification of the central fringe cannot be guaranteed. Using the technique discussed in Chapter 4, two signal processing schemes for the dual wavelength system have been developed. One uses the electrical circuit to square the output of a two wavelength system directly (using one detector) and the other uses two detectors to detect the different wavelength components of the output of the system, which have been separated by a wavelength separation mirror, then the outputs from the two detectors are multiplied and squared using an analogue electrical circuit. With the use of these two techniques, the minimum signal to noise ratio (SNR_{min}) required to identify the central fringe is obviously reduced. It is revealed that the system with one detector has a less complicated optical arrangement, whereas, the SNR_{min} of the system with two detectors (about 19dB) is lower than that of the system with one detector (about 25dB) and independent of the intensity ratio of the two sources.

Phase noise induced by the drift of the interferometers in a WLI system has been defined in Chapter 2 and has been experimentally investigated in Chapter 5. The experimental results show that the rms value of the phase noise induced by the drift of the interferometers is less than 5nm per minute when a WLI system is mounted on the vibration isolation table.

A curve fitting technique has been introduced in Chapter 5 to measure the rms value of the intensity noise in the output fringe pattern. It has been shown that the output signal to noise ratio of the system with a 100μm core diameter fibre (step index) is higher than that with a 50μm core diameter fibre (graded index).

After identifying the central fringe, it was found that a signal processing scheme is required for reducing the effect of noise and increasing the accuracy of the central position measurement. In Chapter 5, a signal processing scheme based on a curve fitting algorithm using a cosine function has been introduced and developed. The theoretical resolution of the system has been given. It has been shown that the resolution increases as the signal to noise ratio and the data points covered by curve fitting increases. The repeatability of the system (of standard deviations) has also been experimentally measured, the result being very close to the theoretically calculated result. Most of the experimentally measured repeatabilities of the system are better than 5nm over a 80μm range.

6.2 Impact of the research and future work

In summary, the work shown in this thesis has contributed to the field of optical fibre sensing based on white light interferometry in the following aspects:

1) Investigating modal noise in a WLI systems when different linking fibres are used.

2) Developing two signal processing schemes to increase the relative intensity of the central fringe of the output fringe pattern from a WLI system.

3) Introducing a signal processing scheme based on a curve fitting algorithm, which can reduce the effect of noise and increase the repeatability of the central position measurement.

As a suggestion, future work may be pursued in the following aspects:

1) From the simulation results in Chapter 4, the minimum signal to noise ratio (SNR_{min}) required to identify the central fringe of a WLI system with two detectors is independent of the output intensity ratio of the two sources. To verify this theoretical result in practice, further experimental investigations should be carried out.

2) In Chapter 5, an encouraging experimental result of displacement measurement has been presented. To enable this system to be applied in practice, further work is required, such as fabricating a rigid sensing interferometer and designing a reference interferometer with high stability and easy alignment.

3) As the fibre Bragg grating is commercially available, the sensing interferometer may be replaced by a fibre grating whose pitch is longer than the coherence length of the illuminating source. An detailed investigation of such a system is required.

Publications by the Author Relevant to the Thesis

Signal processing scheme for central position identification in a white light interferometric system with a dual wavelength source

QI WANG, Y. N. NING, K. T. V. GRATTAN, A. W. PALMER

A signal processing scheme using a curve fitting algorithm to determine the central position of the digitized fringe pattern output of a white light interferometric (WLI) system is discussed. An analytic result for the resolution obtained in the central fringe position measurement using a specific curve fitting scheme has been given and a simulation of measurement of the central position of a computer generated fringe pattern has been carried out. The results from the simulation show good agreement with those from the theoretical analysis. A supporting experiment to investigate this effect has also been carried out and the short term repeatability of the central position measurement using the curve fitting scheme gives close agreement with the theoretical results. © 1997 Elsevier Science Ltd.

KEYWORDS: interferometric systems, fringes, position identification, resolution

Introduction

Optical sensing systems based on white light interferometry have been intensively investigated in recent years[1-6]. The advantage of this approach over conventional interferometric sensors is well known, in that it can be used to determine a quasi-static measurand such as temperature, pressure, and strain with a corresponding displacement range much larger than one wavelength. The performance of a white light interferometric (WLI) system is dependent on how accurately the central position of its output can be measured. In order to determine this central position with high accuracy, several signal processing schemes have been proposed—for example, those including the whole fringe pattern centroid technique[6] and the central fringe of the output of the system cannot readily be identified through simply investigating the amplitude of the fringes due to the inevitable presence of noise. In order to ease the problem of central fringe identification, a system with a dual wavelength illuminating source has been proposed and investigated under practical conditions[8,9]. With the dual wavelength source technique, the signal-to-noise ratio required to identify the central fringe of the output of the system is considerably reduced from ~50 dB, by typically 30 dB, depending on the arrangement used.

The authors are in the Department of Electrical, Electronic and Information Engineering, City University, Northampton Square, London EC1V 0HB, UK. Received 4 June 1997. Revised 15 August 1997

In this paper, a curve fitting signal processing scheme has been proposed for determining the central position of the digitized output from a WLI system with a dual wavelength illuminating source. A theoretical analysis has been described and an analytical result for the resolution of the central position measurement has been given. The measurement results of the central position with simulated fringe patterns are seen to be in good agreement with those from the theoretical analysis; following which, an experimental investigation on a system comprising two Michelson interferometers linked with a multimode fibre, has then been carried out. The variation of the arm length difference (ALD) of the sensing interferometer was determined by measuring the central position variation of the output fringe pattern of the system and the position of one of the mirrors in the reference interferometer was measured utilizing a capacitive displacement sensor. The central position of the output fringe patterns of the system was measured using the curve fitting signal processing scheme and it is seen that the short term repeatability of the central position measurement obtained can be very close to the theoretical result.

Curve fitting signal processing scheme and theoretical analysis

The signal processing scheme using the curve fitting algorithm extends work discussed earlier[9] and was achieved by using the following steps.

(1) *Finding the central fringe of the output fringe pattern and obtaining the position of maximum visibility, χ_c*

The position of the maximum visibility may be defined as the coarse central position, by using the maximum visibility method[7]. Using a two-wavelength source in a WLI system, the central peak is much easier to identify by employing this method[8], which means that the error of the central position measurement using the maximum visibility method can be much smaller than one wavelength if a dual wavelength illuminating source is utilized. However, the accuracy of the maximum visibility method is restrained due to the presence of noise in the system and the limitation of the sampling gap in the digitized output fringe pattern. In order to increase the accuracy of the central position, a curve fitting algorithm can be used to obtain an improved central position, which will be discussed in the next processing step.

(2) *Fitting a cosine function to the central fringe*

The cosine function, $y(x)$, can be used to fit the central fringe of a digitized output, which is given by

$$y(x) = a \cos[4\pi(x - x_0)/\lambda_a] + b \qquad (1)$$

where a is the amplitude of the central fringe, λ_a represents the average wavelength of the illuminating source, b is the DC component of the output signal, and x_0 represents the position of the peak value. When the central fringe of a digitized output fringe pattern is fitted to a function shown in (1), the initial values of the parameters, a, λ_a, b, can be estimated from the output fringe pattern and the initial value of x_0 was set equal to the coarse central position, x_c, at the beginning of the curve fitting signal processing. Then, by adjusting the value of a, λ_a, b, x_0, the sum of squares for error (SSE) can be minimized. The SSE is given by[10]

$$SSE = \sum_i (I[i] - y(X[i]))^2 \qquad (2)$$

where $(X[i], I[i])$ represents the digitized output fringe pattern, $X[i]$ represents the position of the PZT actuator in the reference interferometer at the ith sampling point $I[i]$, and it may be assumed that a', λ_a', b', x_0' are the values of a, λ_a, b, x_0 with which the value of SSE is minimized. The best fitted curve can then be written as

$$y'(x) = a' \cos[4\pi(x - x_0')/\lambda_a'] + b' \qquad (3)$$

where the value of the parameter x_0' of the fitted curve is a new central position of the output fringe pattern. The accuracy of the new central position, x_0', should then be better than that of the coarse central position due to the following two reasons: (1) The new central position is determined by all the data points of the curve fitting and so the noise effect is reduced by averaging; and (2) the fitted curve is described by a continuous function instead of a number of discrete data points. This fitted curve represents a recovered central fringe with which the determination of the central position is not restrained by the sampling gap.

In an analysis of the situation, the central fringe of the output from a WLI system with added random noise may be expressed as

$$X_m = md + n_p(m) \qquad (4a)$$

$$I_m = a \cos[4\pi(md - X_0 + n_p(m))/\lambda_a] + b + n_I(m) \qquad (4b)$$

where m is an integer, d is the sampling gap of the PZT actuator, and $n_p(m)$ and $n_I(m)$ are the phase noise and the intensity noise at the mth sampling point $(m = 0, 1, 2, \ldots)$, which are assumed to be a normally distributed noise with root-mean-square values of σ_p and σ_I, respectively. Suppose a curve described by (1) is used to fit the digitized central fringe given by (4a) and (4b), then in the case that the values of the parameters a, b, λ_a, the digitized central fringe, are determined, the SSE value can be expressed as

$$SSE = \sum_{m=1}^{N} (I_m - y(md))^2$$

$$= \sum_{m=1}^{N} \{a \cos(4\pi(md - X_0 + n_p(m))/\lambda_a)$$
$$- a \cos(4\pi(md - x_0)/\lambda_a) + n_I(m)\}^2 \qquad (5)$$

Assuming $\Delta x = x_0 - X_0$, in the case of $\sigma_p \ll \lambda_a$ and $\Delta x \ll \lambda_a$, then (5) can be rewritten as

$$SSE = \sum_{m=1}^{N} \left\{ -\frac{4\pi a}{\lambda_a} \sin(4\pi(md - X_0)/\lambda_a) \right.$$
$$\left. \times (\Delta x + n_p(m)) + n_I(m) \right\}^2 \qquad (6)$$

where $\Delta x = x_0 - X_0$ is the error of the central position measurement, N is the number of data points covered by the curve fitting. To obtain the value Δx that minimizes the SSE value, the following equation has to be satisfied

$$\frac{\partial(SSE)}{\partial(\Delta x)} = 2 \sum_{m=1}^{N} \left\{ \left(\frac{4\pi a}{\lambda_a}\right) \sin(4\pi(md - X_0)/\lambda_a) \right.$$
$$\left. \times (\Delta x + n_p(m)) - n_I(m) \right\} \frac{4\pi a}{\lambda_a}$$
$$\times \sin(4\pi(md - X_0)/\lambda_a) = 0 \qquad (7)$$

From (7), the error of the central position of the ith measurement, Δx_i, can be expressed as

$$\Delta x_i = \frac{\lambda_a}{4\pi a} \frac{\sum\limits_{m=1}^{N} n_I(m)\sin(4\pi(md - X_0)/\lambda_a)}{\sum\limits_{m=1}^{N} \sin^2(4\pi(md - X_0)/\lambda_a)}$$
$$- \frac{\sum\limits_{m=1}^{N} n_p(m)\sin^2(4\pi(md - X_0)/\lambda_a)}{\sum\limits_{n=1}^{N} \sin^2(4\pi(md - X_0)/\lambda_a)} \qquad (8)$$

where α is the amplitude of the central fringe, λ_a is the average wavelength of the course, X_0 is the central position of the central fringe, m is an integer, d is the sampling gap of the PZT actuator in the reference interferometer, and $n_p(m)$ and $n_l(m)$ are the phase noise and the intensity noise with their root mean square values, σ_p and σ_l respectively. To simplify the analysis, it may be assumed $X_0 = 0$. Then (8) can be simplified to

$$\Delta x_i = \frac{\lambda_a}{4\pi\alpha} \frac{\sum_{m=1}^{N} n_l(m)\sin(4\pi(md)/\lambda_a)}{\sum_{m=1}^{N} \sin^2(4\pi(md)/\lambda_a)}$$

$$- \frac{\sum_{m=1}^{N} n_p(m)\sin^2(4\pi(md)/\lambda_a)}{\sum_{m=1}^{N} \sin^2(4\pi(md)/\lambda_a)} \quad (9)$$

In the case that the intensity noise $n_l(m)$ and the phase noise $n_p(m)$ are independent of each other and $E[n_l(m)] = E[n_p(m)] = 0$ (where $E(z)$ represents the expectation value of z), the theoretical resolution of the system can be expressed as

$$\Delta = \sqrt{D(\Delta x)}$$

$$= \left(\left(\frac{\lambda_a}{4\pi\alpha}\right)^2 \frac{\sigma_l^2 \sum_{m=1}^{N} \sin^2(4\pi(md)/\lambda_a)}{\left[\sum_{m=1}^{N} \sin^2(4\pi(md)/\lambda_a)\right]^2} \right.$$

$$\left. + \frac{\sigma_p^2 \sum_{m=1}^{N} \sin^4(4\pi(md)/\lambda_a)}{\left[\sum_{m=1}^{N} \sin^2(4\pi(md)/\lambda_a)\right]^2} \right)^{1/2} \quad (10)$$

where $D(\Delta x)$ is the variance of Δx. When $d \ll \lambda_a$, (10) can then be described as

$$\Delta = \left(\left(\frac{\lambda_a}{4\pi\alpha}\right) \frac{\sigma_l^2 d}{[\int \sin^2(y)(dy)]} \right.$$

$$\left. + \frac{4\pi d\sigma_p^2 \int \sin^4(y)(dy)}{\lambda_a[\int \sin^2(y)(dy)]^2} \right)^{1/2} \quad (11)$$

If the curve fitting covers just one fringe, (11) can then be written as

$$\Delta = \left(\left(\frac{\lambda_a}{4\pi\alpha}\right) \frac{\sigma_l^2 d}{\left[\int_0^{2\pi} \sin^2(y)(dy)\right]} \right.$$

$$\left. + \frac{4\pi d\sigma_p^2 \int_0^{2\pi} \sin^4(y)(dy)}{\lambda_a\left[\int_0^{2\pi} \sin^2(y)(dy)\right]^2} \right)^{1/2} \quad (12)$$

then

$$\Delta = \left(\frac{\lambda_a^2 \sigma_l^2}{8\pi^2\alpha^2 N} + \frac{3\sigma_p^2}{2N} \right)^{1/2} \quad (13)$$

where $N = \lambda_a/2d$. Equation (13) shows a theoretical resolution of the system when the curve fitting covers just one fringe. It can be seen from the equation that the resolution of the system is inversely proportional to the square root of the number N and becomes better as the RMS values of the noise, σ_l and σ_p, decrease.

In a single-modelinked WLI system, the intensity noise is very small because there is minimum modal noise in such a system and so the effect of the intensity noise on the central position measurement can be ignored. Therefore, the resolution for a WLI system with a single-mode linking fibre can be obtained from (13), which is given by

$$\Delta = \sigma_p \left(\frac{3}{2N}\right)^{1/2} \quad (14)$$

If the number of the sampling points covered by the curve fitting, N, is, for example, 24, the resolution of a single-mode fibre linked WLI system given by (14) is $\sigma_p/4$, which means that the resolution using the curve fitting scheme can be one quarter of that of the position sensor used in the reference interferometer. For instance, if a capacitive position sensor with 2.8 nm resolution were used, the resolution of the system could be 0.7 nm.

Simulation

The output of a WLI system with a dual wavelength illuminating source can be expressed as[11]

$$I(x) = \frac{I_0}{4}\left\{ 1 + \frac{1}{2}\exp\left(-\left(\frac{4(x-x_0)}{L_c}\right)^2\right)\right.$$

$$\left. \times \cos\left(\frac{4\pi(x-x_0)}{\lambda_a}\right)\cos\left(\frac{4\pi(x-x_0)}{\lambda_m}\right)\right\} \quad (15)$$

where I_0 is the output intensity of the illuminating source, L_c represents the coherence length of the illuminating source, x represents the difference of the ALDs of the two interferometers, x_0 represents the central position of the output fringe pattern. m is an integer, d represents the sampling gap, $\lambda_a = (2\lambda_1\lambda_2)/(\lambda_1 + \lambda_2)$ is termed the average wavelength and $\lambda_m = (2\lambda_1\lambda_2)/(|\lambda_1 - \lambda_2|)$ the modulation wavelength.

When a computer is used to collect the output fringe pattern, the fringe pattern needs to be digitized. This digitized output from a WLI system illuminated by a dual wavelength source with added intensity noise and phase noise can be obtained from (15)

$$I_m = \frac{I_0}{4}\left\{ 1 + \frac{1}{2}\exp\left(-\left(\frac{4(md - x_0 + n_p)}{L_c}\right)^2\right)\right.$$

$$\times \cos\left(\frac{4\pi(md - x_0 + n_p)}{\lambda_a}\right)$$

$$\left. \times \cos\left(\frac{4\pi(md - x_0 + n_p)}{\lambda_m}\right)\right\} + n_l \quad (16)$$

where n_p and n_I represent phase noise and intensity noise, and their root mean square (RMS) values are σ_p and σ_I respectively. In a practical system, the phase noise can be induced by the vibration and the drift of the interferometers, by the noise of the position sensor and by the turbulence of air. The intensity noise can be induced by, for example, the fibre lead, the source intensity fluctuations, the turbulence of air, and the shot noise and the thermal noise from the detector. In the case where a system is linked with a multimode fibre, the noise induced by the fibre lead, which is termed the 'modal noise'[3], represents the main part of the total intensity noise.

To determine the central position of the digitized output fringe pattern shown in (16), the curve fitting signal processing scheme discussed in the last section can be used. The values of the parameters in (16) were chosen as: wavelengths λ_1 and λ_2 were equal to 0.78 µm and 0.67 µm respectively, the coherence length L_c was equal to 20 µm, the signal to noise ratio $2\alpha/\sigma_I$ was 1/100, and the RMS value of the phase noise σ_p was 3 nm, where the

central position of the digitized fringe pattern given by (16) was repeatedly measured (100 times) using the curve fitting signal processing scheme and the resolution of the central position measurements, which is equal to the standard deviation of the measurement, was calculated.

Figure 1 is plotted according to the simulation results and the results calculated from (13), which are shown as the circles and the squares respectively. It can be seen from the diagram that the resolution of the system becomes better as the number of sampling points covered by the curve fitting increases and the theoretical possible resolution of the system can be better than 1 nm if the number of sampling points is larger than 20. In addition, the simulation results are in good agreement with those calculated from (13).

Experimental analysis

Figure 2 shows a schematic diagram of the system used for the experimental investigation where light from two multimode laser diodes (LT023MDO and LPM3 670,
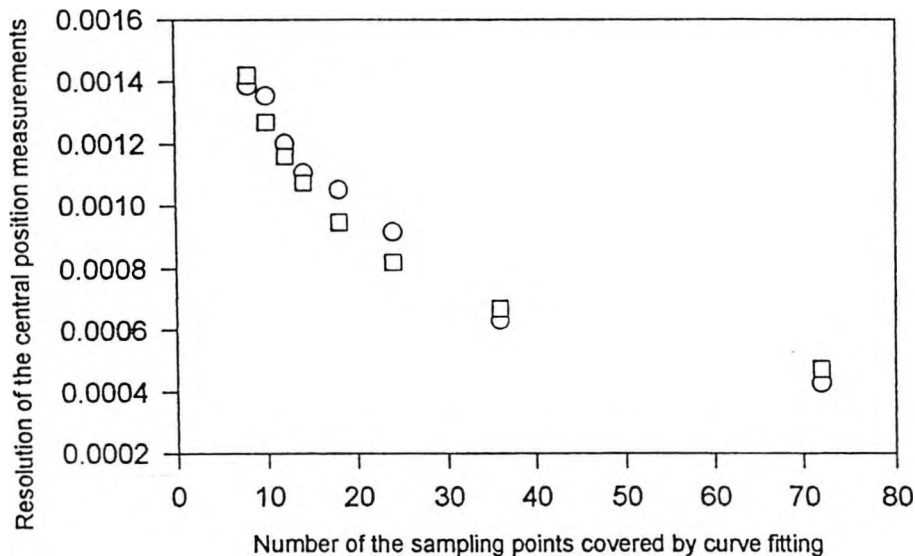
Fig. 1   Comparison between the resolution of the simulation and the resolution given by (13). Circles represent the results from the simulation. Squares represent the results given by (13)
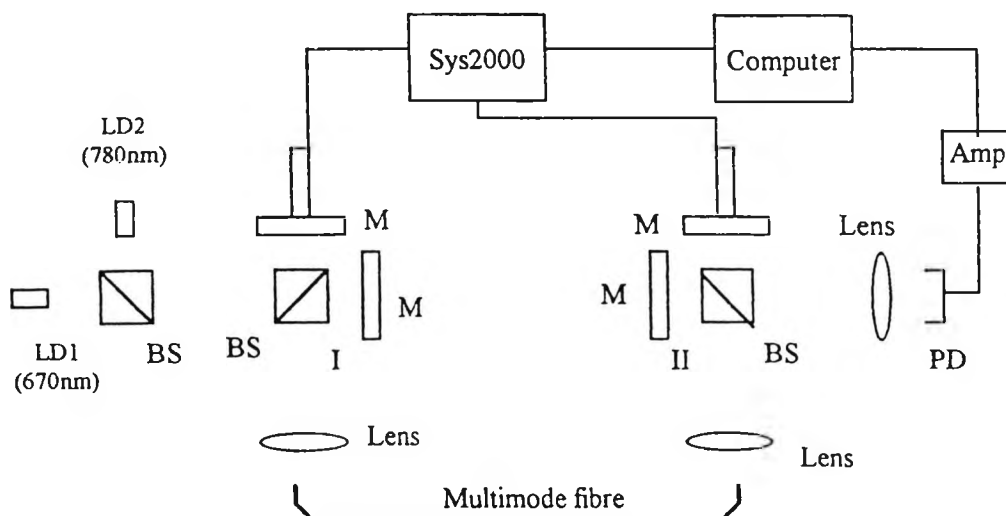
Fig. 2   Schematic diagram of a system consisting of two Michelson interferometers with a multimode linking fibre. lD1: 670 nm wavelength laser diode; LD2: 780 nm wavelength laser diode; BS: beam splitter; M: mirror; PZT0, PZT1: piezoelectric actuators; Sys2000: Controller for PZTs; Amp: amplifier; I, II: interferometers
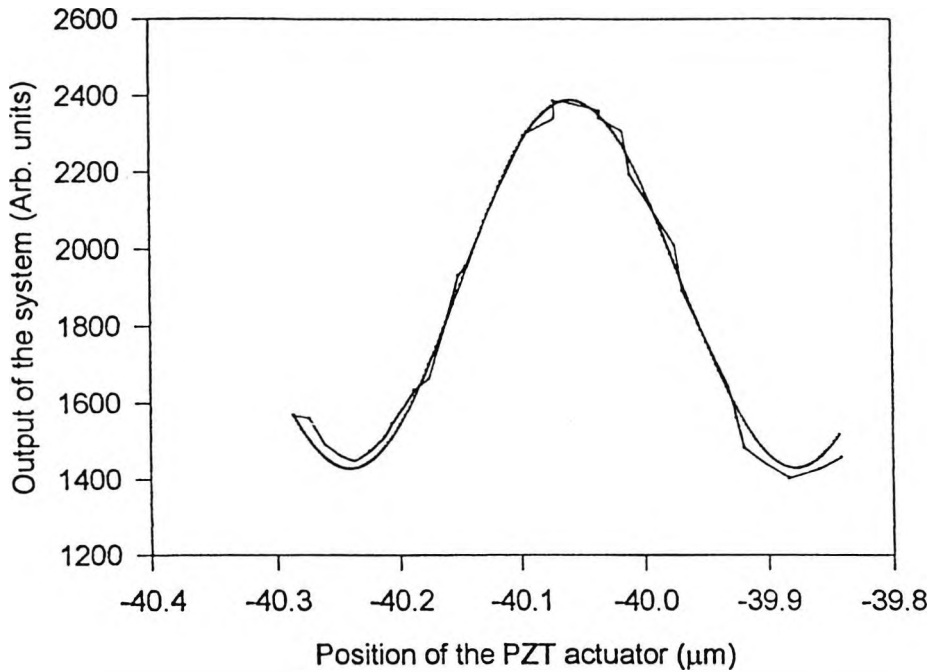
Fig. 3   Comparison between the curve fitting result and the raw data of the central fringe of an output fringe pattern

with central wavelengths of 780 nm and 670 nm, respectively) was launched into the first interferometer (interferometer I), and then injected into a multimode fibre (with a core diameter of 100 μm and a length of 5 m) via a 10 × objective lens. The output from the multimode fibre was collimated and then launched into the second Michelson interferometer (interferometer II). The output of the system was detected with a photodiode. In the experiment, the arm length differences (ALDs) of the two interferometers are set nearly equal to each other so that the difference between the ALDs of the two interferometers is smaller than the coherence length of the source. The PZT actuator in the reference interferometer (PZT1) is then scanned to obtain the output fringe pattern of the system. Interferometer I operates as a sensing interferometer and interferometer II is used as a reference interferometer, i.e. PZT0 is used to set the displacement, and PZT1 is used to measure the central position of the output fringe pattern.

Figure 3 shows the result of the curve fitting to the central fringe of the output fringe pattern. The jagged curve is drawn following the experimental data set, while the smooth curve is the fitted cosine function determined by (3).

The reason that the curve fitting approach can improve the resolution of the central position measurement would appear to be as follows. First, the fitted curve is obtained using the least-mean-squares method, allowing the removal of the high frequency noise by averaging, and secondly, the fitted curve is a continuous function instead of a series of separate experimental data points.

With this continuous function, the determination of the central position is free from the restraint of the sampling gap, allowing the resolution of the system potentially to be smaller than the sampling gap of the PZT actuator.

In the experiment, the output fringe pattern of the system was obtained by using the scanning PZT actuator in interferometer II (PZT1) when the displacement of the mirror in the interferometer I, which is positioned by PZT0, was set to a number of positions. For each position set by PZT0, six fringe patterns were recorded within a short period of about two minutes, allowing negligible interferometer drift to be assumed. The sampling gap of PZT1 was about 12 nm. The central position of each fringe pattern was measured using the curve fitting signal processing scheme. The results obtained are shown in Fig. 4 where the horizontal axis represents the measured positions corresponding to the displacements set by PZT0, and the vertical axis represents the mean value of the measured displacement using the curve fitting signal processing scheme discussed. The number of sampling data points that are covered by the curve fitting was 36. It can be seen from this diagram that the system gives a quite satisfactory measurement result with a 100 μm core diameter linking fibre, even when the fibre was constantly shaken. This confirms the results of previous studies[9].

The repeatability of each measurement is shown in Table 1, where D represents the mean value of the measured displacement, E represents the repeatability of the measurements without the use of the curve fitting signal processing scheme (using just the maximum

Table 1.   Mean value of the measured displacements (D) and the repeatability of the displacement measurements, E and E′ without and using the cosine curve fitting scheme

D (μm)	−40.056	−29.720	−19.450	−9.239	0.910	11.008	21.089	31.147	41.163
E (nm)	9.0 nm	9.0 nm	7.7 nm	7.4 nm	4.4 nm	11 nm	5.0 nm	9.7 nm	4.7 nm
E' (nm)	2.7 nm	2.8 nm	5.0 nm	4.0 nm	2.3 nm	2.7 nm	3.3 nm	1.2 nm	1.8 nm
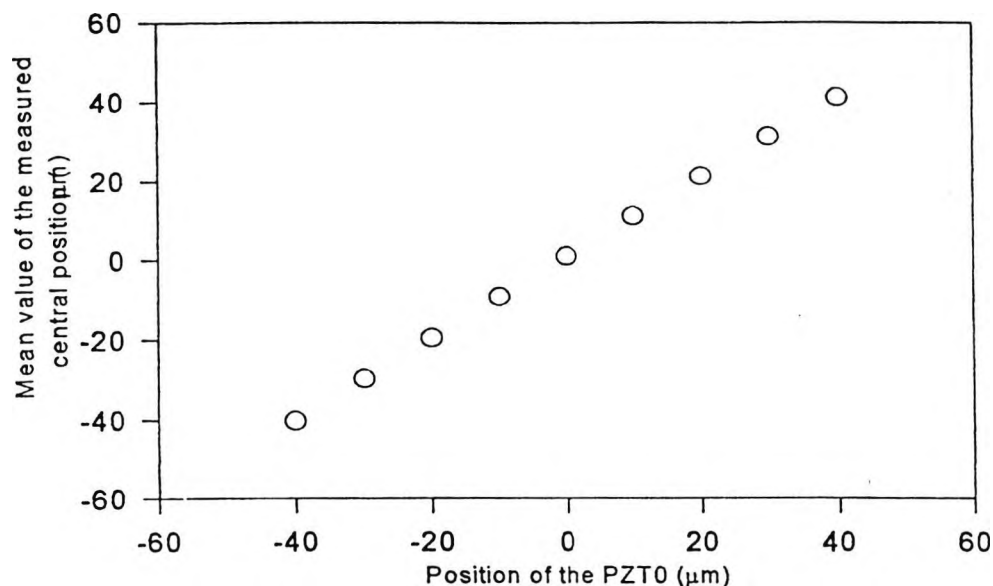
Fig. 4   Displacement measurement results using the multimode fibre linked interferometric system discussed

visibility method[7]), and E' represents the repeatability of the measurement using this curve fitting signal processing scheme. Measurements are obtained with the shaking of the linking fibre and thus modal noise is induced in the output of the system. From Table 1, it can be seen that the worst repeatability of the measurements obtained utilizing the maximum visibility method is about 10 nm and, using the signal processing scheme, the repeatability improved over previous work[9] to values that are better than 5 nm, where the total displacement range of the measurement is 80 μm. Comparing the experimental repeatability with the theoretical resolution shown in Fig. 1 as the number of the sampling data points covered by the curve fitting is 36, it can be seen that the experimentally measured repeatability results are very close to those of the theoretical resolution. The main reason that the experimentally measured repeatability listed in the table is larger than that of the theoretical possible resolution using the curve fitting signal processing scheme, may be an instability in the interferometers.

Conclusions

In this paper, a curve fitting signal processing scheme using a cosine function has been introduced and an analytic result on the resolution of the displacement measurement using the curve fitting scheme has been given. It has been shown from the theoretical analysis that the resolution of the system increases as the number of sampling data points increases and as the RMS values of the intensity noise and the phase noise decrease. A central position measurement of simulated output fringe patterns utilizing the curve fitting scheme has been carried out and the results of the simulated measurement are in good agreement with those from the theoretical analysis. An experimental investigation has also been carried out with a system comprising two Michelson interferometers linked with a step index multimode fibre.

The noise effect on the central position measurement has been shown to be reduced by the curve fitting signal processing scheme discussed. With the use of the curve fitting signal processing scheme, the short term displacement measurement repeatability of the system has been shown to be improved where the discrepancy between the experimentally measured repeatability and the theoretical resolution appears related to the instability of the interferometers.

References

1   Grattan, K.T.V., Meggitt, B.T. *Optical Fiber Sensor Technology*, Chapter 9, Chapman & Hall, London (1995)
2   Koch, A., Ulrich, R. Fiber-optic displacement sensor with 0.02 μm resolution by white light interferometry, *Proc 7th Int Conf on Optical Fiber Sensors*, Sydney (1990) 201–207
3   Chen, S., Palmer, A.W., Grattan, K.T.V., Meggitt, B.T. Extrinsic optical-fiber interferometric sensor that uses multimode optical fibers: system and sensing head design for low noise operation, *Opt Lett*, 17 (1992) 701–703
4   Bossemann, T. Multimode fiber coupled white light interferometric position sensor, *Optical Fiber Sensors*, NATO, ASI Series E: Applied Science, no. 132 (1987) 429–432
5   Beheim, G. Fibre-linked interferometric pressure sensor, *Rev Sci Instrum*, 58 (1987) 1655–1657
6   Dandliker, R., Zimmermann, E., Frosio, G. Noise-resistant signal processing for electronically scanned white-light interferometry, *Proc 8th Int Conf Optical Fiber Sensors*, Monterey, CA (1992) 53–56
7   Chen, S., Palmer, A.W., Grattan, K.T.V., Meggitt, B.T. Digital signal-processing techniques for electronically scanned optical-fibre white-light interferometry, *Appl Opt*, 31 (1992) 6003–6010
8   Rao, Y.J., Ning, Y.N., Jackson, D.A. Synthesized source for white-light sensing systems, *Opt Lett*, 18 (1993) 462–464
9   Wang Qi, Ning, Y.N., Grattan, K.T.V., Palmer, A.W. A multimode optical-fibre sensing system using white-light interferometry and a two-wavelength synthetic source, *Sensors and Actuators A* (1997) to be published
10 Mendenhall, W., Scheafer, R.L., Wackerly, D.D. *Mathematical Statistics with Applications*, Second Edition, Ch. 11, Boston. Duxbury (1978) 426
11 Wang, D.N. White light interferometric sensor systems, PhD Thesis, Chapter 2, City University, London (1995)

OPTICS
COMMUNICATIONS

Noise effects in position measurement using a white light interferometric system linked with different core diameter multimode fibres

Qi Wang, Y.N. Ning, K.T.V. Grattan, A.W. Palmer

Department of Electrical, Electronic and Information Engineering, City University, Northampton Square, London EC1V OHB, UK

Aims and Scope
Optics Communications ensures the rapid publication of contributions in the field of optics and interaction of light with matter.

Abstracted/indexed in:
Chemical Abstracts; Current Contents: Engineering, Computing and Technology; Current Contents: Physical, Chemical & Earth Sciences; EI Compendex Plus; Engineering Index; INSPEC.

Subscription Information 1997
Volumes 133–144 (72 issues) of Optics Communications (ISSN 0030-4018) are scheduled for publication.
Prices are available from the publisher upon request. Subscriptions are accepted on a prepaid basis only. Issues are sent by SAL (Surface Air Lifted) mail wherever this service is available. Please address all enquiries regarding orders and subscriptions to:

Elsevier Science B.V.
Order Fulfilment Department
P.O. Box 211, 1000 AE Amsterdam
The Netherlands
Tel. +31 20 4853642, Fax: +31 20 4853598

Claims for issues not received should be made within six months of our publication (mailing) date.

Advertising Offices
International: Elsevier Science, Advertising Department, The Boulevard, Langford Lane, Kidlington, Oxford, OX5 1GB, UK; Tel: +44 (0)1865 843565; Fax: +44 (0)1865 843976
USA and Canada: Weston Media Associates, Dan Lipner, P.O. Box 1110, Greens Farms, CT 06436-1110, USA; Tel: +1 (203) 261 2500; Fax: +1 (203) 261 0101
Japan: Elsevier Science Japan, Marketing Services, 1-9-15 Higashi-Azabu, Minato-ku, Tokyo 106, Japan; Tel: +81 3 5561 5033; Fax: +81 3 5561 5047

N·H

ELSEVIER

Noise effects in position measurement using a white light interferometric system linked with different core diameter multimode fibres

Qi Wang, Y.N. Ning, K.T.V. Grattan, A.W. Palmer

Department of Electrical, Electronic and Information Engineering, City University, Northampton Square, London EC1V OHB, UK

Received 16 February 1996; accepted 28 March 1996

Abstract

An optical fibre sensing system comprising two Michelson interferometers linked with a multimode fibre has been investigated. The signal to noise ratio of the output, when linking fibres of a range of core diameters were used, was measured and the system analyzed. The signal to noise ratio of the system in the 100 μm fibre case is higher than that with a 50 μm core diameter fibre, these results being obtained while the linking fibre in the system was perturbed to induce noise in a known and reproducible way. The repeatability of the displacement measurement with 50 μm, 100 μm, and 200 μm core diameter linking fibre has been obtained by using the maximum visibility method, this being seen to increase as the core diameter of the linking fibre increases, and for 200 μm core diameter fibre it was measured to be about 22.5 nm (3 standard deviations) under the conditions described.

1. Introduction

Optical fibre sensing systems using white light interferometry have been attracting significant attention recently when used to undertake a variety of measurements [1]. The system may be configured in a way that a fibre is used to link the two interferometers, one of which is termed the "sensing" and the other the "reference" interferometer. If a single mode fibre is used for this purpose it may be difficult to couple the light back into the fibre. Connecting the two interferometers of a white light interferometric system with multimode fibre represents a convenient way to overcome this problem and has led to an investigation to analyze the effect of the noise that is inevitably generated in these multimode fibres when used under these circumstances, in most environments.

Results have been reported on the use of various means of suppressing the modal noise thus induced, by using a short coherence length source [2], or by increasing the length of the linking fibre [3]. It has also been reported that by increasing the core diameter of the fibre [4], the modal noise may also be decreased.

In this investigation, to analyze the output signals, a curve fitting technique is first introduced to enable a measurement of the signal to noise ratio to be made, and then, actual position measurements in the presence of an imposed but representative noise signal have been carried out, using a tandem interferometer system linked with the different core diameter fibres discussed. It was found that with the increasing diameter of the linking fibre, the displacement measurement repeatability of the system was seen to increase.

2. Theory and analysis

When a multimode fibre is used to link the two interferometers, modal noise will be induced in the system due to the presence of environmental perturbations. The signal to noise ratio (S/N) of the output from such a multimode fibre linked system is proportional to the square root of the mode number, M, transmitted in the linking fibre when the fibre is perturbed, i.e. subjected to a reproducible shaking stimulus [4]:

$$S/N \propto \sqrt{M}, \tag{1}$$

where S is the signal amplitude, and N is the noise level. When the core diameter of the linking fibre used is increased, the mode number propagated in the linking fibre will increase. Therefore, according to Eq. (1), the value of the output signal to noise ratio will be higher when a larger core diameter linking fibre is employed, i.e. the signal to noise ratio of the output of the system increases correspondingly.

In order to assess the noise level of the output of such a system, a curve fitting approach using a cosine function, $y(x)$, representing the theoretical output of the interferometer, which is given by

$$y(x) = A \exp\left[-\left(\frac{(x-x_0)}{L_C}\right)^2\right]$$
$$\times \cos\left(\frac{4\pi(x-x_0)}{\lambda_a}\right) + B \tag{2}$$

is carried out where A is the amplitude of the AC component of the signal, and B is the value of the DC component of the signal. L_C is the coherence length of the source, λ_a is the average wavelength of the source, x is the arm length difference (ALD) of the interferometers, with x_0 being the position of the central fringe of the visibility profile.

The curve fitting can be used to minimize the sum of squares for error (SSE) [5] by adjusting the parameters, A, B, L_C, λ_a, and x_0. The value of the SSE factor is given by

$$SSE = \sum_i (I[i] - y(X[i]))^2, \tag{3}$$

where $[X[i], I[i]]$ is the experimental data set, where $X[i]$ is the position of the PZT actuator, and $I[i]$ is

the output of the system. The peak–peak value of the AC component in Eq. (2) is equal to $2A$, and the noise value, termed N, is defined as

$$N = \sqrt{SSE/P}, \tag{4}$$

where P is the number of data points in the data set, and the value of SSE was defined by Eq. (3). The signal to noise ratio is then given by

$$(S/N) = 20 \log\left(\frac{2A}{\sqrt{SSE/P}}\right). \tag{5}$$

To determine the above signal to noise ratio, described by Eq. (5), a simulation has been carried out, where the simulated output signal of the interferometer system, $y'(x)$, is obtained by adding an element of random noise, $n(x)$, into the right-hand side of the Eq. (2):

$$y'(x) = A \exp\left[-\left(\frac{(x-x_0)}{L_C}\right)^2\right]$$
$$\times \cos\left(\frac{4\pi(x-x_0)}{\lambda_a}\right) + B + n(x), \tag{6}$$

where $n(x)$ is normally distributed noise with a square root variance, σ. The signal to noise ratio associated with $y'(x)$, is defined as

$$(S/N)_1 = 20 \log(2A/\sigma). \tag{7}$$

This signal to noise ratio can also be determined by using the same curve fitting technique arrangement
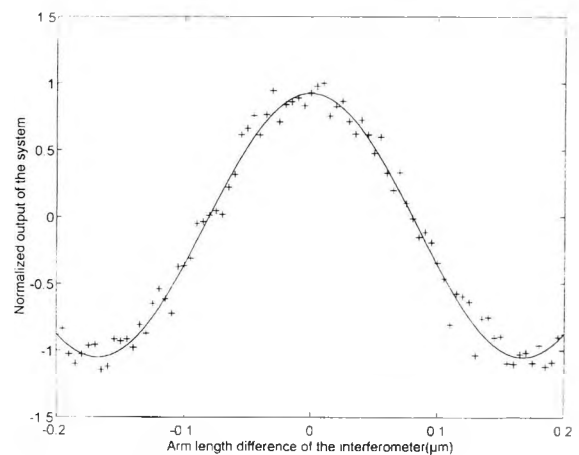
Fig. 1. Result of curve fitting applied to the simulated signal. Crosses: data obtained with the noise effect present. Solid-line: curve fitted to the data.
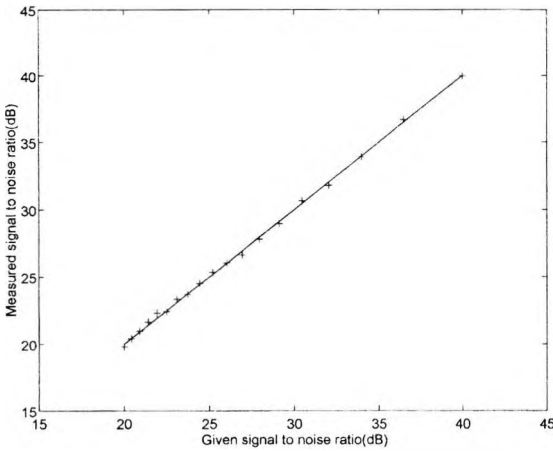
Fig. 2. Comparison of the signal to noise ratios $(S/N)_1$, and (S/N), the latter being the measured signal-to-noise ratio.

discussed earlier, from Eq. (5). Fig. 1 shows a curve fitting approach applied to the simulated signal. The crosses are the values obtained by using Eq. (6) and the solid line is the fitted curve. The noise value (from Eq. (4)) is the deviation of the fitted curve to the simulated signal.

Fig. 2 is a graph comparing the resultant signal to noise ratio, $(S/N)_1$ (see Eq. (7)), and the measured signal to noise ratio, (S/N) (see Eq. (5)). The data point number, P, is chosen to be 800 in the simulation. The data points (crosses) are obtained from the above equations and the solid line represents the

equation $y = x$, i.e. equality between the two values of the signal to noise ratio. It can be seen from this diagram that the measured signal to noise ratio is approximately equal to the given signal to noise ratio, $(S/N)_1$. The maximum difference between the two signal to noise ratios is about 0.5 dB.

The aim of this work is to measure the experimentally determined signal to noise ratio of the output and to investigate the noise effect on the central position measurement when the interferometers are linked by a multimode fibre with different core diameter and perturbed reproducibly. The details of the experimental arrangement used are discussed below.

3. Experimental arrangment

Fig. 3 shows a schematic diagram of the experimental system used, consisting of two Michelson interferometers, linked by a multimode fibre. Two multimode laser diodes, LDs, (with wavelengths of 780 nm and 670 nm, respectively) were used as the light source and after the light from these passed through the first sensing interferometer, it was then launched into the multimode fibre under investigation. The output from this fibre was then collimated and injected into the second recovery interferometer, focused by a lens and detected with the photodiode (PD). Each Michelson interferometer has one mirror driven by a sophisticated piezoelectric actuator (PZT0
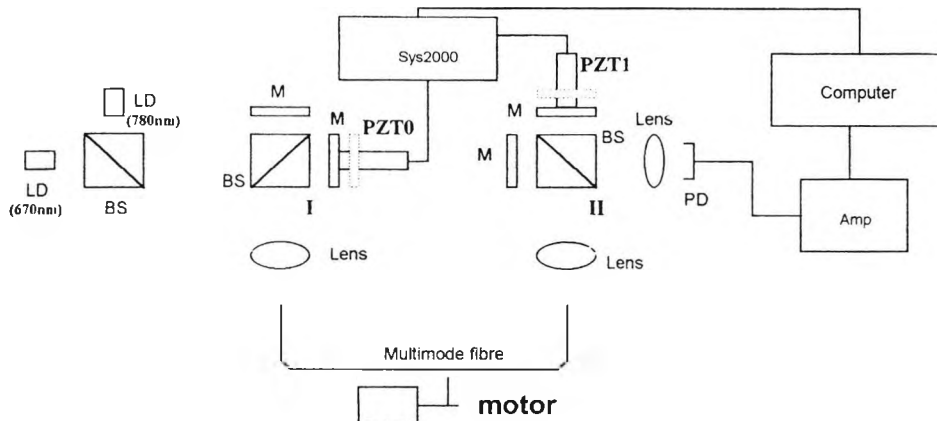
Fig. 3. A schematic diagram of the experimental of system. LD, laser diode; BS, beam splitter; M, mirror, PZT0, PZT1, piezoelectric actuators; PD, photodiode.

& PZT1, type MTP105 Queensgate Instruments Ltd.) and the detector analogue output was converted into a digital signal for computer processing. Part of the fibre of about 60 cm in length was deliberately and reproducibly shaken by a protruding wheel driven by a motor. Thus, repeatable results for the noise generated could be obtained when such a fibre vibrating arrangement was utilized. Both LDs were driven with a current which is below the threshold, so that the corresponding coherence lengths of the LDs are relatively short (about 15 μm).

In the experiment, the arm length differences (ALDs) of the two interferometers are set to be approximately equal to each other, so that the difference of the ALDs is smaller than the coherence length of the source. The PZT actuator in the reference interferometer (PZT1) is then scanned to obtain the output visibility fringe pattern.

Fig. 4 shows such an experimental output fringe profile of the system. Similar results for a one-interferometer system are described in a previous work [7]. In the results obtained here, it should be noted that there is some noise present in the fringe pattern due to the vibration of the multimode linking fibre.

Table 1
The measured signal to noise ratio of the output of the system by using the curve fitting method, (a prime denoting when the fibre was perturbed) for a series of core diameters (50 μm and 100 μm), over a series of measurements (1-5)

	1	2	3	4	5
$(S/N)_{50}$ (dB)	29.9	31.2	30.9	32.0	30.8
$(S/N)'_{50}$ (dB)	27.2	28.2	28.4	28.6	27.1
$\Delta(S/N)_{50}$ (dB)	2.7	3.0	2.5	3.4	3.7
$(S/N)_{100}$ (dB)	32.1	32.5	32.7	33.1	33.0
$(S/N)'_{100}$ (dB)	31.2	31.6	31.4	32.0	31.8
$\Delta(S/N)_{100}$ (dB)	0.9	0.9	1.3	1.1	1.2

A curve fitting algorithm was applied to the fringe pattern and Eq. (5) was used to calculate the signal to noise ratio of the output. Table 1 shows a series of signal to noise ratio measurement results obtained when 50 μm and 100 μm core diameter linking fibres are used. $(S/N)_{50}$, $(S/N)'_{50}$, $(S/N)_{100}$ and $(S/N)'_{100}$ may be defined as the signal to noise ratios of the output when such 50 μm and 100 μm core diameter linking fibre are used, respectively, a prime denoting the ratio when the fibre was perturbed. The signal to noise ratio reductions, which is
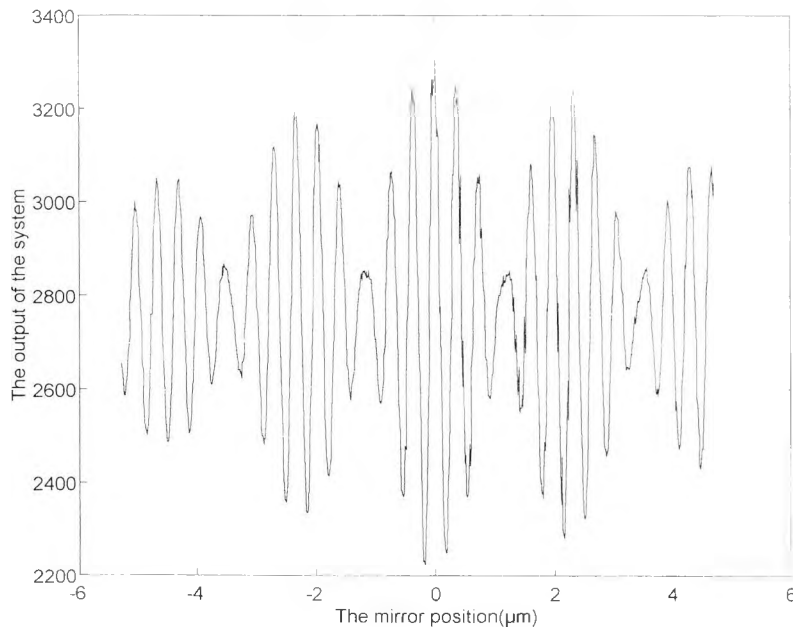
Fig. 4. Experimental output fringe profile.

experienced in these two cases, are represented by $\Delta(S/N)_{50}$ and $\Delta(S/N)_{100}$, and are defined as

$$\Delta(S/N)_{50} = (S/N)_{50} - (S/N)'_{50}, \qquad (8)$$

$$\Delta(S/N)_{100} = (S/N)_{100} - (S/N)'_{100}, \qquad (9)$$

for each linking fibre. Five measurements have been carried out, showing the variations in the measured signal over these cases, as illustrated in Table 1 for each fibre, from which it can be seen that the signal to noise ratio of the output of the system with 100 μm core diameter fibre is higher than that with 50 μm core diameter fibre by, on average, ~ 2 dB, in agreement with the trend of Eq. (1).

In the experiment, interferometer I represents a sensing interferometer and interferometer II a reference interferometer, i.e. PZT0 was used to set the displacement, and the PZT1 to measure central position of the output fringe signal.

A further experiment was carried out to investigate the effect of the modal noise on the central position measurement when fibres with different core diameters were used to link the two interferometers. The values of ALD of the sensing and recovery interferometers were both set to be about 2 mm. The central position of the output was measured by using the scanning PZT actuator (PZT1) in the recovery interferometer. The value corresponding to the central position measurement in the experiment is equal to the arm length difference of the two interferometers when the two PZT actuators (PZT0 and PZT1) are both in the "zero" position. The repeatability, E, (to three standard deviations) of the measurement of the central position was obtained from a number of consecutive central position measurements.

The results are listed in Table 2, showing the fibre core diameters and the measurement repeatability

Table 2
The displacement measurement repeatability of the system with different core diameter linking fibres: D, fibre diameter; E, measurement repeatability; E', measurement repeatability with the fibre vibrated

D (μm)	E (nm)	E' (nm)
200	19.8	22.5
100	24.3	30.6
50	27.0	57.0

(three standard deviations) of the central position measurement with and without the fibre being vibrated, i.e. results shown under the headings E' and E, respectively. The central fringe position was determined using the maximum visibility method [6]. The repeatability of the central position measurement is worse when the fibre is perturbed due to the modal noise present in the system, increasing with the fibre core diameter in agreement with the prediction of Eq. (1).

4. Conclusion

In this paper, the signal to noise ratio obtained in the linked interferometer system with different core diameter fibres has been measured, showing that the signal to noise ratio of the output of the system with a 100 μm core diameter linking fibre in the presence of noise is higher than that with a 50 μm core diameter fibre. The displacement measurement repeatability of the system with these fibres has been measured, showing that the repeatability values (to three standard deviations) of the system with a reproducible vibration of the connecting fibre are 22.5 nm, 30.6 nm, 57.0 nm when the system is linked with a 200 μm, 100 μm and 50 μm, core diameter fibre, respectively.

References

[1] K.T.V. Grattan and B.T. Meggitt, Optical Fiber Sensor Technology, Ch. 9 (Chapman & Hall, London, 1995).
[2] Y.N. Ning, Y. Liu, K.T.V. Grattan, A.W. Palmer and K. Weir, Optics Lett. 19 (1993) 372.
[3] Y.N. Ning, K.T.V. Grattan, A.W. Palmer and K. Weir, Appl. Optics 33 (1994) 7529.
[4] Qi Wang, Y.N. Ning, K.T.V. Grattan and A.W. Palmer, Optics Comm. 118 (1995) 473.
[5] W. Mendenhall, R.L. Scheafer and D.D. Wackerly. Mathematical Statistics with Applications, 2nd Ed. (Boston, Duxbury, 1978) Ch. 11, p. 426.
[6] S. Chen, A.W. Palmer, K.T.V. Grattan and B.T. Meggitt Appl. Optics 31 (1992) 6003.
[7] D.N. Wang, Y.N. Ning, K.T.V. Grattan, A.W. Palmer and K. Weir, Lightwave Technol. 12, 909 (1994) 914.

Instructions to Authors (short version)
(A more detailed version of the instructions is published in the preliminary pages of each volume)

Submission of papers

Manuscripts (one original and three copies), should be sent to one of the Editors, whose addresses are given on the inside of the journal cover.

Original material. Submission of a manuscript implies that the paper is not being simultaneously considered for publication elsewhere and that the authors have obtained the authority for publication, if needed.

Refereeing. Submitted papers will be refereed and, if necessary, authors may be invited to revise their manuscript. Authors are encouraged to list the names (addresses and telephone numbers) of up to five individuals outside their institution who are qualified to serve as referees for their paper. The referees selected will not necessarily be from the list suggested by the author.

Types of contributions

The journal Optics Communications publishes short communications and full length articles in the field of optics and quantum electronics.

Short communications are brief reports of significant, original and timely research results that warrant rapid publication. The length of short communications is limited to six journal pages. Proofs will not be mailed to authors prior to publication unless specifically requested.

Full length articles are subject to the same criteria of significance and originality but give a more complete and detailed account of the research results. Proofs of all full length articles will be mailed to the corresponding author, who is requested to return the corrected version to the publisher within two days of receipt.

Manuscript preparation

All manuscripts snould be written in good English. The paper copies of the text should be prepared with double line spacing and wide margins, on numbered sheets. See notes opposite on electronic version of manuscripts.

Structure. Please adhere to the following order of presentation: Article title, Author(s), Affiliation(s), Abstract, classification codes (PACS and/or MSC) and keywords, Main text, Acknowledgements, Appendices, Ref rences, Figure captions, Tables.

Corresponding author. The name, complete postal address, telephone and Fax numbers and the E-mail address of the corresponding author should be given on the first page of the manuscript.

PACS codes/keywords. Please supply one to four classification codes (PACS and/or MSC) and 1–6 keywords of your own choice for indexing purposes.

References. References to other work should be consecutively numbered in the text using square brackets and listed by number in the Reference list. Please refer to a recent issue of the journal or to the more detailed instructions for examples.

Illustrations

Illustrations should also be submitted in triplicate: one master set and two sets of copies. The *line drawings* in the master set should be original laser printer or plotter output or drawn in black india ink, with careful lettering, large enough (3–5 mm) to remain legible after reduction for printing. The *photographs* should be originals, with somewhat more contrast than is required in the printed version. They should be unmounted unless part of a composite figure. Any scale markers should be inserted on the photograph itself, not drawn below it.

Colour plates. Figures may be published in colour, if this is judged essential by the editor. The publisher and the author will each bear part of the extra costs involved. Further information is available from the full length instructions.

After acceptance

Important. When page proofs are made and sent out to authors, this is in order to check that no undetected errors have arisen in the typesetting (or file conversion) process. No changes in, or additions to, the edited manuscript will be accepted.

Copyright transfer. You will be asked to transfer copyright of the article to the publisher. This transfer will ensure the widest possible dissemination of information.

Electronic manuscripts

The publisher welcomes the receipt of an electronic version of your accepted manuscript (preferably encoded in LaTex). If you have not already supplied the final, revised version of your article (on diskette) to the Journal Editor, you are requested to send a file with the text of the accepted manuscript directly to the Publisher by e-mail or on diskette (allowed formats 3.5" or 5.25" MS-DOS, or 3.5" Macintosh) to the address given below. Please note that no deviations from the version accepted by the Editor of the journal are permissible without the prior and explicit approval by the Editor. Such changes should be clearly indicated on an accompanying printout of the file.

Author benefits

No page charges. Publishing in Optics Communications is free.

Free offprints. The corresponding author will receive 50 offprints free of charge. An offprint order form will be supplied by the publisher for ordering any additional paid offprints.

Discount. Contributors to Elsevier Science journals are entitled to a 30% discount on all Elsevier Science books.

Further information (after acceptance)

SENSORS AND ACTUATORS

A

PHYSICAL

A multimode optical-fibre sensing system using white-light interferometry and a two-wavelength synthetic source

Wang Qi, Y.N. Ning, K.T.V. Grattan *, A.W. Palmer

Department of Electrical, Electronic and Information Engineering, City University, Northampton Square, London EC1V 0HB, UK

ELSEVIER

SENSORS AND ACTUATORS A: PHYSICAL
International Journal Devoted to Research and Development of Physical and Chemical Transducers

Aims and Scope

Sensors and Actuators A brings together multidisciplinary interests in one journal entirely devoted to disseminating information on all aspects of research and development of solid-state devices for transducing physical signals.

Sensors and Actuators A regularly publishes original papers, letters to the Editors and from time to time invited review articles within the following device areas:

● **Fundamentals and Physics** such as: classification of effects, physical effects, measurement theory, modelling of sensors, measurement standards, measurement errors, units and constants, time and frequency measurement.

● **Materials and their Processing** such as: piezoelectric materials, polymers, metal oxides, III–V and II–VI semiconductors, thick and thin films, optical glass fibres, amorphous, polycrystalline and monocrystalline silicon.

● **Optoelectronic sensors** such as: photovoltaic diodes, photoconductors, photodiodes, phototransistors, position-sensitive photodetectors, optoisolators, photodiode arrays, charge-coupled devices, light-emitting diodes, injection lasers and liquid-crystal displays.

● **Mechanical sensors** such as: metallic, thin-film and semiconductor strain gauges, diffused silicon pressure sensors, silicon accelerometers, solid-state displacement transducers, piezo junction devices, piezoelectric field-effect transducers (PiFETs), tunnel-diode strain sensors, surface acoustic wave devices, silicon micromechanical switches, solid-state flow meters and electronic flow controllers.

● **Thermal sensors** such as: platinum resistors, thermistors, diode temperature sensors, silicon transistor thermometers, integrated temperature transducers, PTAT circuits, thermocouples, thermopiles, pyroelectric thermometers, quartz thermometers, power transistors and thick-film thermal print heads.

● **Magnetic sensors** such as: magnetoresistors, Corbino disks, magnetodiodes, Hall-effect devices, integrated Hall devices, silicon depletion-layer magnetometers, magneto-injection transistors, magnistors, lateral magnetotransistors, carrier-domain magnetometers, MOS magnetic-field sensors, solid-state read and write heads.

● **Micromechanics** such as: research papers on actuators, structures, integrated sensors–actuators, microsystems, and other devices or subdevices ranging in size from millimetres to sub-microns; micromechatronics; microelectromechanical systems; microrobots; silicon and non-silicon fabrication techniques; basic studies of physical phenomena of interest to micromechanics; mechanooptics and mechano-chemical systems; analysis of microsystems; exploration of new topics and materials related to micromechanics; microsystem-related problems like power supplies and signal transmission, microsystem-related simulation tools; other topics of interest to micromechanics.

● **Interface electronics**: electronic circuits which are designed to interface directly with the above transducers and which are used for improving or complementing the characteristics of these devices, such as linearization, A/D conversion, temperature compensation, light-intensity compensation, current/frequency conversion and microcomputer interfacing.

● **Sensor Systems and Applications** such as: sensor buses, multiple-sensor systems, sensor networks, voting systems, telemetering, sensor arrays, and automotive, environmental, monitoring and control, consumer, medical, alarm and security, robotic, nautical, aeronautical and space measurement systems.

A multimode optical-fibre sensing system using white-light interferometry and a two-wavelength synthetic source

Wang Qi, Y.N. Ning, K.T.V. Grattan *, A.W. Palmer

Department of Electrical, Electronic and Information Engineering, City University, Northampton Square, London EC1V 0HB, UK

Abstract

A tandem interferometer system linked with a 100 μm core diameter multimode fibre has been investigated and a signal-processing scheme introduced to suppress the noise in the system, simulated by a reproducible vibration of the fibre. The results show a short-term repeatability (to three standard deviations) of better than 15 nm displacement with the use of an appropriate curve-fitting signal-processing scheme, under conditions where the fibre is subjected to a known noise signal by being constantly subjected to vibration.

Keywords: Multimode optical fibres; White-light interferometry

1. Introduction

A number of schemes for optical-fibre sensing using white-light interferometry have been developed over recent years since the pioneering work of Bosselman and Ulrich [1] and further details of the use of the technique have been summarized, for example, by Meggitt [2]. In sensor applications, such systems can be used to determine a displacement or measurands such as temperature and pressure, which can be readily converted to a displacement. The main advantage of white-light interferometry, which uses a broad-band light source of a short coherent length, is the ability to make absolute measurements. Configured as a fibre-optic sensor, it is inherently suitable for use in adverse environments, due to the immunity of the system to both fibre transmission losses and the potential wavelength drift of the source.

When such a system is applied to optical-fibre sensing, multimode fibre is desirable to link the optical components in order to ease the difficulty of optical launch conditions with single-mode fibre. In any practical application of such an interferometer, the fibre will be subject to various perturbations and vibrations, and modal noise will be introduced in the system. Several techniques have been developed to suppress the modal noise thus induced, such as those employing a light source with a short coherence length [3], or linking the components in the system with sufficient lengths of com-

parably large-core-diameter fibre [4]. However, even with the use of these noise-suppression techniques, there is inevitably some residual noise, the presence of which may affect the measurement accuracy of the system.

In this work, a signal-processing approach is introduced to suppress the effect on the measurement of the noise induced in the fibre lead. A comparison of the measurement repeatability with and without the use of this signal-processing scheme is discussed and its implications for employment in a sensor system discussed.

2. The signal-processing scheme

The signal-processing scheme used in this work can be considered under two main aspects: first, identifying the central fringe by using the maximum-visibility method, and then employing an appropriate curve-fitting technique. This is designed to remove the noise present in the fringe profile and thus to determine the central position more accurately. This is achieved by undertaking a process which may be summarized as comprising the following six steps:

2.1. Removing the d.c. components of the signal

If the raw data set representing the results of the measurement is given by $(X[i], I[i])$, and the data point number is N, the new data set, $I'[i]$, after removing the d.c. components, is then given by

* Corresponding author. Tel.: + 44 171 477 8120. Fax: + 44 171 477 8568

$$I'[i] = I[i] - \frac{\Sigma I[i]}{N}$$

Following this processing step, there are two zero points present in each fringe which will then be used in Section 2.5 to determine the fringe central position.

2.2. Finding the central fringe of the output fringe pattern and obtaining the position of the maximum visibility, χ_c'

This may be defined as the coarse central position, used for a first attempt at determining the actual fringe central position, by using the maximum-visibility method described earlier [5]. With the use of a two-wavelength combination source in the system, the central peak can be easily identified, as has been discussed [6,7]. The resultant central position χ_c' is still an approximation as the noise in the system will induce an error, and the finite value of the sampling gap used in the technique will limit the measurement accuracy. In order to increase the quality of identification of the central position measurement, the following steps are required to obtain an improved estimate of the associated resolution, which can be smaller than that of the sampling gap used.

2.3. Subtracting the term χ_c' from the data set, $X[i]$

The new values of the data set $X'[i]$ thus generated are then given by

$$X'[i] = X[i] - \chi_c'$$

Following the implementation of this step, the central position of the fringe given by the new data set $(X'[i], I'[i])$ is close to zero and it is easier to fit a polynomial curve to the shape of the central fringe, as described in Section 2.4.

2.4. Fitting a fourth-order polynomial to the central fringe

The curve-fitting polynomial, $y(z)$, is given by

$$y(z) = az^4 + bz^3 + cz^2 + dz + e$$

where a, b, c, d and e are constants; by adjusting their values, the sum of squares for error (SSE) can be minimized [8], as given by

$$SSE = \sum_i (I[i] - y(X'[i]))^2$$

The best-fit curve is obtained using the constants whose values minimize the value of the SSE factor. Due to the modal noise present and the limitations of the sampling gap size, the fringe central position, χ_c', obtained after the step in Section 2.3, is just an estimate of the central position of the raw data, and the actual central position of the data set, $(X'[i], I'[i])$, does not correspond exactly to zero. Thus a term $\Delta \chi_c$ may be written as an estimate of the offset in the coarse central position, χ_c'. The following two steps are then used to obtain an estimate of the value of $\Delta \chi_c$.

2.5. Finding the two zero-point positions of the fitted curve, X_L, X_R

These two positions are given by

$$y'(X_L) = y'(X_R) = 0$$

An estimate of the error in the coarse central position, χ_c', is obtained by calculating the value of $\Delta \chi_c$, where

$$\Delta \chi_c = (X_L + X_R)/2$$

The final step in the process is then undertaken.

2.6. Calculating the improved value of the central position of the raw data, χ_c

This is simply given by

$$\chi_c = \chi_c' + \Delta \chi_c$$

The resolution obtainable in the measurement of the central position can be smaller than the value of the sampling gap, because the value of $\Delta \chi_c$ is calculated from a knowledge of the equation governing the fitted curve, which itself is a continuous function.

To show the validity of the method in practice, several experiments were carried out to collect and analyse visibility profiles obtained under the conditions where known levels of noise were introduced, achieved by vibrating the fibre in a reproducible way.

3. Experimental method

Fig. 1 shows a schematic of the system used to investigate the practical use of the scheme discussed, and to validate it. It consists of two Michelson interferometers, linked by a multimode fibre. Light from two readily available multimode laser diodes (LD2 and LD1, with wavelengths of 780 and 670 nm, respectively) passed through interferometer I, and then was coupled into a 100 μm core diameter multimode fibre. The light from the fibre was collimated and injected into interferometer II, the output of which was focused by a lens and detected by using a photodiode (PD). Each Michelson interferometer has one mirror controlled by a piezoelectric actuator (PZT0 and PZT1), which was driven using a closed-loop controlled system (System-2000, Queensgate Instruments Ltd). The output of the detector was then obtained and digitized. Part of the fibre (about 60 cm of its length) was continuously and repeatably shaken by a protruding wheel driven by a motor at a frequency of about 5 Hz to induce a reproducible and controlled noise signal in the fibre output. Both LDs are driven at a current which is below threshold, so that their resulting coherence lengths are relatively short (about 15 μm). In the experiment, the optical path-length differences, OPDs, of the two interferometers are set nearly equal to one another so that the difference of the OPDs between the two interferometers used is smaller than
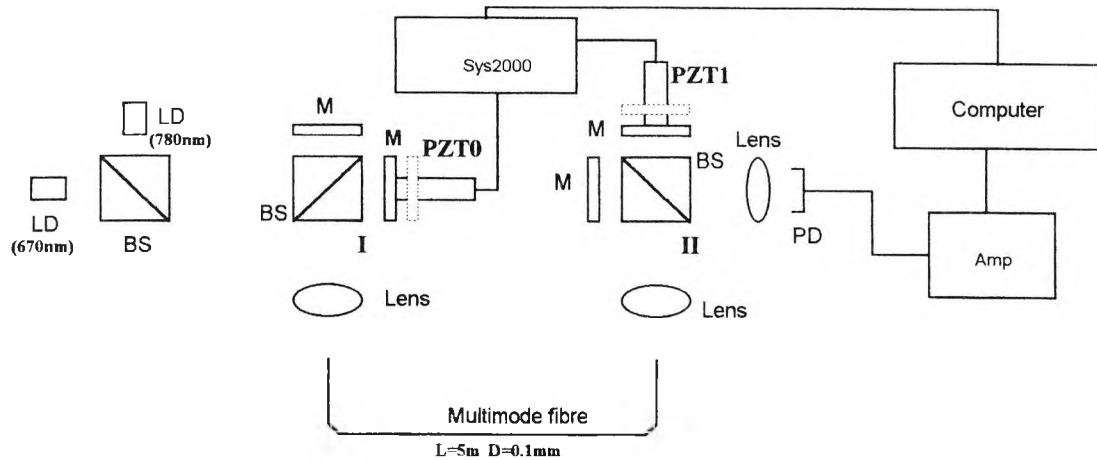
Fig. 1. The tandem interferometer system used in this work: LD1, 670 nm laser diode; LD2, 780 nm laser diode; BS, beam splitter; M, mirror; PZT0, PZT1, piezoelectric actuators; Sys2000, computer controller for PZTs; Amp, amplifier; I, II, interferometers.

the value of the coherence length of the source. The PZT actuator in the reference interferometer (PZT1) is then scanned to obtain the output fringe pattern representative of the system. In this simulation, interferometer I is taken to operate as a sensing interferometer and interferometer II is used as a reference interferometer, i.e., PZT0 is used to set the value of the displacement, and PZT1 to measure the central position of the output signal. Usually, a difference is seen between the position derived from the PZT0 and the central position of the output fringe pattern. This difference equals the difference of the OPDs of the two interferometers when both PZT actuators are at their zero positions and is independent of the position of PZT0 if the two interferometers are stable, this being measured by the use of the capacitance position sensors in the sensitive PZT actuators in the system.

Fig. 2 shows the result of applying a curve-fitting procedure to the central fringe of the output pattern. The jagged profile represents the experiment data set, and the smooth curve is the fitted fourth-order polynomial from the curve-fitting signal-processing scheme (Section 2.4) discussed
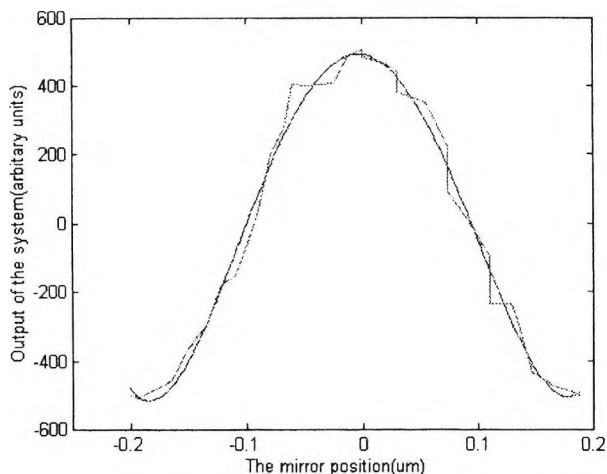
above, using the least-mean-squares method. If the peak-to-peak value of the smooth curve is taken to represent the signal value, the SEE term resulting from the curve fitting with the use of the fourth-order polynomial represents the noise obtained, and the signal-to-noise ratio may be calculated, from Fig. 2, to be about 31 dB.

The curve fitting applied clearly improves the results obtained in two ways. First, the fitted polynomial is determined with the least-mean-squares method, which allows the removal of the high-frequency amplitude and the phase noise by averaging. Secondly, as the fitted curve is a continuous function instead of a series of discrete data points, it can enable an enhancement of the resolution obtainable, which therefore can be much smaller than that determined simply by using the sampling gap obtainable from the PZT actuator.

4. Results

The displacement of the mirror in interferometer I, which is set by PZT0, was measured by using the tandem interferometer system. Each measurement was repeated six times within a short period of about two minutes, which allowed the reasonable assumption of negligible interferometer drift. The scanning gap of PZT1 was about 15 nm. The results obtained from this are shown in Fig. 3 where the x axis represents the displacement, set by PZT0, and the y axis the mean value of the measured displacement using the curve-fitting signal-processing scheme discussed above. It can be seen from this Figure that with the use of a 100 μm core diameter optical-fibre link, the system gives quite a satisfactory result, even when the fibre was constantly shaken and noise thus induced. The repeatability (to three standard deviations) of each measurement is shown in Table 1, where D represents the mean value of the measured displacement, E represents the repeatability of the measurements with the fibre being shaken and subject to noise and without the use of the curve-fitting signal-processing scheme (i.e., using just the

Fig. 2. Comparison between the fourth-order polynomial fit and the raw data for the central fringe of the interferometric visibility profile.
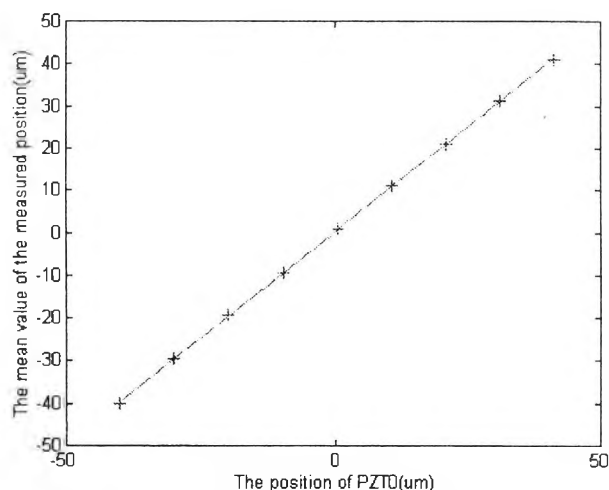
Fig. 3. The displacement measurement result with use of the tandem interferometer system discussed.

Table 1
The mean value of the measured displacements (D) and the repeatability of the measurements, E and E', without and with the use of the curve-fitting scheme discussed

D (μm)	-40.053	-29.569	-19.435	-9.231	0.916
E (nm)	27	27	21	30	24
E' (nm)	9	9	15	6	6
D (μm)	11.014	21.099	31.154	41.171	
E (nm)	21	24	24	15	
E' (nm)	6	6	12	3	

maximum-visibility method [5]), and in contrast E' represents the repeatability of the measurement with the use of the curve-fitting signal scheme. From Table 1, it can be seen that the worst value of the repeatability of the measurements obtained with the use of the maximum-visibility method is about 30 nm; after employing the signal-processing scheme, the repeatability was seen to improve to a value which is better than 15 nm, over a total displacement range of 80 μm.

5. Conclusions

Thus the work has shown that with the use of the simple signal-processing scheme described, the effect of a reproducible noise perturbation on the accurate measurement of the central position of a fringe can be reduced. The signal-to-noise ratio of the output in the system was determined to be about 31 dB when a 100 μm core diameter linking fibre was used in the experiment.

References

[1] T. Bosselman and R. Ulrich, High accuracy position-sensing with fiber coupled white light interferometers, *Proc. 2nd Int. Conf. Optical Fiber Sensors, Berlin, Germany, 1984*, pp. 361–364.

[2] B.T. Meggitt, Fiber optic white light interferometric sensors, in K.T.V. Grattan and B.T. Meggitt (eds.), *Optical Fiber Sensor Technology*, Chapman & Hall, London, 1995, Ch. 9, pp. 269–312.

[3] A.S. Gerges et al., Fiber optic interferometric sensors using a low coherence source: dynamic range enhancement, *Int. J. Optoelectronics, 3* (1988) 311–322.

[4] Y.N. Ning, K.T.V. Grattan, A.W. Palmer and K. Weir, Measurement of up and down-lead fibre sensitivity caused by lead in multimode fibre in an interferometric system, *Appl. Optics, 33* (1994) 7529–7535.

[5] S. Chen, A.W. Palmer, K.T.V. Grattan and B.T. Meggitt, Digital signal processing techniques for electronically scanned optical-fibre white-light interferometry, *Appl. Optics, 31* (1992) 6003–6010.

[6] D.N. Wang, Y.N. Ning, K.T.V. Grattan, A.W. Palmer and K. Weir, The optimized wavelength combinations of two broad band sources for white light interferometry, *IEEE J. Lightwave Technol., 12* (1994) 909–914.

[7] D.J. Webb, J.D.C. Jones and D.A. Jackson, Extended-range interferometry using a coherence-tuned, synthesized dual wavelength technique with multimode fiber link, *Electron Lett., 24* (1988) 1173–1175.

[8] W. Mendenhall, R.L. Scheafer and D.D. Wackerley, *Mathematical Statistics with Applications*, Duxbury, Boston, 2nd edn., 1978, Ch. 11, p. 426.

Biographies

Wang Qi was born in China on 5 October, 1958. He was awarded the B.S. in applied physics by Huazhong University of Science and Technology, Wuhan, China, in 1982 and the M.S. in optical engineering from the same university in 1988. He has been employed since 1988 as a lecturer in the Department of Physics in Huazhong University, teaching courses in advanced physics and transducer techniques. Since 1994 he has been a visiting scholar and a research student at City University, London, where he has now completed a Ph.D. in the field of optical-fibre interferometry, representing his main research interest.

Ya Nong Ning received the B.Sc. degree in physics from the Xian Jiaotong University, Shaanxi, China, in 1982, and the Ph.D. degree in measurement and instrumentation from the City University, London, UK, for research in optical-fibre sensing techniques. From 1991 to 1993, he worked as a research fellow at the Applied Optics Group, Physics Laboratory, University of Kent at Canterbury, UK, where he was responsible for research into miniature optical current and voltage sensors under the SERC/DTI-supported LINK-JIMS scheme. He is currently a research fellow at the Measurement and Instrumentation Centre, City University, doing research in optical-fibre sensing techniques using fibre gratings and interferometric detection schemes. His research interests are currently in the field of optical sensing and measurement techniques for industrial and environmental applications. He has authored or co-authored over 100 international journal and conference publications in the field of optical-fibre sensing and optical measurement. Dr Ning is a member of IEEE.

Kenneth Thomas Victor Grattan was born in County Armagh, Northern Ireland, on 9 December, 1953. He received

the B.Sc. degree in physics and the Ph.D. degree from the Queen's University, Belfast, Northern Ireland, in 1974 and 1978, respectively, and the D.Sc. degree from City University, London, in 1992. His Ph.D. research involved the development of ultraviolet gas discharge lasers and their application to the study of the photophysics of vapour-phase organic scintillators. From 1978 to 1983, he was a research assistant at Imperial College, University of London, UK, working in the field of ultraviolet and vacuum ultraviolet lasers and their application to measurement on excited states of atoms and molecules. In 1983, he was appointed a 'New Blood' lecturer in measurement and instrumentation at City University, London, in 1987, he became a senior lecturer, in 1988, a reader and in 1990, professor of measurement and instrumentation and head of the Department of Electrical, Electronic and Information Engineering at the same institution, where his research interests are currently in the field of optical sensing with industrial, environmental, and bioengi-

neering applications. He has authored and co-authored over 300 journal and conference papers in the field of optical measurement and sensing. Professor Grattan is a fellow and chairman of the Applied Optics Division of the Institute of Physics, a fellow of the Institution of Electrical Engineers, and a fellow of the Institute of Measurement and Control.

Andrew W. Palmer was born in New Zealand on 15 March 1938. He received the B.Eng. degree in electrical engineering from Canterbury University, New Zealand, and the M.Phil. and Ph.D. degrees from the City University, London, UK. He has lectured at the City University in the Department of Electrical, Electronic and Information Engineering, where he is currently doing research in the field of fibre-optic sensing for a range of measurement purposes. He has recently been appointed professor of electrical engineering at City University and is the author of some 200 journal and conference papers in the field.

Guide for Authors

Submission of Papers *(Physical papers only)*

Authors should submit a **disk** together with **three** copies of their articles (complete in all respects) direct to the appropriate Regional or Section Editor at the address listed below.

Professor S. Middelhoek, Delft University of Technology, Department of Electrical Engineering, P.O. Box 5031, 2600 GA Delft, Netherlands *(European papers only),*

or to the Editor for N. & S. America:
Professor J. Van der Spiegel, University of Pennsylvania, School of Engineering and Applied Science, Center for Sensor Technologies, Philadelphia, PA 19104-6390, USA,

or to the Editor for Japan:
Professor K. Takahashi, Teikyo University of Science and Technology, Department of Electronics and Information Science, 2525 Yatsuzawa, Uenohara-machi, Kitatsurugun, Yamanashi Prefecture, 409-01, Japan.

Papers for the *Micromechanics Section* should be submitted in threefold to the Coordinating Editor:
Professor J. E. Wood, Department of Mechanical Engineering, University of New Mexico, Albuquerque, NM 87131,USA.

Contributions are accepted on the understanding that authors have obtained the necessary authority for publication. Submission of an article must be accompanied by a statement that the article is original and unpublished and is not being considered for publication elsewhere. Upon acceptance of an article by the Journal, the author(s) will be asked to transfer the copyright of the article to the publisher. This transfer will ensure the widest possible dissemination of information.

Disk Preparation

The final text should be submitted on a 3.5″ disk (in addition to the hard copies and original figures). Double density (DD) or high density (HD) disks formatted for IBM compatibles or Apple Macintosh are preferred. The files should be saved in the native format of the word processing program used. Most popular word processor file formats are acceptable, though we cannot guarantee the usability of all formats. The disk format, word-processor format, file name(s) and the title and authors of the article should be indicated on the disk. The content of the disk must correspond exactly to the hard copy version of the paper.

Manuscript Preparation

Language. Papers will be published in English. Authors in Japan please note that information about how to have the English of your paper checked, corrected and improved *(before submission)* is available from: Elsevier Science Japan, Editorial Service, 1-9-15 Higashi Azabu, Minato-ku, Tokyo 106, Japan; Tel: +81-3-5561-5032; Fax: +81-3-5561-5045; E-mail: KYF04037@niftyserve.or.jp. Some flexibility of presentation will be allowed, but authors are urged to arrange the subject matter clearly under such headings as *Introduction, Experimental, Results, Discussion,* etc. All contributions should include a concise, informative *Abstract,* and a maximum of six *Keywords.* References should be numbered consecutively throughout the text and should be collected together in a reference list (headed *References*) at the end of the paper. All *equations, tables* and *legends* should be numbered consecutively and separately throughout the paper.

Illustrations. Line drawings should be in a form suitable for reproduction. Illustrations can be printed in *colour* when they are judged by the Editor to be essential to the presentation. The publisher and the author will each bear part of the extra costs involved. Further information concerning colour illustrations and the costs to the author can be obtained from the publisher.

Proofs

Authors will receive proofs which they are requested to correct and return as soon as possible. No new material may be inserted in the text at the time of proof-reading. A *Note added in proof* must be dated and the author must have requested and received the Editor's approval.

Offprints

Twenty-five offprints of each paper will be supplied free of charge to the author(s). Additional offprints may be ordered at prices shown on the offprint order form which accompanies the proofs.

There are no page charges.

Further Information

All questions arising after acceptance of a paper, especially those concerning proofs, should be directed to the Editorial Office, Elsevier Science S.A., P.O. Box 564, 1001 Lausanne, Switzerland; Tel.: +41 (21) 320 73 81; Fax: +41 (21) 323 54 44; E-mail: j.alwachi@elsevier.ch. A more detailed guide for the preparation of manuscripts is available from the Editorial office.

OPTICS
COMMUNICATIONS

Effect of multimode fibre core diameter
on modal noise suppression in white-light interferometry

Qi Wang, Y.N. Ning, K.T.V. Grattan, A.W. Palmer

Department of Electrical, Electronic and Information Engineering, City University, Northampton Square, London, EC1V OHB, UK

N·H

ELSEVIER

Effect of multimode fibre core diameter
on modal noise suppression in white-light interferometry

Qi Wang, Y.N. Ning, K.T.V. Grattan, A.W. Palmer

Department of Electrical, Electronic and Information Engineering, City University, Northampton Square, London, EC1V OHB, UK

Abstract

A study of the effect of modal noise in a Michelson interferometer system with a multimode down-lead fibre is reported. The experimental results show that the larger the core diameter of the multimode fibre used, the higher the signal-to-noise ratio (S/N) obtained at the output of system. A simplified theoretical analysis is used to support this, and indicates that, to a reasonable approximation, the output S/N ratio of the system is proportional to the square root of the mode number of the light propagating in the fibre.

1. Introduction

Optical white light interferometry (WLI) has recently been attracting significant attention in the research area of optical-fibre sensors [1], and several multimode fibre-linked interferometric systems have been studied [2–4]. However, when a multimode fibre is used to deliver light in a WLI system, modal noise will be induced in the system, which will reduce the overall signal-to-noise ratio (S/N) ratio experienced [2,5]. An experimental study on how the S/N of the system is affected by the use of different down-lead fibres of varying core diameters in a Michelson interferometer is reported. Results obtained are compared with those from a simplified theoretical analysis, and agreement seen with the use of serval approximations.

2. Theoretical analysis

It is well known that when a multimode fibre is not perturbed, the electric field supported by each mode of

the fibre will be independent and not cross-couple one to another. Under such an ideal condition, the total optical power delivered by the multimode fibre may be approximated to be the sum of the power delivered by an equivalent group of "single-mode" fibres [2]. Hence, the overall system can be treated in this simplified way as an array of similar sub-systems each with a single mode optical link. If the term "elemental system'" is used to represent such a sub-system which consists of an input light beam delivered by a single mode fibre into the interferometer, each elemental system will give an identical fringe pattern at the output of the interferometer, and the overall output of the system may be considered to be the sum of that of each elemental sub-system, i.e.:

$$P = \sum_k P_k , \qquad (1)$$

where P is the total mean power of the system, and P_k is the mean power of the kth elemental sub-system.

When the fibre is perturbed, the optical power delivered by each of the elemental sub-systems will vary, due to the following reasons.

(a) As the fibre is perturbed, a power exchange across each individual mode, due to the mode coupling effect, will take place randomly along the fibre. This introduces a statistical uncertainty in the modal power distribution. In particular, when the optical power of the radiation modes or the leak modes is concerned, the level of the power in those modes will fluctuate with time, and this causes a variation in the optical power transmitted by the multimode fibre.

(b) The optical components (lenses, mirrors, beam-splitters, etc.) in the interferometer are usually not perfect, as they will induce scattering and absorption of the light beam. Due to the uncertainty in the modal power distribution, the intensity distribution along the cross-section of the light beam will change in time, and therefore any scattering and absorption caused by the optical components in the interferometer also fluctuate in time, resulting in a variation in the optical power in each of the elemental sub-systems.

(c) It is well known that any state of polarization (SOP) of an input beam cannot be preserved through a multimode fibre, and as a result, although the SOP for any particular sub-system may vary, the SOP of the overall output light from many such sub-systems will be randomly distributed, in any possible direction, and no dominant direction may be obtained for the SOP of the output. In fact, since the fibre used in this work serves as the lead fibre to an extrinsic interferometer, any slight variation in the SOP of the output of the fibre will not affect the visibility of the output of the interferometer. Hence the SOP of the output can be statistically considered, to a reasonable approximation, not to vary.

From the above analysis, ignoring polarization effects as discussed, it is clear that as the perturbation of the fibre will cause an output fluctuation of each elemental sub-system, it will therefore induce an output fluctuation of each elemental sub-system, it will therefore induce a fluctuation of the total output. The number of the elemental sub-systems may be approximated to be the number of modes, M, propagating along the fibre, and the following assumptions may be made:

(i) $M \gg 1$. This requirement can readily be met since the number of modes for a graded index multimode fibre, with 50 μm core diameter, is about 340.

(ii) When the electric fields propagating along different modes reach their stationary state, i.e. the attenuation of every mode is the same, the mode distribution

will remain unchanged, and in this case the modal energy of each is independent one from the other. When the fibre is perturbed, modal coupling between adjacent modes will result in an energy variation, and at this level, the output intensity of each sub-system is indeed dependent on the adjacent modes. However, since the modal coupling most commonly occurs between adjacent modes, i.e., between the modes with most nearly equal propagation vectors [6], in considering all the modes involved, in order to simplify the theoretical analysis it can be assumed that the intensity of each sub-system is approximately statistically independent of most of the other nonadjacent modes, although this assumption strictly must be recognized as an approximation, and may be influenced by the partial coherence of beams travelling in different modes, as discussed later.

(iii) Since the propagation of one electric field will not be affected by the presence of another field, even the electric fields of two individual modes might overlap with each other, their interference is only determined by the coherence condition and where they are detected. The modal coupling in a perturbed fibre, in fact, is the modal energy variation and not the interference between the modes, and therefore, if a multimode laser diode or a LED is used as a source in the system, the OPD between most of the modes propagating in a multimode fibre, of say 5 m in length, is larger than the coherence length of the source itself. It is therefore a reasonable assumption that any two modes in the fibre are incoherent with each other at the output of the fibre.

(iv) It may be assumed that the S/N of any one elemental sub-system, $(S/N)_k$ is equal to that of any other sub-system, under the condition that the perturbation to the fibre is fixed and the arrangement of the interferometer is kept unchanged. These requirements are met in this experiment by inducing the same level of perturbation in the fibre, and keeping the alignment of the interferometer fixed, while changing the down-lead fibre itself.

When the interferometer is adjusted to the "balance position" [2], and one of the mirrors modulated by a PZT transducer with an amplitude equal to $\lambda/2$ (where λ is the central wavelength of the source), a signal at the modulation frequency can be obtained. The S/N associated with each elemental system can be written as

$$(S/N)_k = a(P_k/\sigma_k) , \qquad (2)$$

where σ_k is the square root of the variance of P_k, and A is dependent on the fringe visibility of the interferometer. If the alignment of the interferometer is kept unchanged during the experiment, A can be considered as an average value over all the sub-systems, each of which may experience a value which is different to some extent, and the total variance of the system is given by

$$\sigma^2 = \sum_k \sigma_k^2 . \qquad (3)$$

For the case where all guided modes are assumed equally excited at the sending end of the fibre, the optical energy is considered approximately evenly distributed into each mode [7] and the variance of the intensity in any mode is assumed equal to that in any other, then

$$P_k = P_1 . \qquad (4)$$

$$\sigma_k^2 = \sigma_1^2 . \qquad (5)$$

Substituting Eq. (4) and (5) into Eqs. (1) and (3), the following is obtained

$$P = MP_1 , \qquad (6)$$

$$\sigma^2 = M\sigma_1^2 , \qquad (7)$$

where M is the modal number of the fibre. The S/N of overall system is given by

$$(S/N) = AP/\sigma = \sqrt{M}(S/N)_1 . \qquad (8)$$

The square root of the variance, σ, is related to the noise level of the system, and when σ increases in the system, the noise will increase accordingly. In this experiment, the noise spectrum obtained is similar to that of white noise (as shown in the upper curve in Fig. 3). It may be assumed that the square root variance, σ, is proportional to the modal noise level, n, at frequency, f_1, and so

$$\sigma = Bn(f_1) , \qquad (9)$$

where B is a constant, and f_1 is chosen to be 130 Hz in this experiment.

Substitution of Eq. (9) into Eq. (8), yields

$$\frac{S}{n(f_1)} = B\sqrt{M}\,(S/N)_1 , \qquad (10)$$

which may be expressed in dB as

$$\left(\frac{S}{n(f_1)}\right)_{dB} = 20 \log(B(S/N)_1) + 10 \log(M) . \qquad (11)$$

These results indicate that, under the approximations given, the S/N of the interferometer, with a down-lead multimode fibre, is proportional to the square root of mode number in the fibre, where $(S/N)_1$ is the S/N of elemental sub-system, which is dependent on the strength of the perturbation strength applied to the fibre and the quality of the optical components in the interferometer.

3. Experimental arrangement

Fig. 1 shows the experimental arrangement used to study the effect of modal noise induced by the down-lead fibre. Light from a multimode laser diode (LT023MD) was injected into a multimode fibre, 5 meters in length, via a $\times 10$ objective lens. The output light from the fibre was then collimated and launched into a Michelson interferometer which was adjusted to the "balanced position". The recombined output beam from the interferometer was focused by a lens and detected by a photodiode (with a receiving area of 41.3 mm^2), where its output was amplified and then analyzed with a signal analyzer. One of the mirrors in the interferometer was modulated at a frequency which was randomly chosen at 130 Hz, and the amplitude of the PZT motion was driven at about half of the central wavelength of the source used: hence only one interference fringe around the central fringe position was generated, representing an output signal of the interferometer. Part of the fibre (about 90 cm in length) was vibrated with a protruding wheel driven by a motor at a frequency about 5 Hz, introducing a modal noise at the output. The peak value (rms) of the output spectrum at the modulated frequency (130 Hz) is used as the "signal" and the spectral output at 210 Hz is recorded as the average noise level. The above two frequencies were chosen to avoid problems due to pick-up in the electronics and interferometer.

In the experiment, all the conditions of the experimental arrangement were kept unchanged while fibres with different diameter were tested respectively, and therefore, the S/N ratio of the system linked with the different fibres could be studied and compared. Four
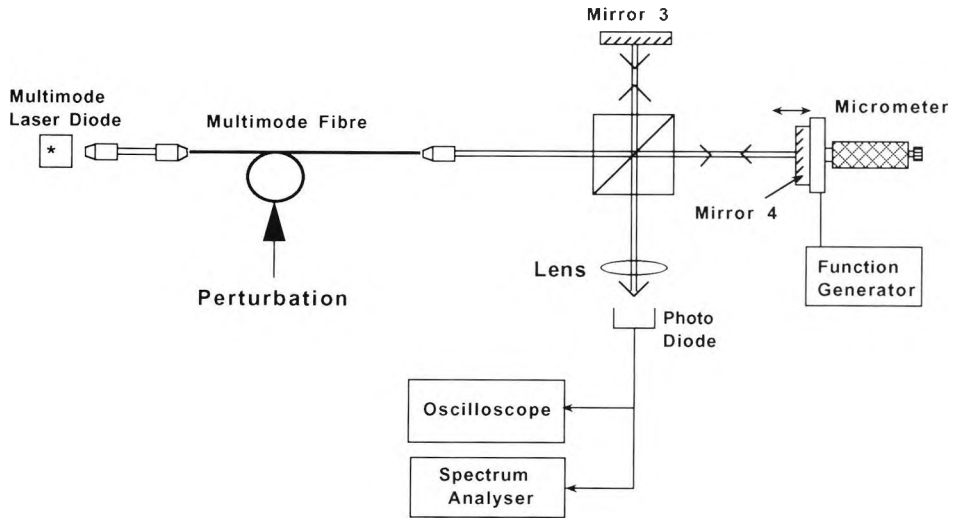
Fig. 1. The experimental arrangement used in this work, including a Michelson interferometer and a range of down-lead fibres.

types of fibres (all 5 meters in length) with core diameters of 50 μm (graded index), 100 μm (step index), 200 μm (step index), and 320 μm (step index), were employed respectively.

4. Results

Fig. 2 shows the results obtained experimentally and compared with those determined theoretically, where
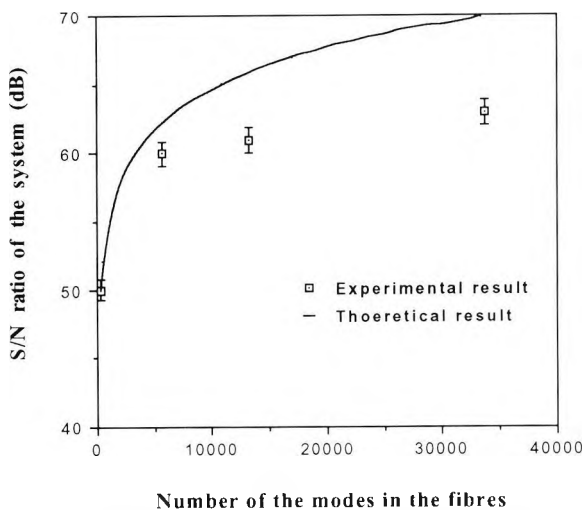
Fig. 2. The S/N ratio in the output of system vs. mode number of the down-lead fibres.

the theoretical result is shown as a solid line, which was calculated from Eq. (11). In this calculation, the value of the first item on the righthand side of the Eq. (11) was determined by utilizing the value of the measured S/N when a 50 μm core diameter fibre was used and the mode number, M, was determined using the theoretical approach described by Snyder and Love [8]. The dots represent experimental values obtained when the fibres with four different core diameters were used as the ''upload'' fibre respectively. From Fig. 2, it can be seen that the results of both the approximate theoretical analysis and the experiment show a similar trend, i.e. as the core diameter of the fibre increases, allowing for a consequent increase in the mode number of the fibre, the S/N of the system is also seen to increase. However, when the mode number reaches to about 6000, the variation of the S/N ratio in both the theoretical and experimental results occurs more slowly and continues with this trend as the mode number increases. This may be parially explained by the fact that for the same fibre length, when the core diameter increases to a certain value, the majority of the modes become incoherent with each other, and thus the vibration-induced modal noise will not increase as much as when a fibre with a smaller core diameter is used, resulting in a slow increase in the S/N ratio.

It also can be noticed that the theoretical S/N value is several dB higher than that obtained from the experiment, especially when the number of modes is relative
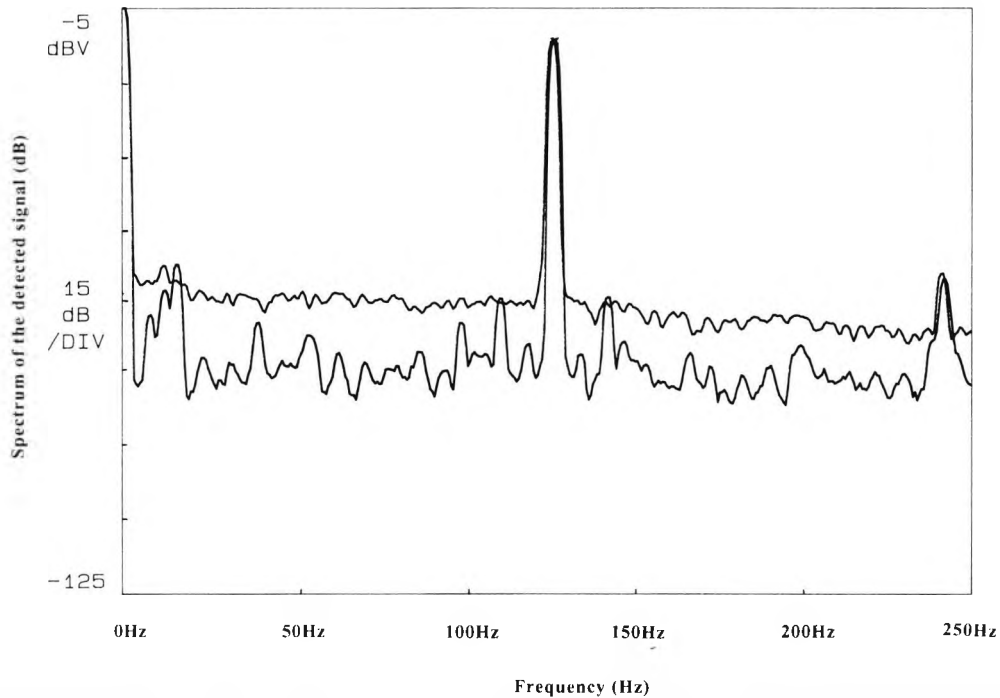
Fig. 3. The output spectrum of the system. The upper curve was obtained with a 50 μm core diameter fibre. The lower curve was obtained with a 320 μm core diameter fibre.

large. This may be due to the following reasons: (1) the output of the fibre in the theoretical model used in this work was considered as a point source. However, in the experiment, when a fibre with a large core diameter was used, the fibre end did not represent a point source, and hence the output beam was not well collimated, and as a result, the fringe visibility was reduced and the SNR obtained from the experiment was shown to be less than that obtained from the theory; and (2) some of the modes in the fibre are still coherent with each other, regardless of how large is the fibre diameter, and thus the earlier assumption (ii) is not strictly valid in this practical situation, although the underlying trend is clearly seen in the results obtained.

Fig. 3 shows a spectrum recorded of the output obtained with a 50 μm core diameter fibre (graded index, upper curve) and 320 μm core diameter fibre (step index, lower curve) as the down-lead fibre, respectively. In the experiment, the output intensity in the fibre was kept at the same value for each fibre. From Fig. 3, it can be seen that the S/N ratio of the system obtained with a larger core diameter fibre (i.e. 320 μm) is higher than that with a smaller core diameter fibre,

this also being in agreement with the results discussed above. The graph also shows some small peaks on the lower curve due to pick-up in the electronics and the interferometer.

5. Conclusion

In this work, the use of multimode fibres with different core diameters as a down-lead fibre in a Michelson interferometer has been studied experimentally. It has been shown that the larger the core diameter of the fibre utilized, the higher the signal-to-noise ratio that may be obtained at the output of the interferometer. A simple theoretical analysis is employed to show the trends in the results, using several reasonable assumptions and approximations and their agreement indicates that S/N ratio of the system is essentially proportional, to a reasonable approximation, to the square root of the mode number in the fibre, i.e. $S/N \sim \sqrt{M}$, where $M \gg 1$. Hence by using larger core diameter fibres in white light interferometric optical sensors, a greater $S/$

N can be obtained, resulting in a further advantage in the construction and use it such a system.

References

[1] H.C. Lefevre, Proc. 7th Optical Fibre Sensors Conference (Institution of Radio and Electronics Engineering, Sydney, Australia, 1990) pp. 345–352.

[2] S. Chen, A.W. Palmer, K.T.V. Grattan and B.T. Meggitt, Optics Lett. 17 (1992) 701.

[3] G. Beheim, K. Fritsch and R.N. Poorman, Rev. Sci. Instrum. 58 (1987) 1655.

[4] Q. Wang, Rev. Sci. Instrum. 64 (1993) 82.

[5] Y.N. Ning, K.T.V. Grattan, A.W. Palmer and K. Weir, Appl. Optics 33 (1994) 7529.

[6] R. Olshansky, Appl. Optics 14 (1975) 4.

[7] D. Gloge, Appl. Optics 10 (1971) 2252.

[8] S.W. Snyder and J.D. Love, Optical Waveguide Theory (Chapman&Hall, London, 1983) pp. 725.

Instructions to Authors (short version)

(A more detailed version of the instructions is published in the preliminary pages of each volume)

Submission of papers

Manuscripts (one original and two copies), should be sent to one of the Editors, whose addresses are given on the inside of the journal cover.

Original material. Submission of a manuscript implies that the paper is not being simultaneously considered for publication elsewhere and that the authors have obtained the necessary authority for publication.

Refereeing. Submitted papers will be refereed and, if necessary, authors may be invited to revise their manuscript. Authors are encouraged to list the names (addresses and telephone numbers) of up to five individuals outside their institution who are qualified to serve as referees for their paper. The referees selected will not necessarily be from the list suggested by the author.

Types of contributions

The journal Optics Communications publishes short communications and full length articles in the field of optics and quantum electronics.

Short communications are brief reports of significant, original and timely research results that warrant rapid publication. The length of short communications is limited to six journal pages. Proofs will not be mailed to authors prior to publication unless specifically requested.

Full length articles are subject to the same criteria of significance and originality but give a more complete and detailed account of the research results. Proofs of all full length articles will be mailed to the corresponding author, who is requested to return the corrected version to the publisher within two days of receipe.

Manuscript preparation

All manuscripts should be written in good English. The paper copies of the text should be prepared with double line spacing and wide margins, on numbered sheets. See notes opposite on electronic version of manuscripts.

Structure. Please adhere to the following order of presentation: Article title, Author(s), Affiliation(s), Abstract, PACS codes and keywords, Main text, Acknowledgements, Appendices, References, Figure captions, Tables.

Corresponding author. The name, complete postal address, telephone and Fax numbers and the E-mail address of the corresponding author should be given on the first page of the manuscript.

PACS codes/keywords. Please supply one or more relevant PACS-1995 classification codes and 1–6 keywords of your own choice for indexing purposes.

References. References to other work should be consecutively numbered in the text using square brackets and listed by number in the Reference list. Please refer to a recent issue of the journal or to the more detailed instructions for examples.

Illustrations

Illustrations should also be submitted in triplicate: one master set and two sets of copies. The *line drawings* in the master set should be original laser printer or plotter output or drawn in black india ink, with careful lettering, large enough (3–5 mm) to remain legible after reduction for printing. The *photographs* should be originals, with somewhat more contrast than is required in the printed version. They should be unmounted unless part of a composite figure. Any scale markers should be inserted on the photograph itself, not drawn below it.

Colour plates. Figures may be published in colour, if this is judged essential by the editor. The publisher and the author will each bear part of the extra costs involved. Further information is available from the publisher.

After acceptance

Important. When page proofs are made and sent out to authors, this is in order to check that no undetected errors have arisen in the typesetting (or file conversion) process. No changes in, or additions to, the edited manuscript will be accepted.

Copyright transfer. You will be asked to transfer copyright of the article to the publisher. This transfer will ensure the widest possible dissemination of information.

Electronic manuscripts

The publisher welcomes the receipt of an electronic version of your accepted manuscript (preferably encoded in LaTex). If you have not already supplied the final, revised version of your article (on diskette) to the Journal Editor, you are requested to send a file with the text of the accepted manuscript directly to the Publisher by e-mail or on diskette (allowed formats 3.5″ or 5.25″ MS-DOS, or 3.5″ Macintosh) to the address given below. Please note that no deviations from the version accepted by the Editor of the journal are permissible without the prior and explicit approval by the Editor. Such changes should be clearly indicated on an accompanying printout of the file.

Author benefits

No page charges. Publishing in Optics Communications is free.

Free offprints. The corresponding author will receive 50 offprints free of charge. An offprint order form will be supplied by the publisher for ordering any additional paid offprints.

Discount. Contributors to Elsevier Science journals are entitled to a 30% discount on all Elsevier Science books.

Further information (after acceptance)

Elsevier Science B.V., Optics Communication
Desk Editorial Department
P.O. Box 103, 1000 AC Amsterdam, The Netherlands
Fax: +30 20 4852319
E-mail: H. OOSTEROM@ELSEVIER.NL

Central fringe identification in a white light interferometer using a multi-stage-squaring signal processing scheme

Q. Wang, Y.N. Ning, A.W. Palmer, K.T.V. Grattan

Department of Electrical, Electronic and Information Engineering, City University, London EC1V OHB, UK

For 1995, volumes 112–121 (60 issues) have been announced. The subscription price for these volumes is available upon request from the publisher.

Subscriptions should be sent to the publisher, Elsevier Science B.V., Journals Department, P.O. Box 211, Amsterdam, The Netherlands, or to any subscription agent or bookseller. Claims for issues not received should be made within six months of publication. If not, they cannot be honoured free of charge.

Central fringe identification in a white light interferometer using a multi-stage-squaring signal processing scheme

Q. Wang, Y.N. Ning, A.W. Palmer, K.T.V. Grattan

Department of Electrical, Electronic and Information Engineering, City University, London EC1V OHB, UK

Received 6 December 1994

Abstract

A new signal processing scheme for central fringe identification in a white light interferometer is described. With the use of a simple, fast and low-cost multi-stage-squaring processing unit, the central fringe in the output fringe pattern can be considerably enhanced and the SNR_{min} required to identify the central fringe can be reduced from about 30 dB to 17 dB in a practical application.

Optical-fibre schemes based on the white light interferometer (WLI) represent a recently developed technology in the field of optical sensing and measurement [1–6]. The method has several distinct advantages over other sensing approaches, such as a large dynamic unambiguous range with high resolution; a passive sensing head; it is "down-lead insensitive", and has immunity to the frequency variation of the optical source. A typical WLI sensing system uses a sensing interferometer which converts the measurand into a variation in the optical path difference (OPD) and a reference or recovery interferometer which will introduce an OPD with the same value as the first in order to recover the profile of the interference fringes. By measuring the variation of the second OPD, the change caused in the first OPD and hence the measurand, can be obtained. Generally speaking, the accuracy of the WLI sensing system is determined by two basic factors: the first is whether the central fringe in the zero-order interference region can be accurately identified, and the second is whether the peak position of the central fringe can be precisely determined. In order to identify correctly the central fringe and thus its position, a number

of novel schemes and new developments have been introduced and reported, such as the use of the centroid algorithm method [3], the calculation of the centre of gravity of the average fringe power [4], or by the use of a two- [5] or three- [6] wavelength combination source to generate a fringe beating pattern. An alternative approach to locate the position is of measuring the phase slope of the Fourier components of the appropriate time domain signatures (sampled interference fringes) in the frequency domain [7]. In this letter, a new signal processing approach which can improve the accuracy of identifying the central fringe from the output of a white light interferometer is reported. This scheme is simple, fast, accurate and low-cost, and it can further reduce the signal-to-noise ratio (SNR) required for high quality identification.

The main goal of the signal processing is to enhance the relative value of the peak value of the central fringe whilst suppressing the peak values of other fringes, thus reducing the requirement on the SNR needed. For an interferometer illuminated using two incoherent light sources with different central wavelengths, as shown in Fig. 1, the light beams from two laser diodes are
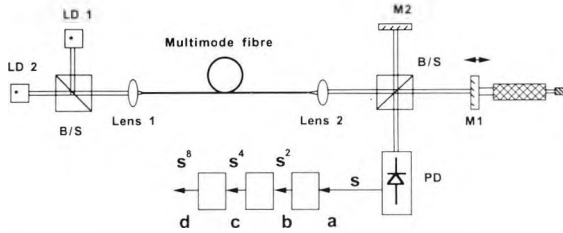
Fig. 1. Schematic diagram of the experimental arrangement used in this work, (the experimental results were recorded at a, b, c, and d respectively).

mutually incoherent with each other, and the output signal obtained from the interferometer is a result of intensity superposition of two sets of interference fringes. In this case, a ''fringe beat pattern'' is created whose intensity, $I(\Delta L)$, can be described by summing the autocorrelation functions of the two light sources, given by

$$
\begin{aligned}
I(\Delta L) &= (1/4)\{2 + \exp[-(2\Delta L/L_c)^2] \\
&\quad \times [\cos(2\pi\Delta L/\lambda_1) + \cos(2\pi\Delta L/\lambda_2)]\} \\
&= (1/2)\{1 + \exp[-(2\Delta L/L_c)^2] \\
&\quad \times [\cos(2\pi\Delta L/\lambda_a)\cos(2\pi\Delta L/\lambda_m)]\},
\end{aligned}
\tag{1}
$$

where λ_1, λ_2 are the central wavelengths of the two sources respectively, ΔL is the OPD introduced by the interferometer, L_c is the source coherence length, and $\lambda_a = 2\lambda_1\lambda_2/(\lambda_1 + \lambda_2)$ is termed the average wavelength and $\lambda_m = 2\lambda_1\lambda_2/|\lambda_1 - \lambda_2|$ the modulation wavelength. When this output signal is fed into a simple three-stage squaring circuit, the resulting output, $I'(\Delta L)$, can be then written as

$$
I_n(\Delta L) = [I(\Delta L)]^n, \qquad n = 2, 4, 8,
\tag{2}
$$

where $n = 2$, 4, 8, $I_n(\Delta L)$ represents the output of the first, the second and the third squaring operations, respectively. With the use of a simple computer program, the output intensity as a function of the optical path difference for the cases of $n = 1$, 2, 4, and 8 are calculated respectively, and the results are shown in Fig. 2.

In order to determine the minimum value of the signal-to-noise ration (SNR_{min}) required to identify the central fringe, the amplitude difference between the central fringe and the second largest fringe within the zero-order fringe packet, ΔI, is defined as the maximum noise level and can be written as

$$
\begin{aligned}
\Delta I &= I'(0) - I'(\lambda_a) \\
&= 1 - \{(1/2[1 + \exp[-2\Delta L/L_c)^2] \\
&\quad \times [\cos(2\pi\Delta L/\lambda_a)\cos(2\pi\Delta L/\lambda_m)]\}^n.
\end{aligned}
\tag{3}
$$

Clearly, if a system has a noise level which is equal to or greater than ΔI, the central fringe cannot be identified directly, simply through inspection of its amplitude. In other words, if the normalized peak value of the central fringe is defined as a unit signal, a minimum signal-to-noise ratio, SNR_{min}, required to identify the central fringe is given by

$$
SNR_{min}(dB) = -20\log(\Delta I/2).
\tag{4}
$$

In order to verify the principle of this signal processing scheme, the experimental arrangement shown in
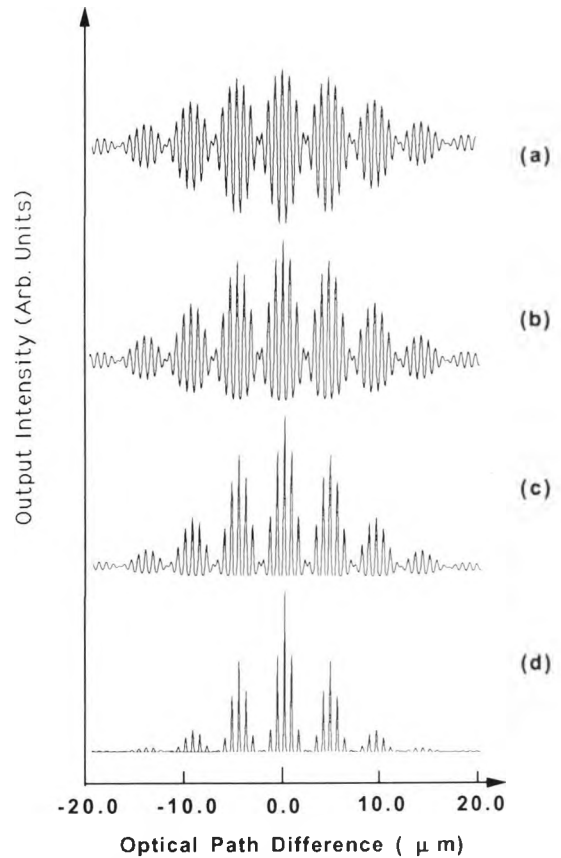
Fig. 2. Simulated results showing the fringe intensity as a function of the optical path difference for the cases of (a) $n = 1$, (b) $n = 2$, (c) $n = 4$, and (d) $n = 8$, respectively.
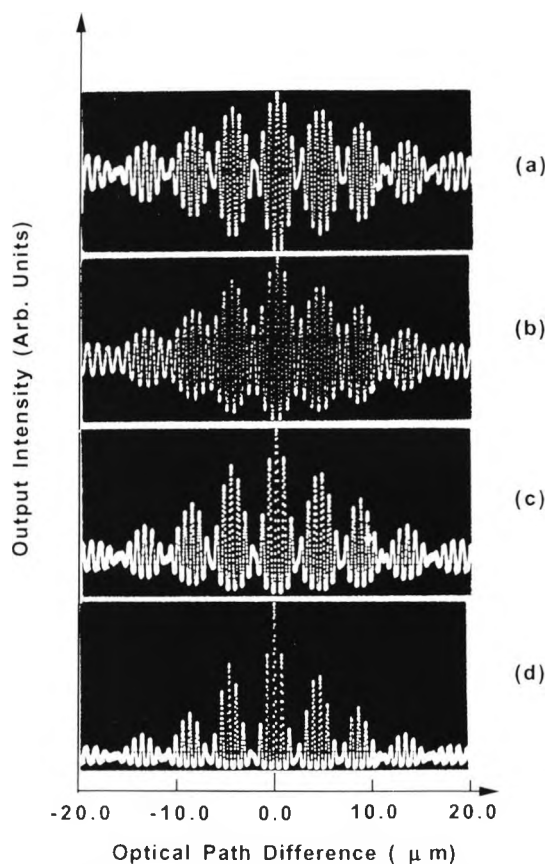
Fig. 3. Experimental results showing the fringe intensity as a function of the optical path difference for the cases of (a) $n = 1$, (b) $n = 2$, (c) $n = 4$, and (d) $n = 8$, respectively.

Fig. 1 was used in this work, where light from two multimode laser diodes (LT023MDO and LPM3.670, with central wavelengths of 780 nm and 670 nm, respectively) was injected into a multimode fibre (with a core diameter of 200 μm and a length of 4 meters) via an $10 \times$ objective lens. The collimated beam is modulated by the Michelson interferometer and detected with a photodiode. The output signals are then recorded before (for the case of $n = 1$) and after each stage of the squaring operation and the results are shown in Fig. 3. The values of the SNR for each cases were measured and plotted in Fig, 4, in which the theoretical value of the SNR_{min} as a function of the value of the power, n, was also shown.

By comparing Figs. 2 and 3, it can be seen that the results obtained from the experiment are in good agreement with those obtained theoretically. It is particularly important to see that as the number of the squaring operations increases, the relative peak value of the central fringe becomes larger and it can be easily identified by the use of a conventional electronic preset threshold device. In Fig. 4, a similar trend in which the value of the SNR_{min} is reduced with the increase of the number of the power can be seen. This is because the maximum "noise" defined here is, in fact, the difference between the peak values of the two fringes and it can be directly increased by a squaring operation. As a result, the identification of the central fringe becomes easier, and the value of the SNR_{min} required is lower.

It should be pointed out that the squaring operation can also increase the noise level induced by other sources, and the SNR of the output signal cannot be improved. However, since the amplitudes of the central fringe and the second largest fringe are much larger than that of the noise, the amplification of the amplitude difference (i.e. the "noise" used to calculate the SNR_{min} required) between these two fringes is larger than that of the overall noise in the squaring operation, resulting the effect of enhancing the central fringe and suppressing other fringes.

In conclusion, with the use of the multi-stage squaring signal processing scheme, the central fringe in the output fringe pattern can be considerably enhanced and the SNR_{min} required to identify the central fringe can be reduced, therefore making fringe identification eas-
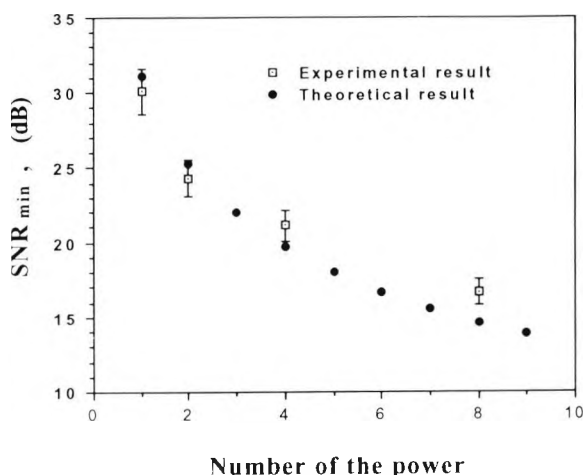
Number of the power

Fig. 4. Both experimental and theoretical results showing that the value of the SNR_{min} is reduced as the increase of the number of the power applied.

ily achieved with simple, conventional analogue devices.

References

[1] H.C. Lefevre, Proc. 7th Optical Fibre Sensors Conference, Sydney, Australia, ISBN0909 394 245 (1990) pp. 345–352.

[2] A.S. Gerges, T.P. Newson and D.A. Jackson, Appl. Optics 29 (1990) 4473.

[3] S. Chen, A.W. Palmer, K.T.V. Grattan and B.T. Meggitt, Appl. Optics 31 (1992) 6003.

[4] R. Dandliker, E. Zimmermann and G. Frosio, Proc. 8th Optical Fibre Sensors Conference, Monterey, CA, USA (1992) pp. 53–56.

[5] Y.J. Rao, Y.N. Ning and D.A. Jackson, Optics Lett. 18 (1993) 462.

[6] D.N. Ning, Y.N. Ning, K.T.V. Grattan, A.W. Palmer and K. Weir, IEEE Photon. Technol. Lett. 5 (1993) 1350.